Universitat de Girona

ANALYSIS OF COOPERATION AND ELECTRON DELOCALIZATION IN INTERMOLECULAR HYDROGEN BONDS

Laia Guillaumes Domènech

Dipòsit legal: Gi. 1382-2015
http://hdl.handle.net/10803/302666

VRIJE UNIVERSITEIT

UNIVERSITY OF GIRONA

Analysis of cooperation and electron delocalization in intermolecular hydrogen bonds

ACADEMISCH PROEFSCHRIFT

ter verkrijging van de graad

Doctor aan de Vrije Universiteit Amsterdam,
op gezag van de rector magnificus
prof.dr. F.A. van der Duyn Schouten,
en
Doctor in de Exacte Wetenschappen aan de University of Girona
op gezag van de rector
prof.dr. S. Bonet i Marull

in het openbaar te verdedigen
ten overstaan van de promotiecommissie
van de Faculteit der Exacte Wetenschappen van de Vrije Universiteit Amsterdam
en de Faculty of Sciences van de University of Girona

op maandag 22 juni 2015 om 15.45 uur
in de aula van de universiteit,
De Boelelaan 1105

door

Laia Guillaumes Domènech

geboren te Girona, Spanje

promotor:	prof.dr. F.M. Bickelhaupt
copromotoren:	dr. C. Fonseca Guerra
	dr. S. Simon Rabasseda

Doctoral Thesis

Analysis of cooperation and electron delocalization in intermolecular hydrogen bonds

Laia Guillaumes Domènech

2015

Doctoral programme in Experimental Sciences and Sustainability

Supervised by:

Dr. Sílvia Simon Rabasseda

Dr. Célia Fonseca Guerra

This manuscript has been presented to opt for the doctoral degree from the University of Girona and the Vrije Universiteit.

Cover design: Cristina Simon

No matter how high the mountain is, surround yourself with people that trust in you and just keep on going to achieve your dreams.

A la meva família

Acknowledgements

Resumir aquests anys amb una sola paraula, *gràcies*, és un objectiu difícil d'assolir. I és que aquesta engloba un camí d'aprenentatge, recerca i divulgació científica amb molts reptes, vivències i coneixences. En primer lloc, un *gràcies* per a tots aquells amb qui he coincidit durant aquest temps, perquè compartir-lo permet fer front als entrebancs, comentar anècdotes o tirar endavant un cop descoberta la pròpia paciència!

Durant aquest període he pogut formar part de dos camps diferenciats però complementaris, el de la recerca i el de la divulgació. La Sílvia i en Miquel ho han fet possible, donant-me l'oportunitat de fer un doctorat i comptant amb mi en l'àrea divulgativa des dels inicis. Perquè vàreu permetre que la meva col·laboració en ambdós àmbits comencés ja un temps abans de l'inici de la tesi i, mirant enrere, t'adones que són molts anys treballant junts per uns mateixos objectius. D'altra banda, gràcies també Sílvia per la tutoria rebuda durant aquests anys.

I would like to thank Célia and Matthias for their kind reception in their group. Thanks Célia for having been my supervisor, for all the objectives we have shared and for your professionalism. I have learnt lots and I am happy to have worked with you. And I would like also to mention other people: Karin, Joss, Francesc, Zoë and Olga. Iedereen van harte bedankt!

Tot i que les tasques divulgatives no estan presents a aquesta tesi, haig d'agrair també a en Pep, en Pep Anton, l'Eva, l'Íngrid, la Cristina, l'Òscar i a tots els membres i col·laboradors de la C4D haver compartit amb mi durant tot aquest temps la idea de treballar per comunicar la ciència.

Gràcies a en Miquel Solà, per l'assessorament a l'inici del doctorat i també per l'ajuda administrativa a l'hora d'encarar l'acabament. A en Marcel, per donar un cop de mà quan calia fer de pont geogràfic entre les dues zones de treball. I a en Sergi, la Mercè, en Majid i la Luz per fer més lleugera la realització del màster. També a en Pedro i l'Eduard per les explicacions dels seus programes i per aclarir sempre els dubtes quan apareixien problemes. I a l'Eloy, la Sílvia, en Ferran, en Marc, l'Eugene, en Quim, en Jordi, la Verònica... pels moments compartits i pel bon ambient de treball. Finalment a la Carme, per donar un cop de mà sempre que ha calgut i pel seu bon caràcter tranquil·litzador en moments d'estrès.

Ja per últim recordar els inicis i mencionar el tancament del cicle. D'una part, gràcies Dani, David i Anna per la bona acollida al despatx i per les anècdotes viscudes. De l'altra, gràcies Sara i Montse per l'ajuda i pels consells rebuts. I també cal anomenar en aquest apartat la Cristina Simon, qui ha posat el toc artístic en aquesta tesi tot fusionant disseny i ciència.

Per acabar gràcies a la família. Perquè les muntanyes no es pugen, el recorregut és més complicat i els reptes costen més d'assolir si no es té qui sempre et dóna suport al costat.

Així que a continuació, ara ja sí, comencem!

List of Publications

The following works are included in this thesis:

- Guillaumes, L.; Salvador, P.; Simon, S. A Fuzzy Analysis of Electron Delocalization of Hydrogen Bonds. *J. Phys. Chem. A.* **2014**, *118* (6), 1142-1149.

- Guillaumes, L.; Simon, S. Dealing with Quasi-Ring Formation by Two Hydrogen Bonds. Cooperativity Analysis with Delocalization Indices. *J. Phys. Chem. A*. **2014**, *118*, 9727–9733.

- Guillaumes, L.; Simon, S; Fonseca Guerra, C. The Role of Aromaticity, Hybridization, Electrostatics and Covalency in Resonance-Assisted Hydrogen Bonds of Adenine-Thymine (AT) Base Pair and Mimics. *ChemistryOpen*, **2015**.
  http://dx.doi.org/10.1002/open.201402132

- Guillaumes, L.; Simon, S; Fonseca Guerra, C. Theoretical Study on the Resonance-Assisted Hydrogen Bonding of DNA Base Pair Guanine-Cytosine (CG) and Mimics. In preparation, **2015**.

List of Abbreviations

Abbreviation	Description
AIM	Atoms In Molecules
AT	Adenine-thymine
bcp	Bond Critical Point
DFT	Density Functional Theory
DI	Delocalization Indices
DNA	Deoxyribonucleic acid
EDA	Energy Decomposition Analysis
E_{RiR}	Ring Reorganization Energy
GC	Guanine-cytosine
GGA	Generalized Gradient Approximation
HB	Hydrogen bonds
IUPAC	International Union of Pure and Applied Chemistry
KS	Kohn-Sham
LDA	Local Density Approximation
QTAIM	Quantum Theory of Atom In Molecules
RAHB	Resonance Assisted Hydrogen Bonds
VDD	Voronoi Deformation Density

List of Tables

Table 1.1: A classification for hydrogen bonds.....11

Table 5.1: Interaction Energy (kcal·mol^{-1}), CP-Corrected Interaction Energy (kcal·mol^{-1}), HB Distance (Å), HB Delocalization Index (DI_{HB} for complex and $DI_{HB90°}$ for perpendicular configuration), I_{NG}, and Ring Reorganization Energy (E_{RiR}, kcal·mol^{-1}).....58

Table 6.1: Bonding analyses (in kcal·mol^{-1}) and populations (in electrons) for AT and its smaller analogues.[a].....78

Table 6.2: Bonding analyses (in kcal·mol^{-1}), populations (in electrons), orbital energies (in eV) and distances (in Å) for adenine-thymine analogues A"T" and a"t".[a].....82

Table 7.1: Bonding analyses (in kcal·mol^{-1}) and populations (in electrons) for GC and its smaller equivalents.....97

List of Figures

Figure 1.1: Resonant forms of benzene (Kekulé structures). 13
Figure 1.2: Resonant forms for the cyclic malonaldehyde with one hydrogen bond. 13
Figure 1.3: On the left, AT. On the right, GC. 15
Figure 2.1: Donor-acceptor σ orbital interaction in the case of HB. Figure extracted from Ref.38. 26
Figure 2.2: Representation of adenine-thymine HB studied when calculating ΔE_{oi} without virtuals. ΔE_{oi} [A(σ,-)T(σ,-)] means analyzing both HB without including π virtuals. In the case of ΔE_{oi} [A(σ,-)T(-,-)] also σ virtuals of thymine have been deleted and only the upper HB takes place. 27
Figure 2.3: Topological analysis of the electron density of formic dimer. Small red points are density maximums (atoms). Big red point in the middle is a ring critical point. Points in green are bcp. Lines: gradient paths (blue), bond paths (light green), density contour lines (dark green), surfaces defining atoms in molecules (red). 31
Figure 2.4: Representation of the weight function of A for a diatomic molecule AB, where radius A is larger than B. The blue vertical line is the location of the interatomic plane. Atom A is located on R_A ($W_A(r)=1$) and B on R_B ($W_A(r)=0$). X axis represents the distance between A and B (R_{AB}). *k* is the stiffness parameter, the order of the polynomial. 33
Figure 4.1: Monomers considered in the simple set, including a number of different substituents (X) for formamide (FA), formamidine (FI) and formic acid (FO). 44
Figure 4.2: DI versus HB distances R_{HB} (Å) for QTAIM (a), Becke and Becke-ρ (b), Hirshfeld (c) and Hirshfeld-Iterative (d) atomic definitions. OH···O (black), NH···O (red), and NH···N (blue). 44
Figure 4.3: DI versus densities at the bcp for QTAIM (a), Becke and Becke-ρ (b), Hirshfeld (c) and Hirshfeld-Iterative (d) atomic definitions. OH···O (black), NH···O (red), and NH···N (blue). 46
Figure 4.4: Fuzzy-atom versus QTAIM DI for the set of hydrogen bonds. OH···O (black), NH···O (red), and NH···N (blue). The *y=x* line is also represented. 47
Figure 4.5: Fuzzy-atom versus QTAIM I_{NG} values for the *quasi*-rings. 48
Figure 5.1: All the monomers with the nomenclature used in this work. 57
Figure 5.2: Half of the interaction energy (E_{int}) with respect to delocalization indices on HB. 57
Figure 5.3: Interaction energy (E_{int}) with respect to the π contribution of the n-center delocalization index, $I_{NG\pi}$. 59
Figure 5.4: Interaction energy with respect to the addition of both DI_{HB}. 60
Figure 5.5: Interaction energy (E_{Int}) with respect to the π contribution of the n-center delocalization index, $I_{NG\pi}$. 60
Figure 5.6: C7-C7 complex with corresponding bond DI. (a) Monomer in the dimer geometry, (b) two-HB system, and (c) one-HB complex. 61

Figure 5.7: E_{RiR} with respect to the π contribution of the n-center delocalization index, $I_{NG\pi}$. 61
Figure 6.1: Hydrogen bond distances (in Å) and energies (in kcal·mol^{-1}) for adenine-thymine AT and its smaller analogues at the BLYP-D3(BJ)/TZ2P level of theory. 74
Figure 6.2: VDD atomic charges (in mili-electrons) of the prepared monomers (see eq. (6.5)). 75
Figure 6.3: Molecular orbital diagram with the most pronounced donor-acceptor interactions in the N6(H)···O4 and N1···(H)N3 hydrogen bonds between adenine and thymine. 75
Figure 6.4: Frontier orbitals of the monomers (HOMO-1, HOMO, LUMO and LUMO+1) in the σ electronic system, with the corresponding energies (eV). 76
Figure 6.5: ΔE_σ(σ,–; σ,–) of both hydrogen bonds and ΔE_σ(σ,–;–,–) for the N(H)···O hydrogen bond, and ΔE_σ(–,–;σ,–) for the N···(H)N hydrogen bond (see main text). 78
Figure 6.6: Voronoi deformation density (VDD) atomic charges ($\Delta Q^{\sigma}_{A,oi}$, in milli-electrons) associated with the formation of the different dimers. The contributions stemming from the σ electrons are given. 79
Figure 6.7: Voronoi deformation density (VDD) atomic charges ($\Delta Q^{\pi}_{A,oi}$, in milli-electrons) associated with the formation of the different dimers. The contributions stemming from the π electrons are given. 80
Figure 6.8: Atomic Voronoi deformation density (VDD) charges (in mili-electrons) for front atoms in A''T'' and a''t''. 80
Figure 6.9: Energy decomposition analysis for A"T" and a"t" at the equilibrium distance R(sp^2) of A"T" and at the equilibrium distance R(sp^3) of a"t". 81
Figure 7.1: Hydrogen bond distances (in Å) and energies (in kcal·mol^{-1}) for GC and its smaller equivalents at the BLYP-D3(BJ)/TZ2P level of theory. 94
Figure 7.2: VDD atomic charges (in mili-electrons) of the prepared monomers (see eq. (7.5)). 95
Figure 7.3: Molecular orbital diagram with the most pronounced donor-acceptor interactions in the O6···(H)N4, N1(H)···N3 and N2(H)···O2 hydrogen bonds between guanine and cytosine. HOMO, LUMO and LUMO+2 of guanine and HOMO-1, HOMO, LUMO of cytosine. 95
Figure 7.4: Frontier orbitals of the monomers (HOMO-1, HOMO, LUMO, LUMO+1 and LUMO+2) in the σ electronic system. 96
Figure 7.5: ΔE_σ(σ,–; σ,–) of both hydrogen bonds and ΔE_σ(–,–;σ,–) for the O···(H)N hydrogen bond and ΔE_σ(σ,–;–,–) for the N(H)···N and N(H)···O hydrogen bonds (see text). 98
Figure 7.6: VDD atomic charges ($\Delta Q^{\sigma}_{A,oi}$, in milli-electrons) associated with the formation of the different dimers. The contributions stemming from the σ electrons are given. 99
Figure 7.7: VDD atomic charges ($\Delta Q^{\pi}_{A,oi}$, in milli-electrons) associated with the formation of the different dimers. The contributions stemming from the π electrons are given. 99
Figure 8.1: DI versus HB distances R_{HB} (Å) for QTAIM. OH···O (black), NH···O (red), and NH···N (blue). 103

Figure 8.2: QTAIM versus Becke-ρ I_{NG} values for the *quasi*-rings.[86] 104
Figure 8.3: Is the addition of both HB energies equal to the total interaction energy?[100] 105
Figure 8.4: Terms of EDA: ΔV_{elstat}, ΔE_{Pauli} and ΔE_{oi} (see eq. (6.3)) for the case of having HB between molecule A and molecule B. 106
Figure 8.5: AT and its smaller mimics, reducing the number of π electrons: A, A', A'' and T, T', T''..... 106
Figure 8.6: sp^3 (A''T'', Cs) and sp^2 (a''t'', chair conformation) hybridized dimers..... 107
Figure 8.7: $G^{I}C^{I}$ and its smaller mimics, reducing the number of π electrons: G^{II}, G^{III}, G^{IV} and C^{II}. 108

Contents

Summary 1

Resum 3

Samenvatting 5

Resumen 7

1. Introduction 9

1.1 Hydrogen bonds 9

1.1.1 Definition of Hydrogen Bonds 9

1.1.2 Classification of Hydrogen Bonds 10

1.1.3 Some experimental features 11

1.2 Resonance Assisted Hydrogen Bonds (RAHB) 12

1.2.1 Resonance 12

1.2.2 Definition of RAHB 13

1.2.3 State of the art in RAHB 14

1.2.4 RAHB in DNA 15

2. Methods 17

2.1 Density Functions and Density Functional Theory 17

2.1.1 Density definitions 17

2.1.2 Hohenberg-Kohn theorems 19

2.1.3 Kohn-Sham (KS) method 20

2.1.4 DFT functionals 22

2.1.5 Dispersion-corrected functionals 24

2.2 Hydrogen bond energy analysis 25

2.2.1 Energy decomposition analysis (EDA) 25

2.3 Voronoi Deformation Density 27

2.3.1 VDD. Working with fragments 28

2.4 Atoms in molecules (AIM) 30

2.4.1 Quantum Theory of Atoms In Molecules (QTAIM) 30

2.4.2 Fuzzy-atom definitions 32

2.5 Delocalization indices (DI) 34

2.6 N-center index: I_{NG} 35

3. Objectives 37

4. A Fuzzy-Atom Analysis of Electron Delocalization On Hydrogen Bonds 39

4.1 Abstract 39

4.2 Introduction 39
4.3 Theoretical methods 42
4.4 Results 43
4.5 Conclusions 49
4.6 References 49
5. Dealing with Quasi-Ring Formation by Two Hydrogen Bonds. Cooperativity Analysis with Delocalization Indices 53
5.1 Abstract 53
5.2 Introduction 53
5.3 Methodology 55
5.4 Results 56
5.5 Conclusions 63
5.6 References 64
6. The Role of Aromaticity, Hybridization, Electrostatics and Covalency in Resonance-Assisted Hydrogen Bonds of Adenine-Thymine (AT) Base Pair and Their Mimics 67
6.1 Abstract 67
6.2 Introduction 67
6.3 Computational Methods 69
6.3.1 General Procedure 69
6.3.2 Bonding Energy Analysis 70
6.3.3 Analysis of the Charge Distribution 71
6.4 Results and Discussion 73
6.4.1 Structure and Stability of AT and its analogues 73
6.4.2 Nature of the hydrogen bond interaction 74
6.4.3 Charge redistribution due to hydrogen bonding 79
6.4.4 sp^2 versus sp^3 hybridization 80
6.5 Conclusions 83
6.6 References 84
7. Theoretical Study on the Resonance-Assisted Hydrogen Bonding of DNA Base Pair Guanine-Cytosine (GC) and Mimics 87
7.1 Abstract 87
7.2 Introduction 87
7.3 Computational Methods 89
7.3.1 General Procedure 89
7.3.2 Bonding Energy Analysis 90
7.3.3 Analysis of the Charge Distribution 91

7.4 Results and Discussion 93
7.4.1 Structure and Stability of GC and its equivalents 93
7.4.2 Nature of the hydrogen bond interaction 94
7.4.3 Charge redistribution due to hydrogen bonding 98
7.5 Conclusions 100
7.6 References 100
8. Results and discussion 103
8.1 Atomic division schemes 103
8.2 Delocalization indices and I_{NG} to study RAHB 104
8.3 RAHB for the DNA base pairs 105
8.3.1 Adenine-thymine 106
8.3.2 Guanine-cytosine 108
8.4 Conclusion from results 109
9. General conclusions 111
Bibliography 113
Appendices 117
Appendix A: Supporting information for CHAPTER 4 119
Appendix B: Supporting information for CHAPTER 5 125
Appendix C: Supporting information for CHAPTER 6 135
Appendix D: Supporting information for CHAPTER 7 143

Summary

In this thesis, different studies are presented on hydrogen bonds that occur between two interacting molecules. Hydrogen bonds (HB) are an essential type of interactions for processes in life, being responsible, among others, for holding together the two chains of the double helix of DNA. It is because of the biological importance of DNA that the base pairs, and other compounds with similar hydrogen bonds as these base pairs, have been studied in this thesis.

The main objective of the thesis is to understand Resonance Assisted Hydrogen Bonds (RAHB). This concept was introduced in the late eighties of the previous century to explain the enhanced stability of the hydrogen bonds between aromatic or sp^2-hybridized monomers that involve π electrons as compared to hydrogen bonds between monomers without π electrons.

There are two well-defined parts in this thesis, which both focus on the same objective of analyzing and understanding the nature of Resonance Assisted Hydrogen Bonds and examining the assistance by the π electrons. First, electron delocalization indices are used in order to analyze the HB formation. Secondly, a decomposition of the hydrogen bond energy will allow us understand which components of the bonding energy are responsible for the stronger hydrogen bonds.

It is essential to know how to divide the 3D-space in order to integrate the electron density for each atom and find delocalization indices (DI) on hydrogen bonds and normalized n-center delocalization indices I_{NG} within the *quasi*-ring. Thus, for the first part, using different ways of dividing the 3D-space permits to compare some fuzzy-atoms schemes to QTAIM. Becke-ρ has resulted to be the best performing fuzzy atom method for reproducing the QTAIM results for both mentioned indices.

Then, the same pairwise delocalization indices (DI) and the π contribution of the n-center delocalization indices ($I_{NG\pi}$) are used to know whether π delocalization, associated with RAHB, is a relevant contribution to the interaction energy between several complexes similar to the DNA bases. The values of π delocalization inside the *quasi*-ring are not directly related to the HB energy. Therefore, more π delocalization in the new ring does not mean a proportional increase in HB energy.

In the second part, a study of the π assistance to the hydrogen bonds of the base pairs adenine-thymine and some smaller mimics is performed based on quantitative Kohn-Sham molecular orbital theory and a corresponding energy decomposition analysis. It is shown that π assistance is not exclusively due to aromaticity, but that the sp^2-hybridization of the proton-donor and acceptor atoms already accounts for the π charge delocalization. The covalent component of the hydrogen bonds is shown to be essential to explain the shortening and strengthening in unsaturated dimers.

Finally, the three hydrogen bonds of the pair guanine-cytosine are analyzed. The number of π electrons is made smaller in a series of corresponding dimers to study the role of π assistance in hydrogen bonds. It is concluded that we can reduce the DNA bases to smaller equivalents with similar

sp^2 front atoms without affecting the hydrogen bond energy, except for guanine. The reduction of the 6-membered ring of guanine leads to a slight deviation from planarity and a weakening of the hydrogen bond energy.

In conclusion, both computational approaches, the delocalization indices and the molecular orbital theory with the corresponding energy decomposition analyses, show that the π electrons are not responsible for the enhanced stability of the RAHB. The latter demonstrates that the better covalent interaction in hydrogen bonded sp^2-hybridized dimers is responsible for the enhanced stability compared to sp^3-hybridized dimers.

Resum

En aquesta tesi es presenten diferents estudis sobre enllaços d'hidrogen que tenen lloc entre dues molècules que interaccionen. Els enllaços d'hidrogen són un tipus d'interacció essencial pels processos vitals, essent responsables, entre d'altres, de la unió de les dues cadenes de la doble hèlix de l'ADN. És la importància biològica de l'ADN la que ha portat a escollir com a sistemes d'estudi les seves parelles de bases i altres compostos que mostren enllaços semblants.

El principal objectiu de la tesi és entendre els enllaços d'hidrogen assistits per ressonància (RAHB). Aquest concepte va ser introduït a finals dels anys vuitanta del segle passat per explicar la millor estabilitat dels enllaços d'hidrogen entre monòmers aromàtics o amb hibridació sp^2 que involucren electrons π, en comparació amb els enllaços d'hidrogen entre monòmers sense electrons π.

En aquesta tesi s'hi troben dues parts ben definides, estant les dues enfocades al mateix objectiu d'analitzar i entendre la naturalesa dels enllaços d'hidrogen assistits per ressonància i d'examinar l'assistència dels electrons π. Primerament, s'usen índexs de deslocalització electrònica per analitzar la formació dels enllaços d'hidrogen. En segon lloc, la descomposició de l'energia dels enllaços d'hidrogen ens permetrà entendre quins són els components de l'energia d'enllaç responsables dels enllaços d'hidrogen més forts.

És essencial saber com dividir l'espai 3D per tal d'integrar la densitat electrónica de cada àtom i trobar els índexs de deslocalització (DI) en els enllaços d'hidrogen i els índexs normalitzats de n centres I_{NG} dins els *quasi*-anells. Així, per la primera part, usar diferents maneres de dividir l'espai 3D permet comparar alguns esquemes de *fuzzy* àtoms amb QTAIM. Becke-ρ ha resultat ser el millor mètode de *fuzzy* àtoms per reproduir els resultats QTAIM pels dos índexs esmentats.

Posteriorment, els mateixos índexs de deslocalització (DI) i la contribució π de l'índex normalitzat de n centres ($I_{NG\pi}$) s'usen per saber si la deslocalització π, associada amb els RAHB, és una contribució rellevant a l'energia d'interacció entre alguns complexos semblants a les bases de l'ADN. Els valors de la deslocalització π dins els nous anells no estan directament relacionats amb l'energia dels enllaços d'hidrogen. Per tant, més deslocalització π en el nou anell no significa un increment proporcional de l'energia dels enllaços d'hidrogen.

A la segona part, s'ha portat a terme un estudi de l'assistència dels electrons π als enllaços d'hidrogen de les parelles de bases adenina-timina i alguns anàlegs més petits; a través de la teoria quantitativa d'orbitals moleculars de Kohn-Sham i la corresponent anàlisi de la descomposició de l'energia. S'ha vist que l'assistència π no és exclusiva de l'aromaticitat, sinó que la hibridació sp^2 als àtoms donadors i acceptors de protons compta en la deslocalització de la càrrega π. El component covalent dels enllaços d'hidrogen s'ha trobat que és essencial per explicar el seu escurçament i enfortiment en els dímers insaturats.

Finalment, s'analitzen els tres enllaços d'hidrogen de la parella guanina-citosina. Es redueix el nombre d'electrons π en una sèrie de dímers corresponents per tal d'estudiar el paper de l'assistència π als enllaços d'hidrogen. Es conclou que podem reduir les bases de l'ADN a molècules equivalents més petites amb àtoms sp^2 frontera semblants, sense afectar l'energia dels enllaços d'hidrogen, excepte per la guanina. La reducció de l'anell de 6 membres de la guanina porta a una lleugera desviació de la seva posició al pla i a un afebliment de l'energia dels enllaços d'hidrogen.

En conclusió, els dos enfocaments computacionals, els índexs de deslocalització i la teoria d'orbitals moleculars amb la corresponent anàlisi de descomposició de l'energia, mostren que els electrons π no són responsables de la millor estabilitat dels RAHB. Per l'últim cas, es demostra que és la millor interacció covalent dels enllaços d'hidrogen en dímers amb hibridació sp^2 la responsable d'un augment de l'estabilitat en comparació amb els dímers amb hibridació sp^3.

Samenvatting

In dit proefschrift worden verschillende studies gepresenteerd over waterstofbruggen, die optreden in het geval van twee wisselwerkende moleculen. Waterstofbruggen (Hydrogen Bonds, HB) zijn een essentieel soort interactie voor processen die aan het leven ten grondslag liggen en die verantwoordelijk zijn voor onder anderen het bij elkaar houden van de twee strengen van de dubbele helix van DNA. Het is vanwege de biologische relevantie van DNA dat de basenparen en andere verbindingen met gelijksoortige waterstofbruggen als deze basenparen zijn bestudeerd in dit proefschrift.

Het hoofddoel van dit proefschrift is het verkrijgen van inzicht in de door resonantie geassisteerde waterstofbruggen (RAHB). Dit concept is eind jaren tachtig van de vorige eeuw geïntroduceerd om de verhoogde stabiliteit te verklaren van de waterstofbruggen tussen aromatische of sp^2-gehybridiseerde monomeren met π-electronen in vergelijking met waterstofbruggen tussen monomeren zonder π-electronen.

Er zijn twee goed gedefinieerde delen in dit proefschrift, die beide op hetzelfde doel focussen, namelijk het analyseren en begrijpen van de aard van de door resonantie geassisteerde waterstofbruggen en het onderzoeken van het werkingsmechanisme achter de assistentie door de π-electronen. Ten eerste, zijn de electronen-delocalisatie-indices (DI) gebruikt om de waterstofbrugvorming te analyseren. Ten tweede, maakt de decompositie van de waterstofbrugenergie het mogelijk om na te gaan welke componenten van de bindingsenergie verantwoordelijk zijn voor de sterkere waterstofbruggen.

Het is essentieel om te weten hoe de 3D-ruimte verdeeld moet worden om de electronendichtheid te integreren voor elk atoom en om delocalisatie-indices (DI) te vinden op waterstofbruggen en genormeerde n-center-delocalisatie-indices I_{NG} in de *quasi*-ring. Wat het eerste deel betreft, stelt het gebruik van verschillende manieren om de 3D-ruimte te verdelen ons in staat om verschillende *fuzzy*-atomen-schema's te vergelijken met QTAIM. Becke-ρ blijkt de best presterende *fuzzy*-atomen-methode te zijn met betrekking tot het reproduceren van de QTAIM-resultaten voor beide genoemde indices.

Daarna, zijn dezelfde paarsgewijze delocalistaie-indices (DI) en de π-contributie van de n-center-delocalisatie-indices ($I_{NG\pi}$) gebruikt om te weten te komen of π-delocalisatie, geassocieerd met RAHB, een relevante bijdrage levert aan de interactie-energie van de verschillende van DNA-basenparen afgeleide modelcomplexen. De waarden van π-delocalisatie in de *quasi*-ring zijn niet direct gerelateerd aan de HB energie. Met andere woorden, meer π-delocalisatie in de nieuwe ring betekent niet een proportionele toename in HB energie.

In het tweede deel, is een studie verricht van de π-assistentie aan de waterstofbruggen in adenine-thymine en in kleinere hiervan afgeleide modelcomplexen, gebaseerd op quantitatieve Kohn-Sham

moleculaire orbital theorie en een corresponderende energie decompositie analyse. Er wordt aangetoond dat de π-assistentie niet exclusief aan aromaticiteit toe te schrijven is. Dit stabiliserende effect komt daarentegen voort uit het feit dat de sp^2-hybridisatie van de proton-donor en -acceptor atomen reeds zonder de π-ladingsdelocalisatie tot een sterkere wisselwerking leidt dan in het geval van sp^3-gehybridiseerde proton-donor en -acceptor atomen. De covalente component in het σ-electronensysteem van de waterstofbruggen is essentieel om de verkorting en de versterking in onverzadigde dimeren uit te leggen.

Ten slotte, zijn de drie waterstofbruggen van het paar guanine-cytosine geanalyseerd. Het aantal π-electronen is verkleind in een reeks van gelijksoortige dimeren om de rol van de π-assistentie aan de waterstofbruggen te onderzoeken. Er kan geconcludeerd worden dat de DNA-basen gereduceerd kunnen worden tot kleinere equivalente basen met dezelfde sp^2-frontatomen zonder de waterstofbrug-energie te beïnvloeden, behalve in het geval van guanine. De reductie van de 6-ring van guanine leidt tot een kleine afwijking van diens planariteit en een verzwakking van de waterstofbrugenergie.

Concluderend, beide computationele benaderingen, de delocalisatie-indices en de moleculaire orbitaal theorie met de corresponderende energie decompositie analyse, laten zien dat de π-electronen niet verantwoordelijk zijn voor de grotere stabilisatie van de RAHB. De laatst genoemde methode toont aan dat de betere covalente interactie verantwoordelijk is voor de grotere stabiliteit in de waterstofbrug-gebonden sp^2-gehybridiseerde dimeren vergeleken met de sp^3-hybridiseerde dimeren.

Resumen

En esta tesis se presentan diferentes estudios sobre enlaces de hidrógeno que tienen lugar entre dos moléculas que interaccionan. Los enlaces de hidrógeno son un tipo de interacción esencial para los procesos vitales, siendo responsables, entre otros, de la unión de las dos cadenas de la doble hélice del ADN. Es la importancia biológica del ADN la que ha llevado a escoger como sistemas de estudio a sus pares de bases y a otros compuestos que muestran enlaces semejantes.

El principal objetivo de la tesis es entender los enlaces de hidrógeno asistidos por resonancia (RAHB). Este concepto fue introducido a finales de los años ochenta del siglo pasado para explicar la mejor estabilidad de los enlaces de hidrógeno entre monómeros aromáticos o con hibridación sp^2 que involucran electrones π, en comparación con los enlaces de hidrógeno entre monómeros sin electrones π.

En esta tesis se encuentran dos partes bien definidas, estando ambas enfocadas al mismo objetivo de analizar y entender la naturaleza de los enlaces de hidrógeno asistidos por resonancia y de examinar la asistencia de los electrones π. Primeramente, se usan índices de deslocalización electrónica para analizar la formación de los enlaces de hidrógeno. En segundo lugar, la descomposición de la energía de los enlaces de hidrógeno nos permitirá entender cuáles son los componentes de la energía de enlace responsables de los enlaces de hidrógeno más fuertes.

Es esencial saber cómo dividir el espacio 3D para integrar la densidad electrónica de cada átomo y encontrar los índices de deslocalización (DI) en los enlaces de hidrógeno y los índices normalizados de n centros I_{NG} dentro de los casi-anillos. Así, para la primera parte, usar diferentes formas de dividir el espacio 3D permite comparar algunos esquemas de *fuzzy* átomos con QTAIM. Becke-ρ ha resultado ser el mejor método de *fuzzy* átomos para reproducir los resultados QTAIM por los dos índices mencionados.

Posteriormente, los mismos índices de deslocalización (DI) y la contribución π del índice normalizado de n centros ($I_{NG\pi}$) se utilizan para saber si la deslocalización π, asociada con los RAHB, es una contribución relevante en la energía de interacción entre algunos complejos similares a las bases del ADN. Los valores de la deslocalización π dentro de los nuevos anillos no están directamente relacionados con la energía de los enlaces de hidrógeno. Por lo tanto, más deslocalización π en el nuevo anillo no significa que vaya a haber un incremento proporcional de la energía de los enlaces de hidrógeno.

En la segunda parte, se ha llevado a cabo un estudio de la asistencia de los electrones π en los enlaces de hidrógeno de las parejas de bases adenina-timina y algunos análogos más pequeños; a través de la teoría cuantitativa de orbitales moleculares de Kohn-Sham y el correspondiente análisis de la descomposición de la energía. Se ha visto que la asistencia π no es exclusiva de la aromaticidad, sino que

la hibridación sp^2 en los átomos donadores y aceptores de protones cuenta en la deslocalización de la carga π. El componente covalente de los enlaces de hidrógeno se ha encontrado que es esencial para explicar su acortamiento y fortalecimiento en los dímeros insaturados.

Finalmente, se analizan los tres enlaces de hidrógeno de la pareja guanina-citosina. Se reduce el número de electrones π en una serie de dímeros correspondientes para estudiar el papel de la asistencia π en los enlaces de hidrógeno. Se concluye que podemos reducir las bases del ADN a moléculas equivalentes más pequeñas con átomos sp^2 frontera similares, sin afectar la energía de los enlaces de hidrógeno, excepto por la guanina. La reducción del anillo de 6 miembros de la guanina lleva a una ligera desviación de su posición en el plano y a un debilitamiento de la energía de los enlaces de hidrógeno.

En conclusión, los dos enfoques computacionales, los índices de deslocalización y la teoría de orbitales moleculares con el correspondiente análisis de descomposición de la energía, muestran que los electrones π no son responsables de la mejor estabilidad de los RAHB. Para el último caso, se demuestra que es la mejor interacción covalente de los enlaces de hidrógeno en dímeros con hibridación sp^2 la responsable de un aumento de la estabilidad en comparación con los dímeros con hibridación sp^3.

1. Introduction

1.1 Hydrogen bonds

1.1.1 Definition of Hydrogen Bonds

Hydrogen bonds (HB) are an essential type of interactions for life processes. They can be found in a wide variety of biochemical systems. For example, they are the interactions that allow the two chains of the double helix of DNA holding together and, because of their importance, they have received a great deal of attention.[1-3]

The real discovery of HB is not clear, as their consequences were probably observed before their identification, or before a name for them was introduced. What is known[2] is that the words *nebenvalenz* (near valence) and *innere komplexsalzbildung* ("internal complex salt-bridge") were used by Werner[4] in 1902, Hantzsch[5] in 1910 and Pfeiffer[6] in 1914 to describe intra- and intermolecular HB. The term *weak union* was used in 1912 by Moore and Winmill in describing the properties of amines in aqueous solution.[7]

The concept of the hydrogen bond, according to Pauling, must be attributed to both M. L. Huggins (who claimed[8] to have been the first to propose it in his M.Sc. thesis in 1919) and W. M. Latimer and W. H. Rodebush. These last two authors published a paper[9] in 1920 with the sentence "The hydrogen nucleus held between 2 octets constitutes a weak "bond"". After these publications there were some more studies that involved hydrogen bonding. In 1931 a paper of Pauling[10] about the nature of chemical bonds used the term *hydrogen bond*, and it was also present in a paper of Huggins[11] of the same year about the role of hydrogen bonds in conduction by hydrogen and hydroxyl ions. However, the classic book published by Pauling[12] in 1939 was a very relevant step for the term *hydrogen bond*.

The definition for this type of bonds has been discussed and modified along the years. There are several books[1-2, 13] that focus the attention on hydrogen bonding, but it is worth mentioning the first text dedicated totally to it, by Pimentel and McClellan.[14]

Pauling stated that "It was recognized some decades ago that under certain conditions an atom of hydrogen is attracted by rather strong forces to two atoms, instead of only one, so that it may be considered to be acting as a bond between them. This is called the hydrogen bond".[12] There was also said that hydrogen atoms could form only one covalent bond, that the hydrogen bond was largely ionic in character and also that it was formed only between the most electronegative atoms. Although it is difficult to know where the hydrogen bonds were first mentioned, Pauling pointed out that the recognition of their importance and of their extensive occurrence was developed by Latimer and

Rodebush.[9] During the last years, the significance of hydrogen bonding has been demonstrated by its presence in a huge amount of publications.

The evidence for the existence of the HB can be experimental, theoretical or both. However, the meaning of the term "hydrogen bond" has always been surrounded by discussion. Recently, the International Union of Pure and Applied Chemistry (IUPAC)[15] has published the following recommended definition for the hydrogen bond: "The hydrogen bond is an attractive interaction between a hydrogen atom from a molecule or a molecular fragment X-H in which X is more electronegative than H, and an atom or a group of atoms in the same or a different molecule, in which there is evidence of bond formation".

Accompanying this definition, it is said that typical hydrogen bonds may be represented as X-H···Y-Z, where X is the hydrogen donor atom and Y is the acceptor (may be an atom or an anion, or be Y-Z as a fragment or a molecule). The acceptor is an electron rich zone such as a lone pair of Y or π-bonded pair of Y-Z. The IUPAC definition above is followed by a list of experimental and theoretical criteria which can be used to check the presence of this type of bonds. A total of six points, followed by some characteristics of HB, include detailed insight about the forces involved in the formation of the HB, geometrical requirements and some experimental evidences. These and more aspects are also well-developed in the IUPAC account[16] about the definition of HB. One of the ideas it states is that original examples for the HB[12] involved the donor groups FH, OH or NH, and this led to the conclusion that only them could form HB. F, O and N are among the most electronegative elements in the periodic table and so the H bonded with them will bear a relevant partial positive charge. However, even in the early days and until nowadays at the current IUPAC definition in the "Gold Book",[17] it has been specified that both X and Y are not limited to N, O or F. Some other donor and acceptor atoms have been actually declared also to be able to form HB.[16] For example, it has been realized that the hydrogen donor atom may be any element if it has a larger electronegativity than the one of H (F, N, O, C, P, S, Cl, Se, Br, and I).[18]

Defining the concept of hydrogen bonds has been demonstrated not to be a straightforward job, for being it a complex phenomenon. Thus, the criteria published by IUPAC[15-16] "are found to be satisfied in most hydrogen-bonded systems".

1.1.2 Classification of Hydrogen Bonds

The formation of HB implies a wide variety of interactions, and so their characterization is sometimes not very clear. One way to classify the different HB is by taking into account their strength and interatomic distances. Historically, HB studies pointed out that distances between the atoms X and Y were smaller than the sum of both van der Waals radii (which is only true for strong HB).[12] This led to a difficulty in situating the H atom and so also in a definition of the hydrogen bond radius. However, Desiraju and Steiner[19] and Jeffrey[2] talked about strong, medium and weak hydrogen bonds in reference to the X-Y distance.

Some classifications for the HB have already been published in the literature.[1-2] One example is shown in Table 1.1,[2] built from a set of 32 amino acid crystal structures. The H···Y distance of weak hydrogen bonds can be situated in the range between 2.2-3.2 Å, and 3.2-4.0 Å concerning the X···Y one, having been them described as electrostatic in type. Moderate HB are mostly electrostatic, involving their strength range distances from approximately 1.5 to 2.2 Å for H···Y and 2.5-3.2 Å when looking at X···Y. Finally, there are the mostly covalent ones, the strongest ones (very strong HB were mentioned by Emsley in 1980).[20] H···Y distances for the strongest HB are located in the approximated range 1.2-1.5 Å, while the numbers are 2.2-2.5 Å for X···Y.

Table 1.1: A classification for hydrogen bonds.

	Strong	Moderate	Weak
X-H···Y interaction	Mostly covalent	Mostly electrostatic	Electrostatic
Bond lengths	X-H ≈ H···Y	X-H < H···Y	X-H << H···Y
H···Y (Å)	~1.2-1.5	~1.5-2.2	2.2-3.2
X···Y (Å)	2.2-2.5	2.5-3.2	3.2-4.0
Bond angles (°)	175-180	130-180	90-150
Bond energy (kcal·mol^{-1})	14-40	4-15	<4

Strong HB can be found, for example, when the proton donor group shows a deficiency of electron density or there is an excess of it in the proton acceptor moiety. They also take place when the neutral donor and acceptor groups are forced to a contact closer than normal. However, the most usual HB are the moderate ones, generally built by neutral interacting groups. Being one or another, it must be highlighted that the nature of HB will depend on the donor and acceptor groups involved.

Also other characteristics, some of them experimental in character, have to be mentioned when considering different types of HB depending on their strength. For example, a H-bond angle for strong HB has been considered to be 175-180°, while it is 130-180° for moderate ones and 90-150° for the weakest. The fact that H-bond strength depends on the angle and length results in concluding that it has directionality.

Moreover, considering HB strength expressed in an energetic point of view, a value less than 4 kcal·mol^{-1} is linked with weak HB, 4-15 kcal·mol^{-1} for the moderate ones, and finding an energy of 14-40 kcal·mol^{-1} means having strong HB.

1.1.3 Some experimental features

Recently, both theoretical and experimental outcomes are appearing for the topic of HB. In the experimental field, one of the recent works that caught the attention was published in 2013. Zhang *et*

al.[21] reported the first visualization of HB using atomic force microscopy (AFM), which was a step further within the studies based on HB characterization.

There are quite a large amount of properties of molecules that depend on HB, and some experimental tools to detect the presence of them. Following the criteria recently published by the IUPAC,[15-16] the bond length X-H usually increases when the hydrogen bond is formed, leading to a red shift in the IR X-H stretching frequency. Thus, if we have a bond X-H···Y, it can be said that a stronger H···Y bond will be found for a larger lengthening of the bond X-H. Moreover, as it will take place the formation of H···Y, new vibrational modes will be generated. On the other hand, proton deshielding for H in X-H is one characteristic NMR signature. As the ^{1}H magnetic resonance detects sensibly the electron surroundings of the proton, NMR spectroscopy is useful to prove the existence of the HB. Another indication in IR that there are HB is that the width of the band corresponding to the X-H stretching peak increases and also its intensity.

It has to be mentioned that, although HB usually show a red shift in the X-H stretching frequency, and so a decrease of it linked with a weakening of the bond X-H, some HB have been found to show a blue shift. This opposite characteristic to what is expected to be found in classical HB was related to C-H proton donors and called by Hobza and Havlas[22] as “improper, blue-shifting” HB. Nowadays, it has been demonstrated that there are no major differences between these two types of HB.[23]

1.2 Resonance Assisted Hydrogen Bonds (RAHB)

1.2.1 Resonance

In 1960 Pauling[12] stated that the first to introduce the concept of resonance into quantum mechanics had been Heisenberg[24] when talking about quantum states of the helium atom.

Pauling wrote that when a ground state is described by a linear combination of different wave functions ($\Psi = \sum_i c_i \psi_i$), each of them corresponding to different structures, that state should be named as *resonating* between these structures mentioned, or as being a *resonance hybrid* of them. The energy of the system would have its minimum value (it is, the energy for the ground state) which would be an amount below the ones of the structures involved.

In the Gold Book[17] of IUPAC we can also find a definition for the concept of resonance as a “representation of the electronic structure of a molecular entity in terms of contributing structures. Resonance among contributing structures means that the wave function is represented by 'mixing' the wave functions of the contributing structures. The concept is the basis of the quantum mechanical valence bond methods. The resulting stabilization is linked to the quantum mechanical concept of 'resonance energy'. The term resonance is also used to refer to the delocalization phenomenon itself”. Thus, resonance is related to the idea of the delocalization of electrons in molecules where one single

Lewis formula cannot represent the overall bonding pattern, and this result in obtaining resonant structures (one Lewis representation for each, where only electrons change their place).

As π electrons are essential when it comes to talking about delocalization, it has to be said that the expected behavior is for single bonds to become shorter and a lengthening of the double bonds. As an example, benzene is shown in Figure 1.1, the archetypal structure with resonant forms.

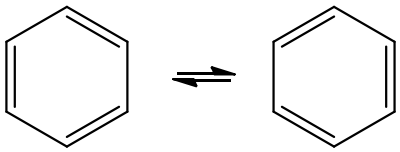

Figure 1.1: Resonant forms of benzene (Kekulé structures).

1.2.2 Definition of RAHB

The behavior of π electrons in the structure of the interacting compounds forming hydrogen bonds has been widely studied from different points of view. The presence of π electrons is usually linked with the appearance of an extra stabilization due to the effect known as Resonance Assisted Hydrogen Bonding (RAHB).

Although resonance was previously stated by Huggins[25] to stabilize rings containing hydrogen bridges, it was in 1989 when the concept of RAHB was first mentioned by Gilli *et al.*[26] They observed that a delocalization appeared in the π-conjugated system HOCR=CR-CR=O when an intramolecular or also an infinite-chain of intermolecular hydrogen bonds were formed. They found experimentally a relevant correlation between the strength of the new HB formed and the delocalization of the conjugated bonds that the system exhibited.

They demonstrated that thanks to the partial polarization generated by this resonance effect a shortening of the distance between proton acceptor and donor atoms occurred and that the distance between proton donor atom and proton increased. They suggested that it could have also biological and biochemical implications as in DNA, which shows both hydrogen and conjugated double bonds.

Another study[27] also revealed that the RAHB model was in agreement with experimental data. Thus, the analysis of the intramolecular hydrogen bond built by the fragment HO-C=C-C=O (Figure 1.2) showed that i) the O···O distance was very short, ii) the heteroconjugated fragment had a strong delocalization, iii) the O-H bond lengthened, iv) there was a lowering of the IR ν(OH) stretching frequency and v) the ^{1}H NMR chemical shift corresponding to the enolic proton increased.

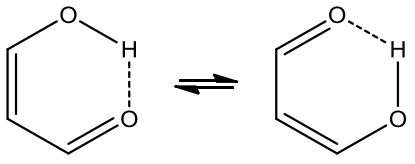

Figure 1.2: Resonant forms for the cyclic malonaldehyde with one hydrogen bond.

Additional investigations[28-29] have been performed complementing these data. For example, homonuclear (X-H···X) and symmetrical HB have been claimed[29] to be stronger for existing two isoenergetic resonance forms that can mix.

1.2.3 State of the art in RAHB

Gilli *et al*.[26] proposed RAHB as a mechanism of synergistic interplay of resonance and the formation of HB in π-conjugated systems. However, the idea of RAHB has led to different opinions since it was first stated.

In a work of Krygowski *et al.*[30] about derivatives of o-hydroxy Schiff bases it was pointed out that π-electron effects were important for the stabilization of the HB. Grabowski[31] established correlations between the energy associated to π-electron delocalization and some parameters used to describe HB strength in the case of malonaldehyde and derivatives.

Intermolecular HB of formamides and carboxylic acids were studied by Grabowski.[32] Delocalization interaction energy, which correlated well with other parameters that described the strength of HB, was mentioned to be the reason for their stability. Moreover, in a study of Lenain *et al.*[33] where they dealt with water and some cyclic compounds with π electrons, they analyzed HB reinforcing depending on aromatic electron delocalization (whether it could facilitate the donation of the proton and whether it enhanced the nucleophilic character of the molecule that had to accept it).

In addition, it was shown by Palusiak *et al.*[34-35] that not only was RAHB a matter of the atoms that were directly involved in HB, but also there was cooperation between adjacent aromatic rings and the effect of RAHB. An example, by Raczyńska *et al.*[36], can be the influence of a phenyl ring on a tautomeric equilibrium with an intramolecular HB, which has been studied in terms of variations of π-electron delocalization and stabilization.

Beck and Mo[37] recommended to highlight the importance of the electrostatics more than the covalent nature when it comes to talking about the stabilization in RAHB. Thus, they proposed the term "resonance-assisted binding (RAB)". They switched off the resonance effect, the resonance of π electrons, and developed an energy analysis that ended up concluding that RAHB was basically enhanced by dipole-dipole electrostatic interaction and polarization effect. However, hydrogen bonds in DNA were proved by Fonseca Guerra *et al*.[38] not to be only an essentially electrostatic phenomenon, as the charge transfer between σ interacting orbitals was seen to be of the same order of magnitude as the electrostatic term.

Recently, Kurczab *et al*.[39] arrived at the conclusion that both σ and π electronic frameworks suffered a charge rearrangement, but that the stabilization due to σ one was four times as important as the one associated with π, and so σ gave the dominant contributions to the HB.

Sanz *et al*.[40,41-42] published some studies of unsaturated compounds with intramolecular hydrogen bonds pointing out that the enhanced strength, which in principle would be due to RAHB, had to do with the much higher intrinsic basicity and acidity of the donor and acceptor groups that built the HB, or the structure of the σ-skeleton of the system that made the proton donor and acceptor be coplanar and nearer to each other.

A lot of studies related to RAHB have been developed, and a lot of points of view have arisen. Thus, there is still some controversy about the explanation of this effect.

1.2.4 RAHB in DNA

DNA is a molecule where the genetic information of all known living organisms and many viruses can be found. Thus, it is one of the most important macromolecules for the known types of life.

DNA is based on 4 nucleobases: adenine (A), thymine (T), cytosine (C) and guanine (G). Then, there are nucleotides, which include one of these nucleobases, a five-carbon sugar (deoxyribose) and one or more phosphate groups. Nucleobases are joined to the sugars. DNA is a long polymer with the shape of a double helix, where nucleotides are repeated and which is formed by two anti-parallel strands.

As mentioned in 1953 by Watson and Crick,[43] hydrogen bonds between the two helical chains of nucleotides are the basic interactions of the structure of DNA. Nucleobases interact thanks to HB, so adenine bonds thymine, while cytosine does it with guanine.

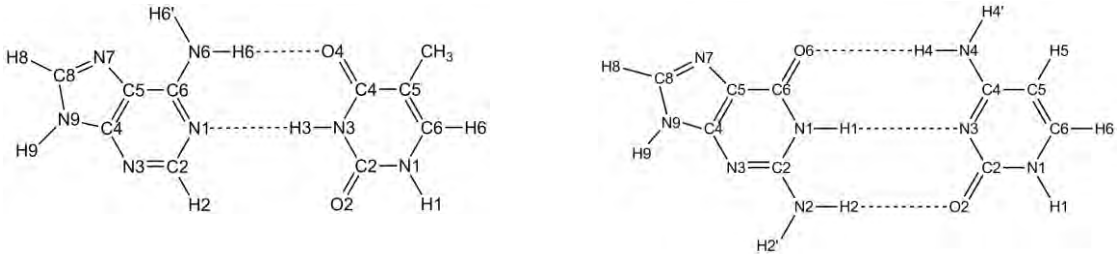

Figure 1.3: On the left, AT. On the right, GC.

As the four nucleobases have both double conjugated bonds and hydrogen bonds between them, they have the characteristics needed for RAHB to be studied. Gilli *et al.*[26] actually cited AT and GC as examples of the concept when it was first mentioned. Although it could seem quite straightforward to think about the appearance of RAHB in AT and GC examples, some controversy has been generated around this topic. The role of RAHB in proteins and DNA is a hypothesis that can neither be excluded nor confirmed in some cases.[13]

The nature of HB in DNA was studied by Fonseca Guerra *et al.*,[38] arriving at some conclusions which questioned the participation of resonance assistance of π electrons in the stability linked with the formation of base pairs due to HB. They did an energy decomposition analysis for the system and they saw that HB were not an essentially electrostatic phenomenon, because donor-acceptor interactions between lone pairs of proton acceptor atoms and σ*-acceptor orbitals had the same order of magnitude

as the electrostatic term (a conclusion also published[44] when the HB NH···O and N···HN were replaced by NH···F and N···HC, which resulted in making longer and weaker the HB between the base pairs). Moreover, π polarization of the bases contributed with only a small amount to the orbital interaction term of the interaction energy, so to the stabilization. In addition, substantial synergism neither between HB (C-H···O was rejected to be characterized as HB) nor between σ orbital interactions and π polarization was detected. Therefore, with the help of Voronoi Deformation Density analyses, they concluded that charge-transfer and electrostatics rather than resonance assistance due to π electrons would explain the behavior of these HB interactions in DNA.

Also in a publication of the same group[45] about the stability of guanine quartets, it was established that the cooperativity in them was because of the charge separation that went to lone-pair donor σ orbitals to $\sigma^*_{N\text{-}H}$ acceptor ones of the other guanine. Resonance assistance by the π electrons contributed only slightly to the HB strength but not to the cooperativity.

Guanine quartets have been also an experimental object of study by Otero *et al.*[46] They found the first experimental evidence that charge-transfer effects had an influence on the strength of the HB among nucleobases. They attributed to RAHB a strengthening of the HB and also a substantial participation in the HB energy of the G quartets in G quadruplexes.

Mitoraj *et al.*[47] analyzed the interaction between adenine-thymine fragments and found that three deformation density components contributed to their bonding. The energetically most important ones came from the donor-acceptor interactions between σ orbitals. However, the π deformation density showed a minor participation of π type orbitals. Thus, the so-called RAHB amounted only to -2.6 $kcal \cdot mol^{-1}$.

On the other hand, a weak covalence in the HB was confirmed by Mo[48] after finding a modest electron-transfer effect in AT, GC and Hoogsteen AT. There it was stated that electrostatics and polarization were the most important for binding energies and enhanced stabilization, especially in GC (with a favorable dipole-dipole electrostatic interaction). Moreover, the effect of π resonance on the covalence of HB was identified to be very limited, and when removing the aromatic rings in DNA bases a reduction of the electrostatics took place.

Modifications in the structure of the bases show that the change of H8 of guanine or H6 of cytosine (see Figure 1.3) for neutral substituents has a small effect on the strength of HB.[49] However, a change for charged substituents induced to modifications. An anionic substituent reduces the capability of proton donor to donate it and makes the acceptance of the proton easier, and the other way around for a cationic substituent.

Many works have been published about the way of dealing with resonance of π conjugated electrons that are part of systems formed with HB. Therefore, the possible appearance of an extra stability when having this type of interactions is still being studied for its important role in biological systems such as DNA.

2. Methods

2.1 Density Functions and Density Functional Theory

The Density Functional Theory (DFT) started in the 1920s with the seminal works in the homogeneous electron gas by Thomas[50] and Fermi.[51-52] Contrary to the wave function methods, which formally depend on 4N degrees of freedom (being N the number of electrons), this theory has the advantage of being solely based on the one-electron density of the system $\rho(\vec{r}\cdot s)$, where $\vec{r}$ and *s* indicate the spatial and spin coordinates, respectively. It was not until 1960s with the two theorems of Hohenberg and Kohn,[53] and specially the Kohn-Sham approach,[54] that the foundations of the modern DFT were established.

The high efficiency and the relatively high accuracy are perhaps the two characteristics of Kohn-Sham Density Functional Theory (DFT)[55-57] that have made it widely used not only for accurate calculations but also when a deeper insight on chemical bonding is desired.

2.1.1 Density definitions

Having a system with N electrons described by a normalized wave function $\Psi(\vec{x}_1, \vec{x}_3, \vec{x}_3 ... \vec{x}_N)$, where $\vec{x} = (\vec{r}\cdot s)$, the probability of finding an electron 1 between $\vec{x}_1$ and $\vec{x}_1 + d\vec{x}_1$ independently of where the others are is

$$\int \Psi(\vec{x}_1, \vec{x}_2, ... \vec{x}_N) \Psi^*(\vec{x}_1, \vec{x}_2, ... \vec{x}_N) d\vec{x}_2, ... d\vec{x}_N \qquad \textbf{(2.1)}$$

Moreover, electrons are indistinguishable, so knowing that N is the total number of electrons, one can consider

$$\rho(\vec{x}_1) = N \int \Psi(\vec{x}_1, \vec{x}_2, ... \vec{x}_N) \Psi^*(\vec{x}_1, \vec{x}_2, ... \vec{x}_N) d\vec{x}_2, ... d\vec{x}_N \qquad \textbf{(2.2)}$$

as the *first-order density*, which indicates the number of electrons between $\vec{x}_1$ and $\vec{x}_1 + d\vec{x}_1$.

Then, the *spinless electronic density*, taking into account both spins, can be obtained after integrating for the spin coordinate s

$$\rho(\vec{r}_1) = \int \rho(\vec{x}_1) ds_1 = N \int \Psi(\vec{x}_1, \vec{x}_2, ... \vec{x}_N) \Psi^*(\vec{x}_1, \vec{x}_2, ... \vec{x}_N) ds_1 d\vec{x}_2, ... d\vec{x}_N \qquad \textbf{(2.3)}$$

As the wave function is normalized, the integral of the electronic density will give the number of electrons N

$$\int \rho(\vec{r})d\vec{r} = N \qquad \rho(\vec{r}) \geq 0 \tag{2.4}$$

Similarly, the *second-order density* gives the information of the number of pairs of electrons that can be indistinctly one between $\vec{x}_1$ and $\vec{x}_1 + d\vec{x}_1$ and another between $\vec{x}_2$ and $\vec{x}_2 + d\vec{x}_2$, independently of the location of the others. It is obtained as

$$\gamma_2(\vec{x}_1, \vec{x}_2) = N(N-1)\int \Psi(\vec{x}_1, \vec{x}_2, ...\vec{x}_N)\Psi^*(\vec{x}_1, \vec{x}_2, ...\vec{x}_N)d\vec{x}_3, ...d\vec{x}_N \tag{2.5}$$

where N(N-1) accounts for all the possible electron pairs. Seemingly to (2.3), if the spin part is integrated, the result is the *spinless pair density* or *two-electron density*,

$$\gamma_2(\vec{r}_1, \vec{r}_2) = \int \gamma_2(\vec{x}_1, \vec{x}_2)ds_1 ds_2 \tag{2.6}$$

which stands for the number of pairs of electrons that can be one between $\vec{r}_1$ and $\vec{r}_1 + d\vec{r}_1$ and another between $\vec{r}_2$ and $\vec{r}_2 + d\vec{r}_2$, no matter the spin of both.

From the first- and second-order densities one can conveniently define the so-called exchange-correlation density $\rho_{XC}(\vec{r}_1, \vec{r}_2)$ as

$$\rho_{XC}(\vec{r}_1, \vec{r}_2) = \gamma_2(\vec{r}_1, \vec{r}_2) - \rho(\vec{r}_1)\rho(\vec{r}_2) \tag{2.7}$$

where $\rho(\vec{r}_1)\rho(\vec{r}_2)$ is the product of densities of uncorrelated independent particles, related to the probability of finding in $\vec{r}_1$ one electron and another in $\vec{r}_2$. So $\rho_{XC}(\vec{r}_1, \vec{r}_2)$ accounts for the fact that around a reference electron, the others are excluded in some degree. The exchange-correlation density $\rho_{XC}(\vec{r}_1, \vec{r}_2)$ accounts for the correlation between same spin (also known as exchange or Fermi contribution) and odd spin electrons (Coulomb or simply correlation contribution). Single Slater determinant wave functions include by construction only the exchange contribution because of the fulfilment of the Pauli repulsion principle. For the particular case of a closed-shell single-determinant wave function built from a set of doubly-occupied molecular orbitals, $\{\phi_i(\vec{r})\}$, one can make use of the so-called non-diagonal terms of the first-order density matrix

$$\rho(\vec{r}_1|\vec{r}_2) = 2\sum_i^{occ} \phi_i^*(\vec{r}_1)\phi_i(\vec{r}_2) \tag{2.8}$$

to write the exchange-correlation density (which in this case it includes only the exchange contribution) simply in terms of the molecular orbitals as

$$\rho_{XC}(\vec{r}_1,\vec{r}_2) = -\frac{1}{2}\rho(\vec{r}_1|\vec{r}_2)\rho(\vec{r}_2|\vec{r}_1) = -2\sum_{i}^{occ}\sum_{j}^{occ}\phi_i^*(\vec{r}_1)\phi_j^*(\vec{r}_2)\phi_j(\vec{r}_1)\phi_i(\vec{r}_2) \quad \textbf{(2.9)}$$

2.1.2 Hohenberg-Kohn theorems

In 1964, Hohenberg and Kohn[53] stated that any observable of a stationary non-degenerate ground state can be written as a functional of the electronic density $\rho(\vec{r})$ of the ground state.

There is a relationship between the density and the wave function via the external potential $v(\vec{r})$:

$$\rho(\vec{r}) \rightarrow v(\vec{r}) \rightarrow \hat{H} \rightarrow \Psi \quad \textbf{(2.10)}$$

The electron density $\rho(\vec{r})$ determines the Hamiltonian $\hat{H}$ and the wave function Ψ of the ground state and, therefore, its observables. It is worth highlighting that for the first Hohenberg-Kohn theorem to be accomplished, conditions (2.4) must be fulfilled (it means $\rho(\vec{r})$ being N-representable). Also, $\rho(\vec{r})$ must be *v*-representable, what means that the relationship (2.10) is guaranteed. Thus, the density of the ground state associated with the external potential cannot be reproduced by another potential (that is, this potential is totally determined by the density, except in an additive constant).

The expression of the energy as a functional of the density the can be formally expressed as

$$E[\rho] = T[\rho] + V_{Ne}[\rho] + V_{ee}[\rho] \quad (+V_{NN}) \quad \textbf{(2.11)}$$

where V_{NN} is the nuclear repulsion and is constant within the Born-Oppenheimer approximation. $V_{Ne}[\rho]$ is the attraction of an electron with the nuclei. Two terms do not depend on the external potential, being them the electron-electron interaction energy $V_{ee}[\rho]$ and the kinetic energy $T[\rho]$. They are usually included in the so-called universal Hohenberg-Hohn functional $F_{HK}[\rho]$ resulting in the equation

$$E[\rho] = \int \rho(\vec{r})v(\vec{r})d\vec{r} + F_{HK}[\rho] \quad \textbf{(2.12)}$$

When talking about the variational principle for $E[\rho]$, the Hohenberg-Kohn second theorem has to be invoked. It states that the electronic density of a non-degenerate ground state can be calculated by determining the density that minimizes the energy of the ground state (eq. (2.13))

$$E_0 \leq E[\tilde{\rho}(\vec{r})], \quad \textbf{(2.13)}$$

being $\tilde{\rho}(\vec{r})$ a trial density defined with the same characteristics as in the first theorem, that is, being N and v-representable. Thus, having a $\tilde{\rho}(\vec{r})$, the exact energy functional gives an energy higher or equal than the one obtained for the exact ground state. Although the definitions of these two theorems are useful, there was no indication on how to systematically build or find $E[\rho]$.

This section should not be finished without mentioning the Levy's constrained-search formulation.[58] An external potential is not needed for the derivation of the density (electronic density does not have to be v-representable) and degenerate ground states are possible. For this, an ensemble of Ψ that integrates an exact density for the studied state is required.

2.1.3 Kohn-Sham (KS) method

The exact expression of the $F_{HK}[\rho]$ functional it is not known. The exact form of T[ρ] is not accurate enough, what does not happen when using the expression T[Ψ]. In 1965 Kohn and Sham[54] proposed a practical computational manner to obtain the energy from $\rho(\vec{r})$. The model was made up of a reference system of N non-interacting electrons (but being Coulomb interactions with the nuclei) moving under an effective external potential $v_s(\vec{r})$, usually known as Kohn-Sham potential. This fictitious non-interacting system has the same density as the real system. For this non-interacting system, the Hamiltonian $\hat{H}_s$ is only built by one electron terms as

$$\hat{H}_s = \sum_{i=1}^{N} -\frac{1}{2}\nabla^2(i) + \sum_{i=1}^{N} \hat{v}_s(i) \qquad \textbf{(2.14)}$$

The Slater determinant

$$\Psi_s = \frac{1}{\sqrt{N!}}\left|\chi_1(1)\chi_2(2)\chi_3(3)...\chi_N(N)\right| \qquad \textbf{(2.15)}$$

gives the exact solution for this a non-interacting system, where the orthonormalized molecular orbitals would be eigenfunctions of the one-electron Hamiltonian operator (known as the Kohn-Sham operator),

$$\left[-\frac{1}{2}\nabla^2 + v_s\right]\chi_i = \varepsilon_i\chi_i \qquad \langle\chi_i|\chi_j\rangle = \delta_{ij} \qquad \textbf{(2.16)}$$

The corresponding electron density is obtained as a sum over densities of the occupied orbitals $\rho(\vec{r}) = \sum_{i=1}^{occ}\left|\chi_i(\vec{r})\right|^2$. With these orbitals the fictitious kinetic energy can be exactly calculated as

$$T_s[\rho] = \sum_{i=1}^{N_{occ}}\left\langle\chi_i\left|-\frac{1}{2}\nabla^2\right|\chi_i\right\rangle \qquad \textbf{(2.17)}$$

The energy of this non-interacting system is not the exact one (but $\rho(\vec{r})$ it is). The kinetic energy $T_s[\rho]$ is different from that of the real system, as it is calculated with Kohn-Sham orbitals found without taking into account interactions between electrons.

The energy of the real system as a functional of the density and including electron-electron interactions is

$$E[\rho] = T[\rho] + \int \rho(\vec{r})v(\vec{r})d\vec{r} + V_{ee}[\rho] \quad \textbf{(2.18)}$$

In the real system, the electron-nuclear attraction energy and the Coulomb repulsion among electrons are exact terms, as they can be expressed by using $\rho(\vec{r})$ and it is the exact one. Equation (2.18) can be reorganized by adding and subtracting the exact Coulomb repulsion energy J[ρ] and the kinetic energy for the non-interacting electrons system $T_s[\rho]$, resulting with the expression

$$E[\rho] = T_s[\rho] + \int \rho(\vec{r})v(\vec{r})d\vec{r} + J[\rho] + (T[\rho] - T_s[\rho]) + (V_{ee}[\rho] - J[\rho]) \quad \textbf{(2.19)}$$

The difference between the real kinetic energy and the one of the reference system, $T_c[\rho]=T[\rho]-T_s[\rho]$, together with the so-called electronic exchange-correlation term, $W_{XC}[\rho]=V_{ee}[\rho]-J[\rho]$, constitute the unknown exchange-correlation functional, $E_{XC}[\rho]=T_c[\rho]+W_{XC}[\rho]$. Eq. (2.19) can alternatively be written as

$$E[\rho] = T_s[\rho] + \int \rho(\vec{r})v(\vec{r})d\vec{r} + J[\rho] + E_{XC}[\rho] \quad \textbf{(2.20)}$$

We can use an expression for the Hamiltonian similar to (2.14) but by finding the definition of the effective potential $v_s(\vec{r})$ for the interacting system. In order to derive the expression of $v_s(\vec{r})$, we need to use Lagrange multipliers and take into account the N-representability condition. With the aim of minimizing the energy in eq. (2.20), the fundamental equation can be obtained as

$$\mu = \frac{\delta E[\rho]}{\delta \rho(\vec{r})} = v(\vec{r}) + \frac{\delta F_{HK}[\rho]}{\delta \rho(\vec{r})} \quad \textbf{(2.21)}$$

where μ is the chemical potential and $\frac{\delta F_{HK}[\rho]}{\delta \rho(\vec{r})}$ is defined as

$$\frac{\delta F_{HK}[\rho]}{\delta \rho(\vec{r})} = \frac{\delta T_s[\rho]}{\delta \rho(\vec{r})} + \frac{\delta J[\rho]}{\delta \rho(\vec{r})} + \frac{\delta E_{XC}[\rho]}{\delta \rho(\vec{r})} \quad \textbf{(2.22)}$$

The latter term is known as the exchange-correlation potential $v_{XC}[\rho]$,

$$v_{XC}[\rho] = \frac{\delta E_{XC}[\rho]}{\delta \rho[\vec{r}]} \quad \textbf{(2.23)}$$

and we finally arrive at the expression for the effective potential

$$v_s(\vec{r}) = v(\vec{r}) + \int \frac{\rho(\vec{r}_2)}{|\vec{r}_1 - \vec{r}_2|} d\vec{r}_2 + v_{XC}(\vec{r}) \quad \textbf{(2.24)}$$

The expression of the potential $v_s(\vec{r})$ includes the external potential $v(\vec{r})$, the classical electronic Coulomb repulsion $J[\rho] = \int \frac{\rho(\vec{r}_2)}{|\vec{r}_1 - \vec{r}_2|} d\vec{r}_2$ and the potential for exchange-correlation effects $v_{XC}(\vec{r})$.

The procedure is based on starting from an initial guess of orbitals, and a density is calculated. With the density and $v_s(\vec{r})$ the Kohn-Sham operator can be determined and by using eq. (2.16) a new set of other orbitals are obtained. This iterative process continues until a convergence for the density is achieved.

However, the exact analytical expression functional of the term $E_{xc}[\rho]$ is not known. Thus, although with DFT we could obtain an exact solution, the use of an approximate $E_{xc}[\rho]$ is a way of error for not knowing its exact definition. Because of this, some approximations have been developed to solve the problem, such as local density approximation (LDA) or the generalized gradient approximations (GGA).

2.1.4 DFT functionals

DFT has to deal with the difficulty of finding an expression for the $E_{XC}[\rho]$. There are many types of density functional methods that use different approximations for the exchange-correlation functional. Three families of them are explained below, relevant for the present work: Local Density Approximation (LDA), Generalized Gradient Approximation (GGA) and Hybrid functionals.

Local Density Approximation (LDA)

This is a simple approximation where $E_{XC}[\rho]$ depends only on the density at each point of the space. The model is based on a uniform electron gas which has a constant density. However, LDA functionals are known to underestimate the exchange energy by approximately 10%, they tend to produce too long bond distances and they are not appropriate for regions near the nucleus or for describing weak bonds.

The method is called Local Spin Density Approximation (LSDA) for open-shell systems, where σ and β densities are treated distinctly and both densities are minimized separately. Kinetic energy and the exchange one will depend only either on σ or β, but Coulomb repulsion and correlation term depends on both.

Generalized Gradient Approximation (GGA)

In order to improve LDA, one can introduce the dependence upon density gradients into the exchange-correlation functional. It is, taking into account the density in each point and also how it varies around them.

There are many GGA approximate functionals, but for the exchange part Becke's[59] (B88, exchange) is one of the most widely used. For the correlation part it can be mentioned the functional of Perdew[60] (P86, correlation), Perdew-Wang[61] (PW86, exchange and correlation) and the one by Lee-Yang-Parr[62] (LYP, correlation). BLYP,[59, 62] that combines B88 for the exchange and LYP for the correlation, is one of the functionals used in this thesis.

Hybrid functionals

On the basis of DFT, hybrid methods incorporate some characteristics from Hartree-Fock theory. They are a type of approximations for the exchange-correlation energy which combine a portion of the exact exchange from the Hartree-Fock-like formula (expressed with Kohn-Sham orbitals) with conventional LDA or GGA exchange and correlation functionals. Such hybrid approach can be justified by the formalism known as the *adiabatic connection*, by which the exchange-correlation energy is formally expressed as

$$E_{XC}[\rho] = \int_0^1 W_{XC}^{\lambda}[\rho] d\lambda \qquad \textbf{(2.25)}$$

where $W_{XC}^{\lambda}[\rho]$ stands for the exchange-correlation energy (excluding the kinetic energy term) of a system with the electron-electron interaction damped by a parameter λ**.** When λ=0 there is no electron-electron interaction in the system and when λ=1 the electrons interact. So the KS model and real systems are linked through this parameter λ. The Half and Half method introduced by Becke[63] proposed to express $W_{XC}^{\lambda}[\rho]$ with a linear dependence on λ. Hence, the integral of eq. (2.25) becomes

$$E_{XC}[\rho] = \frac{1}{2} W_{XC}^{\lambda=1}[\rho] + \frac{1}{2} W_{XC}^{\lambda=0}[\rho] \qquad \textbf{(2.26)}$$

Here, when λ=0, $W_{XC}^{0}[\rho]$ corresponds to the Hartree-Fock exchange energy, whereas $W_{XC}^{1}[\rho]$ is obtained using some known expressions for the exchange-correlation energy.

Another example of hybrid functional used in some calculations of this thesis is the widely used B3LYP functional proposed by Becke[64]

$$E_{XC}[\rho] = E_X^{LDA}[\rho] + a_0\left(E_X^{exact} - E_X^{LDA}[\rho]\right) + a_x\left(E_X^{B88}[\rho] - E_X^{LDA}[\rho]\right) + \\ + E_C^{VWN}[\rho] + a_c\left(E_C^{LYP}[\rho] - E_C^{VWN}[\rho]\right) \qquad \textbf{(2.27)}$$

which combines the exact Hartree-Fock exchange E_X^{exact}, the LDA and GGA (B88) exchange functionals and the LDA (VWN) and GGA (LYP) correlation functionals with three fitted parameters, with values a_0=0.20, a_x=0.72 and a_c=0.81.

2.1.5 Dispersion-corrected functionals

The aim of finding density functionals that correctly model van der Waals interactions is an important field of investigation nowadays. Being the weakest intermolecular forces, London dispersion attractive forces appear when the electrons of two adjacent molecules or atoms are redistributed, thus forming temporary dipoles. The amount of dispersion depends on the facility of the electrons to move, so greater dispersion is found for electrons that can polarize easier (when they are located far from the nucleus, for larger molecules). Hence, taking these forces into account is essential when dealing with systems with weak bonds, in order to obtain accurate results.

In some works of this thesis a dispersion correction known as DFT-D3(BJ)[65] has been added to the total energy. When starting with atomic fragments, dispersion correction is both inter and intramolecular. However, when dealing with molecules as fragments, it is only intermolecular.

The DFT-D3(BJ) correction is composed by the parametrization DFT-D3[66] and the BJ-damping proposed by Becke and Johnson.[67-69] Thus, DFT-D3(BJ) takes characteristics from both. The general formula for dispersion energy correction with the DFT-D3(BJ) method is

$$E_{disp}^{D3(BJ)} = -\frac{1}{2}\sum_{A\neq B} s_6 \frac{C_6^{AB}}{R_{AB}^6 + \left[f(R_{AB}^0)\right]^6} + s_8 \frac{C_8^{AB}}{R_{AB}^8 + \left[f(R_{AB}^0)\right]^8} \qquad \textbf{(2.28)}$$

with

$$f(R_{AB}^0) = a_1 R_{AB}^0 + a_2 \qquad \textbf{(2.29)}$$

where the sum runs over all pairs of atoms, and the fitted parameters a_2 and a_1 are introduced by a damping function making dispersion energy contribute as a constant in the total correlation energy for close atoms. In addition, s_6 is set to unity for hybrid functionals and GGA, and s_8 adjusts the dispersion correction to the short and medium range repulsive character of the exchange-correlation functional. Finally R_{AB} is the distance between atoms A and B, and the cut-off radius R_{AB}^0 introduced by the BJ-approach is obtained by

$$R_{AB}^0 = \sqrt{\frac{C_8^{AB}}{C_6^{AB}}} \qquad \textbf{(2.30)}$$

where C_n^{AB} (n=6,8) are the atom pairwise dispersion coefficients for six and eight-order terms (the latter are obtained by using recursion relations from C_6 ones). Thus, in short, this dispersion correction uses three free fit parameters for each density functional, namely s_8, a_1 and a_2.

The effect of dispersion correction is large when dealing with non-covalent interactions and D3(BJ) description has demonstrated to improve results better than DFT-D3.[65] To sum up, DFT-D3(BJ) is said[65] to be a consistent and theoretically adequate adjustment of DFT-D3. However, the accuracy is determined by the choice of the exchange-correlation functional. The shape of the damping function, if the global parameters are correctly adjusted, shows no important effect on results. Nevertheless, at short distances there is the advantage for BJ-scheme to have a good physical performance.

2.2 Hydrogen bond energy analysis

In this thesis we apply different ways of decomposing the total energy of the molecular systems under study, in order to better analyze the origin of hydrogen bond features. When using DFT in the framework of Kohn-Sham MO theory (2.1.3), the Energy Decomposition Analysis (EDA) is used. The treatment of two hydrogen bonded interacting molecules as fragments leads to a thorough study of the total interaction energy.

2.2.1 Energy decomposition analysis (EDA)

This energy decomposition analysis[38, 55, 70] is made by considering the two interacting molecules as fragments.

The overall stabilization energy Δ*E* between two fragments is first decomposed as

$$\Delta E = \Delta E_{prep} + \Delta E_{\text{int}} \qquad \textbf{(2.31)}$$

Two terms build Δ*E*. The first is the preparation energy ΔE_{prep}, which is defined as the amount of energy necessary to deform the individual molecules from their equilibrium structure to the geometry that they acquire after the interaction. Secondly, the interaction energy ΔE_{int} stands for the energy change when the prepared compounds are joined to form the final interacting structure. Then, a quantitative EDA can be further applied on this ΔE_{int} resulting in different contributions, namely electrostatic interaction, Pauli repulsion, orbital interactions and dispersion.[55, 71-75]

$$\Delta E_{\text{int}} = \Delta V_{elstat} + \Delta E_{Pauli} + \Delta E_{oi} + \Delta E_{disp} \qquad \textbf{(2.32)}$$

The first step of the EDA method is bringing the unperturbed fragment charge distributions from infinity to their final interacting positions. The energy change related to the superposition of fragment densities is ΔV_{elstat}, the classical electrostatic interaction between fragments which is normally attractive

for neutral systems. Secondly, a wave-function for the final compound is built by taking into account the antisymmetry and renormalization requirements, and so ΔE_{Pauli} comprises the destabilizing interactions between occupied orbitals and is responsible for steric repulsions. Finally, there is a relaxation of the system to its final ground state. Virtual orbitals mix with the occupied ones, a fact that is included into the term ΔE_{oi}. The orbital interaction ΔE_{oi} in any MO model, and also in Kohn-Sham theory, accounts for charge transfer (i.e., donor–acceptor interactions between occupied orbitals on one moiety with unoccupied orbitals of the other, including the HOMO-LUMO interactions) and polarization (empty/occupied orbital mixing on one fragment due to the presence of another fragment). The term ΔE_{disp} accounts for the dispersion corrections,[76-79] which includes the correction to the DFT energy (section 2.1).

At the same time, the orbital interaction energy can be further decomposed into the contributions from each irreducible representation Γ of the point group of the interacting system.[71-73] For example, for C_S symmetry it is decomposed into:

$$\Delta E_{oi} = \Delta E_{\sigma} + \Delta E_{\pi} \qquad \textbf{(2.33)}$$

In planar systems with a clear σ/π separation (such as the planar DNA bases) the symmetry partitioning in this approach gives interesting information.

Deletion of virtual orbitals

If the aim of the study is the analysis of one single HB in the presence of two that are in opposite directions, an analysis without the virtual orbitals on one of the monomers is used to prevent charge-transfer in one direction. This allows analyzing the strengths of the hydrogen bonds separately. For example, it is well-known[38] that, in the case of adenine-thymine (Figure 1.3) of DNA, two hydrogen bonds are taking place and an orbital analysis shows that σ occupied lone pairs of proton acceptor atoms of one base point towards (also overlap and give charge into) σ^*-acceptor unoccupied orbitals of the other base. When dealing with HB interactions between DNA base pairs, this process (see Figure 2.1 for a molecular orbital representation) is an important part of the orbital interaction ΔE_{oi} term of the ΔE_{int}.[38]

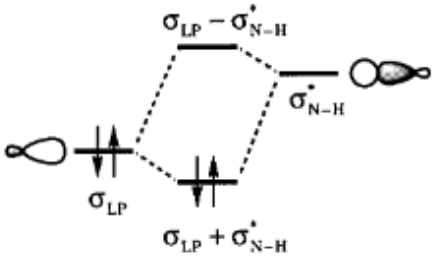

Figure 2.1: Donor-acceptor σ orbital interaction in the case of HB. Figure extracted from Ref.38.

The deletion of the σ virtuals (the ones that accept charge) of one base switches off the possible charge transfer between the donor and acceptor orbitals for that bond, and this allows studying the σ energetic orbital interaction contribution of the other hydrogen bond.

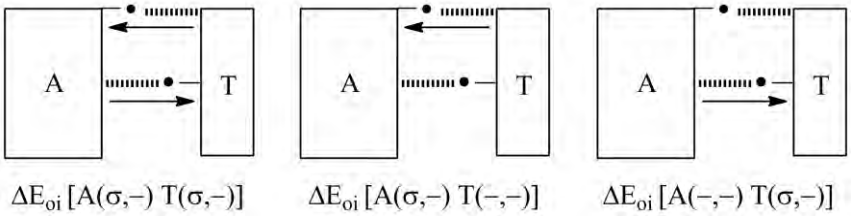

Figure 2.2: Representation of adenine-thymine HB studied when calculating ΔE_{oi} without virtuals. ΔE_{oi} [A(σ,-)T(σ,-)] means analyzing both HB without including π virtuals. In the case of ΔE_{oi} [A(σ,-)T(-,-)] also σ virtuals of thymine have been deleted and only the upper HB takes place.

In Figure 2.2, arrows stand for the direction of the charge donation and the discontinuous lines represent the HB. While ΔE_{oi} [A(σ,-)T(σ,-)] is the total σ energetic orbital interaction contribution calculated without π virtuals, deleting also the σ accepting orbitals of thymine, ΔE_{oi} [A(σ,-)T(-,-)], permits obtaining this energy only for the upper bond, and the same for the lower one if removing the virtuals of adenine.

2.3 Voronoi Deformation Density

Voronoi Deformation Density[80-81] (VDD) is a method used for the analysis of atomic charges, particularly useful when there is a charge reorganization, for instance due to bond formation of intermolecular interactions. Computation of the VDD atomic charges consists on integrating the deformation density in a particular atomic domain. This atomic space is the Voronoi polyhedron of the atom,[82] defined, for a given atom A, as the part of space limited by the bond midplanes on and perpendicular to all bond axes between nucleus A and its neighboring nuclei. Simply speaking, the Voronoi cell of an atom A gathers all points of space that are closer to the nucleus A than to any other nucleus.

This method is based on the numerical integral of the deformation density $\Delta\rho(\vec{r}) = \rho(\vec{r}) - \sum_B \rho_B(\vec{r})$, which is the change between the superposition of unperturbed atomic densities $\rho_B(\vec{r})$ of a fictitious promolecule (it doesn't have any chemical interactions and is associated with the situation in which all atoms are neutral) and $\rho(\vec{r})$, the electron density of the molecule after switching on the interaction between the atoms.

There is a straightforward interpretation to study the changes in densities. Having a region of space close to nucleus A, Q_A^{VDD} measures the amount of electronic charge that flows, due to interactions, out of (Q_A^{VDD} >0, charge decreases) or into (Q_A^{VDD} <0, charge increases) the Voronoi cell of atom A. The value

of Q_A^{VDD} depends on the reference density of the promolecule and the shape of the non-overlapping Voronoi cells,[83] and its definition is

$$Q_A^{VDD} = -\int_{\text{Voronoi cell of A}} \left(\rho(\vec{r}) - \sum_B \rho_B(\vec{r})\right) dr \qquad \textbf{(2.34)}$$

Thus, this directly measures the flow of electrons due to the formation of chemical bonds, going from one atom to another. This is the gain or loss of electrons in the Voronoi cell of an atom.

2.3.1 VDD. Working with fragments

If hydrogen bonds are considered, small charge redistributions take place because of the weak interactions between the monomers. This is the case of DNA,[38, 80] where each nucleobase is considered to be a fragment and the study is based on analyzing the charge rearrangement due to their interaction, especially for the front atoms, which are the ones that point toward the other base. Thus, calculating the difference between the atomic charge of one atom in the base pair $Q_{A,pair}^{VDD}$ and in the separate base $Q_{A,base}^{VDD}$ is not a good idea at least for the front interacting atoms. This is known as the front-atom problem.[38] The explanation is that the charge rearrangements due to the first process of bonding formation within individual bases, $Q_{A,base}^{VDD}$, are an order of magnitude larger than the ones resulting from hydrogen bonding, $Q_{A,pair}^{VDD}$. Both $Q_{A,pair}^{VDD}$ and $Q_{A,base}^{VDD}$ differ in molecular densities (ρ_{pair} and ρ_{base}), promolecules and the shape of the Voronoi cell. This last aspect is important since in an isolated base the Voronoi cell will extend to infinity in the direction where the other base is situated. But, when the base is forming a pair with another one, the Voronoi cell of the frontier atom is limited by the bond midplane perpendicular to the bond to the other base, dividing the bond in half. The effect of this change on the Voronoi cell is as important on the value of VDD charge as the small change on the densities from ρ_{base} to ρ_{pair}. Thus, the subtraction (2.35) is not useful.

$$\Delta Q_A^{VDD} = Q_{A,pair}^{VDD} - Q_{A,base}^{VDD} = -\int_{\substack{Voronoi\,cell\,of\\ A\,in\,pair}} \left(\rho_{pair}(\vec{r}) - \sum_{\substack{atoms\,in\\ pair}} \rho_C(\vec{r})\right) dr + \int_{\substack{Voronoi\,cell\,of\\ A\,in\,base}} \left(\rho_{base}(\vec{r}) - \sum_{\substack{atoms\,in\\ base}} \rho_B(\vec{r})\right) dr \qquad \textbf{(2.35)}$$

In order to solve this problem, one can consider the initial density to be the superposition of the densities of the bases and the final one the density of the pair.

$$\Delta Q_A^{VDD} = -\int_{\substack{Voronoi\,cell\\ of\ A\ in\ pair}} \left[\rho_{pair}(\vec{r}) - \rho_{base1}(\vec{r}) - \rho_{base2}(\vec{r})\right] dr \quad \textbf{(2.36)}$$

Thus, being both bases fragments of a total pair, we will obtain the charge flow due to the formation of HB (interactions between fragments and not just atoms).

Decomposition of VDD charges

Similarly to the energy, VDD charges can be also decomposed. Thus, two steps must be taken into account for the bond formation. The first is Pauli repulsion, corresponding to a wave function Ψ^0 that incorporates the antisymmetry and renormalization requirements for the product of the ground state wave functions of the two fragments. From it, $\rho^0_{complex}(\vec{r})$ can be obtained, where orbitals are orthogonal. Then there is the relaxation to achieve the ground state wave function of the complex thanks to the mixing of virtual orbitals (charge transfer and polarization). Knowing this, the deformation energy of the complex $\Delta\rho_{complex}$ can be divided into a Pauli-repulsion component and an orbital interaction one as follows

$$\Delta Q_{Pauli,A} = -\int_{\substack{Voronoi\,cell\\ of\ A\ in\ complex}} \left[\rho^0_{complex}(\vec{r}) - \sum_{subsystems}\rho_i(\vec{r})\right] dr \quad \textbf{(2.37)}$$

$$\Delta Q_{oi,A} = -\int_{\substack{Voronoi\,cell\\ of\ A\ in\ complex}} \left[\rho_{complex}(\vec{r}) - \rho^0_{complex}(\vec{r})\right] dr \quad \textbf{(2.38)}$$

where $\Delta Q_{Pauli,A}$ and $\Delta Q_{oi,A}$ are the Pauli-repulsion and orbital interaction contributions to charges, respectively. Here, $\rho^0_{complex}(\vec{r})$ corresponds to the density of the complex before taking place charge transfer and polarization, and $\rho_{complex}(\vec{r})$ after it. Finally, subsystems are the fragments that interact.

By excluding the virtual orbitals in the fragment calculation only the Pauli contribution of VDD charges is obtained. Then, the subtraction between the total VDD charges and the Pauli contribution to them results in the orbital interaction part of VDD charges. Moreover, each contribution can be decomposed into σ and π components in planar molecules (such as DNA pairs AT or GC). Following the nomenclature used at the beginning of the section 2.3.1 for the DNA example, such decomposition is expressed as

$$\Delta Q_A^{\Gamma} = -\int_{\substack{Voronoi\,cell\\ of\ A\ in\ pair}} \left[\rho^{\Gamma}_{pair}(\vec{r}) - \rho^{\Gamma}_{base1}(\vec{r}) - \rho^{\Gamma}_{base2}(\vec{r})\right] dr \quad \textbf{(2.39)}$$

where $\rho^{\Gamma}_{pair}(\vec{r})$ is the sum of the orbital densities of the occupied orbitals within the irreducible representation Γ for the pair studied and for each of the interacting bases it is $\rho^{\Gamma}_{base}(\vec{r})$.

2.4 Atoms in molecules (AIM)

In this section different ways to divide the 3D-space into atomic domains are presented. Two main groups will be shown. On one hand, Quantum Theory of Atoms In Molecules (QTAIM) introduced by Bader.[84] On the other hand, several fuzzy-atom schemes. In the case of QTAIM, these atomic divisions consist on assigning every point of the 3D-space to one atom, similarly to the Voronoi cells. For fuzzy-atom schemes, atomic weight functions in each point are constructed, their value depending on the contribution of that point of the space to each atom.

2.4.1 Quantum Theory of Atoms In Molecules (QTAIM)

QTAIM[84] provides both a real-space atomic portioning and a topological analysis of the electron density. Indeed, the molecular charge distribution is used to determine the boundaries.

Within QTAIM, the atoms within molecules are limited by zero-flux surface in the gradient electron field of the electron density. This condition can be expressed as

$$\nabla\rho(\vec{r})n(\vec{r}) = 0 \qquad \forall\vec{r} \in S(\vec{r}) \tag{2.40}$$

where $S(\vec{r})$ is the zero-flux surface that define the boundaries of the atom, perpendicularly to the unit vector $n(\vec{r})$, and $\nabla\rho(\vec{r})$ is the gradient of the density.

When it comes to perform a topological analysis of the electron density, its gradient gives information about the critical points (extreme points of density):

$$\nabla\rho(r_c) = 0 \tag{2.41}$$

In order to characterize the resulting stationary points of the density, the diagonalization for the Hessian matrix must be carried out. Then, principal axes are the eigenvectors and the eigenvalues represent the curvatures on the critical point. The critical points are expressed as (ω,σ), where the *rank* ω is the number of eigenvalues different from zero and the *signature* σ is the algebraic sum of the signs of the curvatures (+1 for a positive curvature and -1 otherwise). By following this notation, different types of stationary of *critical points* of the density are defined:

(3,-3) Attractor or Nuclear Critical Point: All the curvatures are negative and so it is a local maximum of $\rho(\vec{r})$. It usually corresponds to an atomic position, or close to it.

(3,-1) Bond Critical Point (bcp): Two negative curvatures and one positive. The density is a maximum on the critical point in the plane limited by two axes. Along the third axis, perpendicular to the plane, $\rho(\vec{r})$ is a minimum (connecting two atoms). Bcps are useful for studying the interaction between hydrogen bonded atoms.[85-87]

(3,+1) Ring Critical Point: Two positive curvatures and one negative. It is usually linked with the presence of a ring.

(3,+3) Cage Critical Point: Three positive curvatures and so a local minimum of ρ. It is found in a group of bonded atoms with an enclosed structure.

Some of the mentioned topological characteristics are represented in Figure 2.3 for the case of formic dimer.

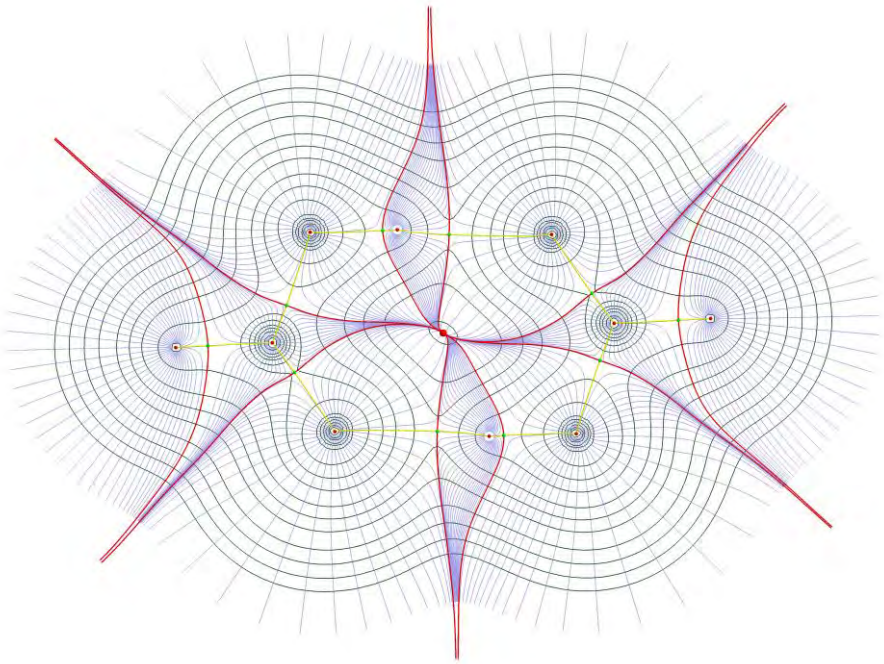

Figure 2.3: Topological analysis of the electron density of formic dimer. Small red points are density maximums (atoms). Big red point in the middle is a ring critical point. Points in green are bcp. Lines: gradient paths (blue), bond paths (light green), density contour lines (dark green), surfaces defining atoms in molecules (red).

Also, by looking at the Laplacian of the density $\nabla^2\rho$ (sum of the trace values of the density Hessian matrix of the density), one can obtain additional interesting information. Thus, for example, a negative value of it on the bcp, $\nabla^2\rho_{(bcp)} < 0$, is linked with a locally concentrated electronic charge and with a shared-shell interaction. Alternatively, if $\nabla^2\rho_{(bcp)} > 0$ there is a depletion of density, it indicates the presence of a closed-shell interaction.

A drawback of the QTAIM method is its high computational cost due to the cumbersome integration of the atomic domains and the exhaustive examination of the topology of the electron density.

2.4.2 Fuzzy-atom definitions

There are different methods of defining an atom in a molecule, being one of them fuzzy-atoms, which have the advantage of being computationally easier than QTAIM. For fuzzy-atom schemes, where atomic domains overlap to some extent, a weight function for each atom in each point of the space is used, which determines to which extent this point is part of each atom. It must be a positive function for each atom A and each point $\vec{r}$ of the space fulfilling

$$w_A(\vec{r}) > 0 \qquad \sum_A w_A(\vec{r}) = 1 \tag{2.42}$$

It is worth pointing out that if QTAIM was expressed with weight functions, as a point in space is part only of an atom, one would obtain $w_A(\vec{r}) = 1$ if $\vec{r}$ belongs to the atomic domain of atom A and $w_A(\vec{r}) = 0$ otherwise. For fuzzy-atoms, they are close to 1 in the vicinity of atom A and gradually tend to 0 when going further. Fuzzy-atoms definitions differ in the shape of these weight functions $w_A(\vec{r})$. Below there is a discussion of the form of the most relevant ones.

Becke atoms

The shape of Becke atoms[88] (the value of the atomic weights) comes from a set of atomic radii and a so-called stiffness parameter. Becke atoms are based on Voronoi cells (section 2.3) but the boundaries are not sharp, and the location of the interatomic plane is given by the ratio between the empirically introduced atomic radii of two atoms, which accounts for a relative size of the atomic basins. Since the method introduced fuzzy Voronoi cells, the position for the interatomic surface must be established between all pair of atoms, not only between those pairs of atoms whose Voronoi cells are in contact.

In order to obtain fuzzy Voronoi cells this scheme uses a polynomial function that shows a value of 1 on the atomic nucleus and decreases tending to 0 when going further. It is controlled by a stiffness parameter, k, related to the order of the polynomial, which determines the shape of the limiting profile of the atomic boundary (for a higher stiffness, polynomial decreases quicker and less overlapping atoms are obtained). The interatomic plane controls where the two polynomials associated to two atoms cross. Figure 2.4 shows the behavior of the weight function of A for a diatomic molecule AB where radius A is larger than B, and in the case of different stiffness parameters for the polynomic definition of atom A.

The drawback of the method is that a fixed covalent atomic radius is used for the same atoms independently of its chemical environment, so partial ionic character is not well accounted for.

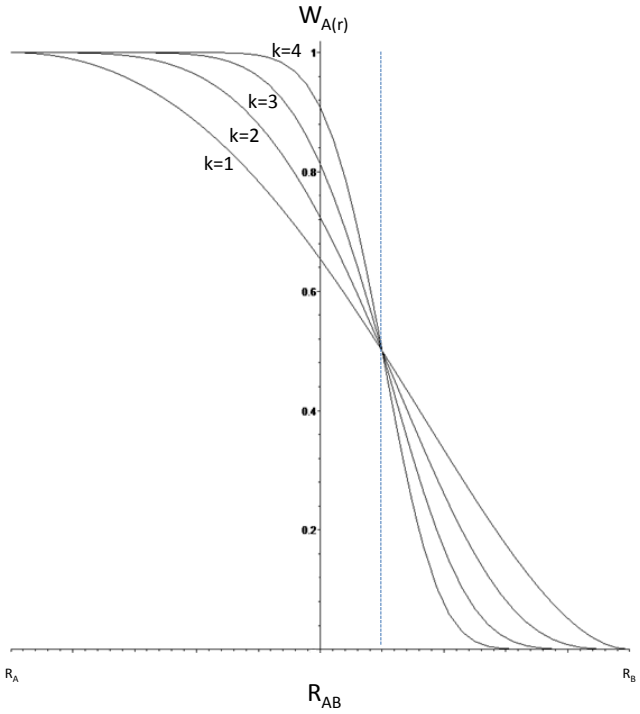

Figure 2.4: Representation of the weight function of A for a diatomic molecule AB, where radius A is larger than B. The blue vertical line is the location of the interatomic plane. Atom A is located on R_A ($W_A(r)=1$) and B on R_B ($W_A(r)=0$). X axis represents the distance between A and B (R_{AB}). *k* is the stiffness parameter, the order of the polynomial.

Becke-ρ

In order to solve the problem mentioned above, one can use Becke-ρ.[89] It is based on Becke scheme but by determixning the ratio of the atomic radii for a pair of chemically bonded atoms by taking into account the position of the minimum[90] of the total density along the internuclear axis. This will determine the position of the intersecting plane. Hence, the possible partial ionization of the atoms is better described. Becke-ρ cell boundaries are obtained as in Becke's atoms for non-bonded atoms or when two atoms are assumed to be too far to be 'neighbours'. In Becke-ρ scheme, some QTAIM ideas are included and the results for bond orders and electron populations are similar.[91]

Hirshfeld atoms

Hirshfeld atoms[92] are based on the use of promolecular densities. The weight of an atom A at a specific point of the space is defined as

$$w_A(\vec{r}) = \frac{\rho_A(\vec{r})}{\sum_B \rho_B(\vec{r})} \qquad \textbf{(2.43)}$$

where $\rho_A(\vec{r})$ is the promolecular density of an atom A, typically obtained from spherically averaging the density of the ground state for free atoms. The addition $\sum_B \rho_B(\vec{r})$ is the total promolecular density, the superposition of isolated atomic densities in the geometry of the molecule. The shape of the atoms

in the molecule depends on the promolecular state chosen for an atom (on their number of electrons, which will change if it is neutral or ionic). Thus, there is the same problem as in Becke atoms in the sense of having an initial promolecular density that it is always the same for a given atom type, regardless of its chemical environment.

Hirshfeld-iterative

An improvement to include partial ionization appears with the Hirshfeld-iterative method.[93-94] This problem is corrected thanks to a converging iterative process, where atomic promolecular densities that integrate to the same number of electrons as the ones that atoms have in the molecule are obtained. So the aim is to reach a promolecular density that integrates to the real atomic electronic population in the molecule, N_A, and not to the atomic number Z_A, as the original Hirshfeld scheme does.

The process is iterative. In the first iteration (i = 1), freely chosen atomic promolecular densities that integrate to N^{i-1}_A (usually $N^{i-1}_A = Z_A$) are used to obtain the atomic weights, with the Hirshfeld-type expression

$$w_A^{i-1}(\vec{r}) = \frac{\rho_A^{N_A^{i-1}}(\vec{r})}{\sum_B \rho_B^{N_B^{i-1}}(\vec{r})} \qquad \textbf{(2.44)}$$

The atomic populations are obtained simply as

$$N_A^i = \int w_A^{i-1}(\vec{r})\rho(\vec{r})d\vec{r} \qquad \textbf{(2.45)}$$

For the next iteration, atomic promolecular densities that integrate to N^i_A (usually fractional) are needed. They are defined as a linear combination of neutral and ionic free atom densities as

$$\rho_A^{N_A^i}(r) = \rho_A^{\mathrm{lint}(N_A^i)}(r)\left[\mathrm{uint}(N_A^i) - N_A^i\right] + \rho_A^{\mathrm{uint}(N_A^i)}(r)\left[N_A^i - \mathrm{lint}(N_A^i)\right] \qquad \textbf{(2.46)}$$

where lint(N^i_A) is the integer part of N^i_A and uint(N^i_A) the upper integer part. Then, a new set of atomic weight functions is obtained using eq. (2.44), and so on. The iterative process continues until the difference in the atomic populations between consecutive iterations is below a given threshold, namely

$$abs(N_A^i - N_A^{i-1}) < 0.001 \quad \forall A \qquad \textbf{(2.47)}$$

So Hirhsfeld-iterative takes into account the partial ionization of the atoms.[86]

2.5 Delocalization indices (DI)

Delocalization indices (DI) are popular bonding indicators. They give a quantitative information about the shared electrons between two atoms/fragments A and B,[95] i.e. about the degree to which electrons

in A are delocalized in B and vice versa. Not only is the bielectronic density needed to obtain delocalization indices, but also a definition for an atom in the molecule.

The delocalization index between two atoms A and B is defined as

$$\delta_{AB} = -\int_{\Omega_A}\int_{\Omega_B} \rho_{XC}(\vec{r}_1,\vec{r}_2)d\vec{r}_1 d\vec{r}_2 - \int_{\Omega_B}\int_{\Omega_A} \rho_{XC}(\vec{r}_1,\vec{r}_2)d\vec{r}_1 d\vec{r}_2 = -2\int_{\Omega_A}\int_{\Omega_B} \rho_{XC}(\vec{r}_1,\vec{r}_2)d\vec{r}_1 d\vec{r}_2 \quad \textbf{(2.48)}$$

where $\rho_{XC}(\vec{r}_1,\vec{r}_2)$ is the exchange-correlation density of eq. (2.9), and Ω_A indicates that the integration is performed over the domain of atom A. Hence, there is a double integration over atomic basins of the exchange-correlation density. If using DFT, the first-order density is in principle exact, but the bielectronic density is not. The usual approach is to invoke the Kohn-Sham wave function Ψ^{KS} of the non-interacting system to build an approximated exchange-correlation density. Thus, in the particular case of a closed-shell system described with KS-DFT, one can use eq. (2.9) in (2.48) to obtain

$$\delta_{AB} = 4\sum_{i,j}^{occ}\int_{\Omega_A}\phi_i^*(\vec{r}_1)\phi_j(\vec{r}_1)d\vec{r}_1\int_{\Omega_B}\phi_j^*(\vec{r}_2)\phi_i(\vec{r}_2)d\vec{r}_2 = 4\sum_{i,j}^{occ} S_{ij}^A S_{ji}^B \quad \textbf{(2.49)}$$

where S_{ij}^A and S_{ij}^B are the overlaps between occupied molecular orbitals *i* and *j* on the domains of atoms A and B, respectively.

In the fuzzy-atom framework, the delocalization index is obtained by introducing the atomic weight function, instead of the space-resctricted integrals of eq. (2.49), leading to the analogous expression

$$\delta_{AB} = 4\sum_{i,j}^{occ}\int w_A(\vec{r}_1)\phi_i^*(\vec{r}_1)\phi_j(\vec{r}_1)d\vec{r}_1\int w_B(\vec{r}_2)\phi_j^*(\vec{r}_2)\phi_i(\vec{r}_2)d\vec{r}_2 = 4\sum_{i,j}^{occ} S_{ij}^A S_{ji}^B \quad \textbf{(2.50)}$$

2.6 N-center index: I_{NG}

Several indices can be calculated to measure the electronic delocalization in a ring with π electrons, i.e. aromaticity. The one used in this thesis has been the normalized I_{ring},[96] known as I_{NG}.[97]

I_{ring}[96] was introduced as an index to quantify the multicentre electron delocalization among a set of atoms $R_n=(A_1,A_2,\ldots A_n)$ that are sequentially connected to form a particular n-member ring. It is defined as

$$I_{ring}(R_N) = \sum_{i_1,i_2,..i_n}^{occ} S_{i_1,i_2}(A_1)S_{i_2,i_3}(A_1)\ldots S_{i_n,i_1}(A_n) \quad \textbf{(2.51)}$$

It allows measuring the aromaticity and so a ring is considered to be more aromatic for a larger value of I_{ring}, as it means a larger simultaneous sharing of electrons among the atoms of the ring.[98] However, its values depend on the size of the ring, as the number of atoms that build it determine the number of

overlaps that constitute the expression for the I_{ring}. Consequently, it is known that a decrease in the values of this multicentre index occurs when the size of the ring increases.[98]

In order to be able to work with comparable electron delocalization measures when having rings with different sizes, I_{NG}[97] was defined as

$$I_{NG}(R_N) = \frac{\pi^2}{4}\frac{G(N_\pi)}{NN_\pi} I_{ring}(R_N)^{1/N} \qquad \textbf{(2.52)}$$

where *N* is the number of atoms that takes part of the ring, N_π is the number of π electrons involved and $G(N_\pi)$=1 for aromatic or $G(N_\pi)$=-3 for antiaromatic systems. These $G(N_\pi)$ values were introduced[98] for this index in order to be compared with the topological resonance energy per π electron (TREPE)[99] index. Thus, $G(N_\pi)$=1 can be chosen as a general way to study aromaticity.

When considering different ways of 3D-space partitioning of the atoms and I_{NG} is calculated, Hirshfeld and Hirshfeld-iterative (2.4.2) methods have been demonstrated[98] not to be reliable. For these mentioned methods some scaled aromatic values revealed that benzene was the less aromatic compound among the ones calculated, contrary to the expected results. Hence, Heyndrickx *et al.*[98] suggested using I_{NG} calculated with AIM definitions with a small or zero overlaps among the atomic domains. In this thesis different fuzzy-atom methods have been used[86] with the objective of knowing which of them behaves more similar to QTAIM (with no overlap among atomic domains) when dealing with hydrogen bonds. As it will be shown, it is the Becke-ρ scheme.

3. Objectives

The aim of this thesis is to shed more light on the concept of Resonance Assisted Hydrogen Bonds in systems that have two or more intermolecular hydrogen bonds and π electrons within their structure. It is known from theoretical and experimental work[26] that in these systems an extra stabilization (RAHB) occurs. Different computational tools have been applied in order to analyze, quantify and understand this possible gain of stability.

In chapter 4 some fuzzy-atoms schemes have been compared to QTAIM. The aim is to know which of them is the most similar to QTAIM and also shows a good description of the nature of hydrogen bonds at a much reduced computational cost. Delocalization indices on hydrogen bonds and the normalized n-center delocalization index I_{NG} have been chosen to establish a comparison between the behavior of the different schemes.

In chapter 5, our aim is to reach a further understanding of the interaction energy between complexes based on DNA base pairs, which interact with more than one hydrogen bond and form a *quasi*-ring, and finding out if π delocalization associated to RAHB is an important contribution to it. Pairwise and n-center electron delocalization indices have been used to study qualitatively the interaction energies.

In chapter 6, we want to determine if the π assistance to the hydrogen bonds of the base pairs adenine-thymine and some smaller mimics is exclusively due to aromaticity, or if the sp^2 hybridization of the proton-donor and acceptor atoms already accounts for the π charge delocalization. Linked with this, another objective is to analyze the reason of the strengthening of the hydrogen bonds in the sp^2 hybridized dimer.

Finally, in chapter 7, there is a study of the importance of π resonance in the guanine and cytosine monomers upon dimerization. The aim is to determine up till where the molecular skeleton of these monomers can be decreased without the hydrogen bond energy becoming weaker than in the natural Watson-Crick base pair GC.

4. A Fuzzy-Atom Analysis of Electron Delocalization On Hydrogen Bonds

4.1 Abstract

The extent of electron delocalization is quantified for set of cyclic complexes exhibiting two or more hydrogen bonds (HB). In particular, the delocalization indices (DI) between the atoms directly involved in the HB, and the I_{NG} (normalized n-center delocalization indices) have been evaluated using several fuzzy-atom schemes, namely Becke, Becke-ρ, Hirshfeld and Hirshfeld-Iterative. The results have been compared with the widely used Quantum Theory of Atoms in Molecules (QTAIM) atomic definition. The DI values are found to correlate very well with geometrical or topological descriptors widely used in the literature to characterize HB systems. Among all fuzzy-atom methods, the ones that can better accommodate the different partial ionic character of the bonds perform particularly well. The best performing fuzzy-atom scheme for both pairwise and n-center electron delocalization is found to be the Becke-ρ method, for which similar results to QTAIM model are obtained with a much reduced computational cost. These results open up a wide range of applications of such electron delocalization descriptors based on fuzzy-atoms for non-covalent interactions in more complex and larger systems.

4.2 Introduction

Hydrogen bonds (HB) are of utmost importance in chemistry and biology. Their theoretical study has received a great deal of attention during the last decades,[1-4] leading to a very recent IUPAC recommendation for its proper definition.[5-7] Hydrogen bonds and intermolecular interactions in general, can be classified according to energetic, geometrical or topological criteria. Nowadays, topological analysis is one of the most useful tools to characterize intra- and intermolecular interactions. It borrows many elements from the so-called Quantum Theory of Atoms in Molecules (QTAIM).[8] For instance, the topological analysis of the electron density, $\rho(\vec{r})$, in the intermolecular region yields a number of descriptors at the so-called bond critical points (bcp) of the density, such as the value of the electron density, its laplacian, and the principal curvatures, to name a few.

One can find in the literature many applications of QTAIM topological analysis devoted to hydrogen bonding systems.[9-13] A very complete study from weak to strong hydrogen bonds was carried out by Espinosa *et al.*,[9] who performed a comprehensive analysis of the topology and local energetic properties of $\rho(\vec{r})$ in the intermolecular region. Koch and Popelier[13] proposed a set of topological criteria that a bond must fulfil to be considered a hydrogen bond. Weinhold *et al.*[14] suggested that the topological

criteria should be complemented with additional geometrical and energetic parameters. In a very recent paper, Lane *et al.*[15] have questioned the mere use of local descriptors and properties associated to the bcp. They have used the NCI index (index of non-covalent interactions) to show that the existence of a bcp is not a necessary condition in order to have a hydrogen bonding interaction.

In this context, the electron delocalization indices (DI) are among the most popular bonding indicators. The delocalization index between atoms *A* and *B*, $\delta(A,B)$, is obtained by double integration of the exchange-correlation density, $\rho_{XC}(\vec{r}_1,\vec{r}_2)\rho_{xc}(\overrightarrow{r_1},\overrightarrow{r_2})$, over their respective atomic domains Ω_A and Ω_B as

$$\delta(A,B) = -2\int_{\Omega_A}\int_{\Omega_B}\rho_{XC}(\vec{r}_1,\vec{r}_2)d\vec{r}_1 d\vec{r}_2 \qquad \textbf{(4.1)}$$

In the particular case of a single-determinant closed-shell wave function, the delocalization index can be expressed solely in terms of the elements of the atomic overlap matrices **S**(A) in the molecular orbital basis

$$\delta(A,B) = 4\sum_{i,j}^{occ} S_{ij}(A)S_{ji}(B) \qquad \textbf{(4.2)}$$

where the summation runs over all doubly-occupied molecular orbitals.

It has been demonstrated that DI are a very useful tool to unravel the electronic structure of molecular systems.[16] They have been also used to study changes on the electronic distribution upon chemical processes.[17,18] For the particular case of intermolecular interactions, the QTAIM theory were used in an electron-pair characterization of hydrogen bonding in terms of the number of electrons shared between the atoms involved in the HB.[17,19,16] Non-conventional HB such as dihydrogen bonded complexes have also been characterized using DI.[19]

On the other hand, the strength of the HB interaction can be enhanced when the H-donor and H-acceptor are connected by a π-delocalized system. This phenomenon can be observed for hydrogen-bonded systems involving carboxylic acids or amides, as well as DNA bases.[20,21] Gilli *et al.* referred to it as resonance-assisted hydrogen bonds (RAHB).[22-24] Some authors have criticized this interpretation, concluding that the main contribution to the extra stabilization comes from a shorter distance between hydrogen donor and acceptor.[25,26] Very recently, Góra *et al.*[20] have analyzed a set of RAHB, concluding that charge-delocalization is the main contribution to the enhancement of the intermolecular HB interaction. Unfortunately, different conclusions were obtained for intramolecular RAHB interactions. In a series of o-hydroxyaryl ketones, where an intramolecular RAHB can be formed, the stabilization energy upon HB formation was shown to exhibit good correlation with the DI between the proton and

proton-acceptor atoms.[27-29] Thus, the electron delocalization induced when an HB leads to the formation of a ring is closely related to the strength of the HB.

In fact, the electronic delocalization in rings involving π electrons is one of the key aspects of aromaticity. Several indices measuring cyclic electron delocalization have been proposed to quantify global and local aromaticity in molecules.[30-32] For instance, Giambiagi introduced[33] long ago an index that measures the n-center electron delocalization among a set of atoms $\mathrm{R_n} = \{\mathrm{A_1}, \mathrm{A_2}, .. \mathrm{A_n}\}$ that are sequentially connected to form a particular n-member ring. The so-called I_{Ring} index is defined as

$$I_{ring}(R_n) = \sum_{i_1, i_2, \ldots i_n}^{occ} S_{i_1 i_2}(A_1) S_{i_2 i_3}(A_2) \ldots S_{i_n i_1}(A_n) \qquad \textbf{(4.3)}$$

where the summation runs over all occupied MOs.

Both the I_{ring} and the more involved MCI index[34] (the latter considers all permutations of the elements of the R_n set in eq. (4.3)) have shown to give similar performance for the quantification of ring aromaticity of a general set of heterocyclic compounds. However, the value of these indices is strongly ring-size dependent, which would introduce difficulties when comparing cyclic electron delocalization in intermolecular complexes that lead to the formation of rings of different size. Matito *et al.* recently introduced a renormalization[30] that accounts for the ring-size dependence of the n-center delocalization indices using both the number of π electrons and the number of atoms involved in the ring. The I_{NG} index for aromatic systems is defined as

$$I_{NG} = \frac{\pi^2}{4} \frac{1}{n N_\pi} I_{ring}(R_n)^{1/n} \qquad \textbf{(4.4)}$$

where the N_π is the number of π electrons of the n-member ring. In this work we will consider only properly normalized I_{NG} indexes.

In the QTAIM framework, the atomic boundaries are determined from the zero-flux surface conditions of the gradient of the one-electron density. The required numerical integrations over the atomic domains can be both costly and cumbersome from a computational point of view, particularly for large systems. A more efficient alternative to QTAIM can be provided in the framework of the fuzzy-atoms. The fuzzy atomic domains have no strict boundaries but are overlapping to some extent. This makes the numerical integrations over the atomic domains much more efficient computationally speaking.

Several authors have explored over the last years the use of different fuzzy-atom definitions to characterize electron delocalization, using both DI and n-center electron delocalization indices such as I_{ring} or MCI. Matito *et al.* tested the performance of the DI computed for a large set of five-member ring systems using a fuzzy-atom scheme. Aromaticity indices calculated using fuzzy-atom DI exhibited very good performance for a set of polycyclic aromatic hydrocarbons.[31] Recently Heyndrickx *et al.*[35] carried

out an exhaustive analysis of the performance of different atomic definitions for the calculation of several electron delocalization descriptors. It was concluded that, whereas all methods performed well for DI between bonded atoms, significant discrepancies between some fuzzy-atom schemes and QTAIM were observed for non-bonded interactions. These differences ultimately lead to changes in the trends of the I_{ring} and MCI aromaticity indices.

Different studies can be found in the literature using n-center delocalization indices to characterize RAHB systems. In particular, Lenain *et al.* have used several of them to demonstrate the validity of the resonance model for different intra- and intermolecular RAHB.[36,37] Also, Palusiak *et al.* analyzed the interplay between electron delocalization within the *quasi*-ring and its hydrogen bond strengths.[28,29]

Whether or not the fuzzy-atom schemes perform equally well compared to QTAIM for hydrogen bonding interactions is still an open question. It is of particular interest to test their performance in HB complexes that lead to the formation of *quasi*-rings, for which the I_{NG} index can also be computed. This is the main goal of this work.

4.3 Theoretical methods

The most different fuzzy-atom schemes can be described in a common framework by introducing a non-negative weight function $w_A(\vec{r})$ for each atom *A* and each point $\vec{r}$ of the physical space, satisfying the requirement $\sum_A w_A(\vec{r}) = 1$. The value of $w_A(\vec{r})$ is expected to be large inside the atom *A* (close to 1 in the vicinity of the nucleus) and quickly decrease to zero outside. Note that the same general framework can be used in the special case of QTAIM, for which $w_A(\vec{r}) = 1$ for points inside the atomic domain of *A* and $w_A(\vec{r}) = 0$ outside of it.

These atomic weight functions can be derived from several atomic definitions within the fuzzy-atom framework. In the past, we have made use of the simplest Becke's atoms[38] to show how several quantities such as bond orders, overlap populations, energy components or local spins can be retrieved in the general framework of fuzzy-atoms. The shape of such Becke atoms is determined by a so-called "stiffness parameter" and a set of fixed atomic radii that define the relative size of the atomic basins (more precisely, the position of the plane that intersects the interatomic axis). One can also use the position of the minimum of the total density along the internuclear axis for each pair of atoms[39] to determine the position of that intersecting plane. Such a scheme, referred to as Becke-ρ in Ref.40, can be viewed as an efficient adaptation of some of the ideas of Bader's QTAIM.

A different way to retrieve the atomic weights using promolecular densities was first proposed by Hirshfeld[41] many years ago. Recently, the Hirshfeld-iterative approach,[42,43] improving over classical Hirshfeld's, has been introduced. In both schemes, the atomic weight of atom *A* at a given point of the space is determined by the ratio

$$w_A(\vec{r}) = \frac{\rho_A^0(\vec{r})}{\sum_B \rho_B^0(\vec{r})} \quad \textbf{(4.5)}$$

where $\rho_A^0(\vec{r})$ represents a promolecular density of the atom *A*, typically obtained from spherically-averaged free atom calculations. In the classical Hirshfeld, the resulting shape of the atoms in the molecule is strongly dependent on the choice of the promolecular state of the atoms, in particular their number of electrons. The improved Hirshfeld-iterative scheme corrects this problem through an iterative process to obtain promolecular atomic densities that integrate to the same (usually fractional) number of electrons as do the atoms within the molecule. In this work we have made use of all fuzzy-atom definitions mentioned above, as well as QTAIM.

All monomers and dimers considered in this study have been optimized at the nonlocal three-parameter hybrid B3LYP level of theory.[44] The 6-311++G(d,p) basis set was chosen for being one of the most widely used basis sets used in the study of medium and large sized hydrogen bonded systems, and for yielding a very small BSSE, with Counterpoise-corrected values comparable to those of the larger 6-311++G(3df,2pd) basis set.[45] Vibrational analysis of optimized structures showed that, in general, the structures are minima of the potential energy surface. Some of them do exhibit an imaginary frequency due to the planarity imposed to the systems (see Table S1, p.119). All calculations were carried out with the Gaussian 03 package.[46] Bond critical points for all complexes were characterized using the AIM2000 program,[47] while DI and I_{NG} were obtained using APOST-3D[48] and ESI-3D[49] programs, respectively. The accuracy of the numerical integrations of the different fuzzy-atoms schemes was thoroughly tested. The results reported here have been obtained using atomic grids consisting of 60 radial and 266 angular points.

4.4 Results

Our set consists of 59 intermolecular complexes, from which a total of 89 different hydrogen bonds were formed. These were grouped into three types depending upon the donor and acceptor atoms, namely OH···O, NH···O and NH···N. The sample was based on dimers that show some analogy to the Watson Crick pairs, that is extra rings are formed upon HB formation. Apart from the guanine-cytosine (GC) and adenine-thymine (AT) pairs, Figure 4.1 shows all monomers that have been considered in this study as building blocks of the cyclic hydrogen bonded dimers.

In the case of formamide (FA), formamidine (FI) and formic acid (FO), different substituents have been considered to incorporate chemical diversity on the set. All dimers have been calculated ensuring C_{2h} symmetry, while the rest of the mixed complexes belong to the C_s point group. All structural data can be found in the Supporting Information (p.119) (Tables S1-S2), as well as the linear correlation parameters for all Figures (Tables S3-S5).

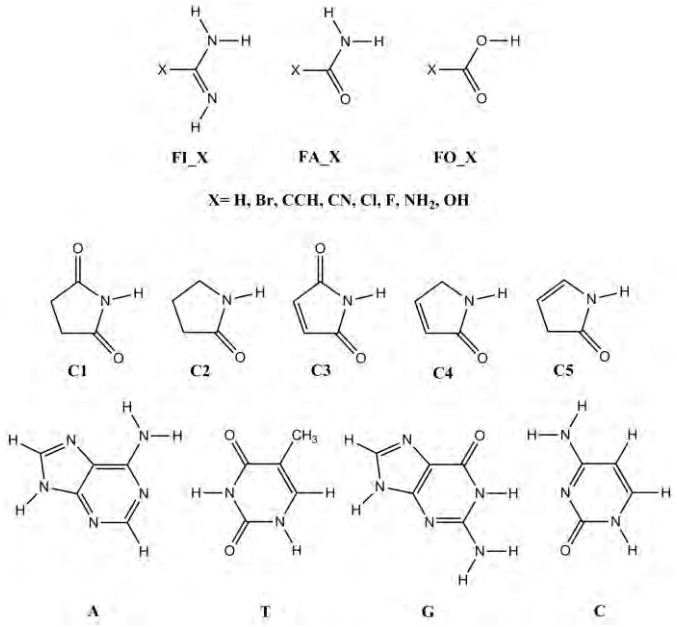

Figure 4.1: Monomers considered in the simple set, including a number of different substituents (X) for formamide (FA), formamidine (FI) and formic acid (FO).

First of all, we will analyze the influence of the different 3D-space atomic definitions upon pairwise DI values. In the second part, the same analysis will be carried out for the I_{NG} cyclic delocalization indices associated with the *quasi*-rings formed upon HB formation.

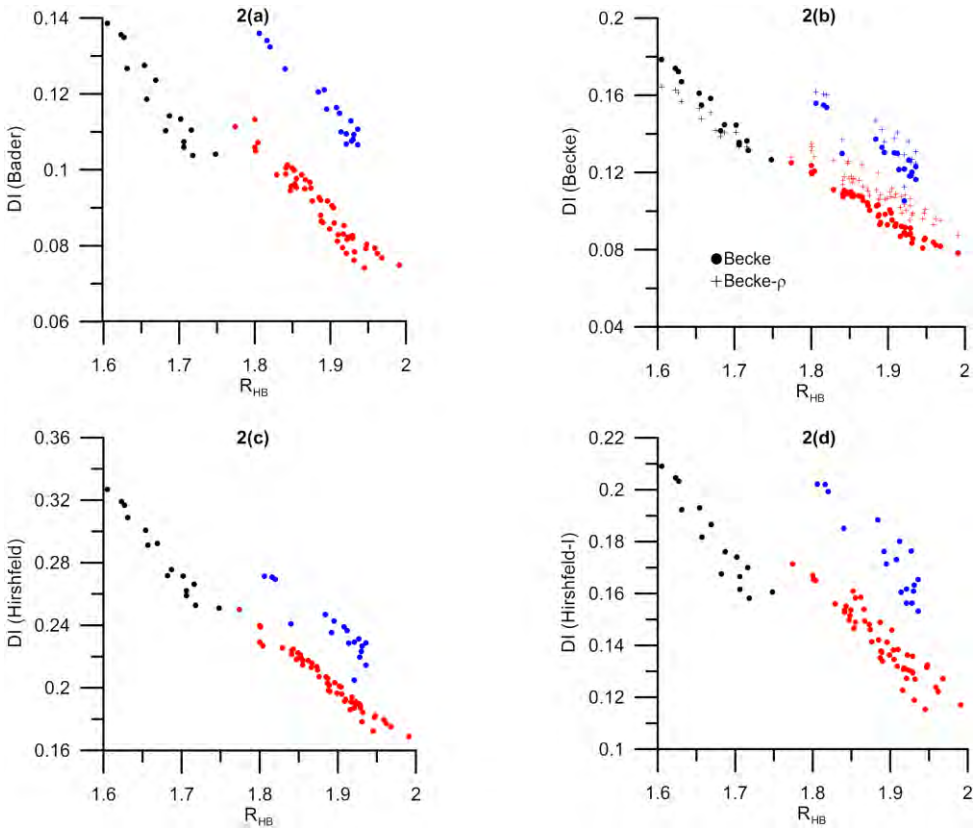

Figure 4.2: DI versus HB distances R_{HB} (Å) for QTAIM (a), Becke and Becke-ρ (b), Hirshfeld (c) and Hirshfeld-Iterative (d) atomic definitions. OH···O (black), NH···O (red), and NH···N (blue).

In Figure 4.2 the DI between the H and H-acceptor atoms for all HB are represented in front of the respective HB distances. The DI have been obtained with different fuzzy-atom definitions, namely Becke (DI Becke), Becke-ρ (DI Becke-ρ), Hirshfeld (DI Hirshfeld) and Hirshfeld-Iterative (DI Hirshfeld-I), as well as in the framework of QTAIM.

As mentioned above, all hydrogen bonds of the set can be classified according to the nature of the proton donor and/or acceptor as OH···O, NH···O and NH···N type. In a previous study,[19] a linear relationship was established between the HB distance at equilibrium geometries (distances between the H atom and the H-acceptor atom), RHB, and the corresponding DI for a set of hydrogen-bonded complexes studied in the framework of QTAIM. Different correlations were obtained depending on the nature of the proton donor and acceptor atoms. In the present study similar linear correlations are obtained for each bond type for all fuzzy-atom definitions used. The respective R^2 values range from 0.705 to 0.954 (see Table S3, p.119). General trends for both QTAIM (Figure 4.2a) and fuzzy-atom (Figure 4.2b, Figure 4.2c and Figure 4.2d) approaches are comparable. For instance, for the same RHB distances, NH···O (red) interactions show systematically lower DI values than NH···N ones (blue).

In QTAIM the slopes for the linear regression of the data corresponding to the three different bond-types is very similar. The clear separation between the curves is basically due to the different values of the y-intercepts. This feature is apparently best captured by the Hirshfeld-Iterative method (see Figure 4.2d). However, both the slopes and y-intercepts (and hence the DI values) are significantly larger than in QTAIM. Becke-ρ yield similar overall trends, and also a much better agreement with QTAIM DI values. On the other hand, both Hirshfeld (Figure 4.2c) and Becke (Figure 4.2b, circles) DI are not affected by the nature of the proton donor. Very similar linear correlation parameters are obtained for the OH···O and NH···O bond types.

It is worth mentioning the fundamental differences between the simplest Becke and the Becke-ρ schemes. In the former, the relative size of each pair of bonded atoms is given by a fixed set of atomic radii, whereas in the later it is established by the position of the bcp of the density between the two atoms. Thus, the partial ionic character of the bonds is not captured by the Becke approach, as the same atoms are treated on equal footing in different chemical environments. Similar argument holds for the Hirshfeld approach. On the contrary, the iterative version does permit larger atomic polarizations. The observed differences between bond-types in QTAIM essentially lie on the different relative atomic sizes of the atoms, and this is best captured by Hirshfeld-Iterative or Becke-ρ schemes.

On the other hand, the value of the electron density at the bcp (ρ_{bcp}) has also been found to be a good descriptor for HB systems. One can find many studies where it is demonstrated that ρ_{bcp} correlates quite well with hydrogen bond strength.[9,10,50,51,14] In Figure 4.3 the DI associated to the HB are represented in front of the respective ρ_{bcp} values. QTAIM DI (Figure 4.3a) exhibit an excellent linear correlation with the ρ_{bcp} values. Again, the differences in the *y*-intercept are responsible for the clustering of the data associated to each bond-type. For a given ρ_{bcp} value the NH···N bonds tend to

show the highest DI values, followed by the NH···O ones. The OH···O bonds exhibit the lowest *y*-intercept but also larger values of DI, as the respective ρ_{bcp} values are significantly larger than for the NH···O contacts. The Hirshfeld-Iterative method (Figure 3d) performs similarly, but the correlation is significantly worst, particularly for the NH···N bonds.

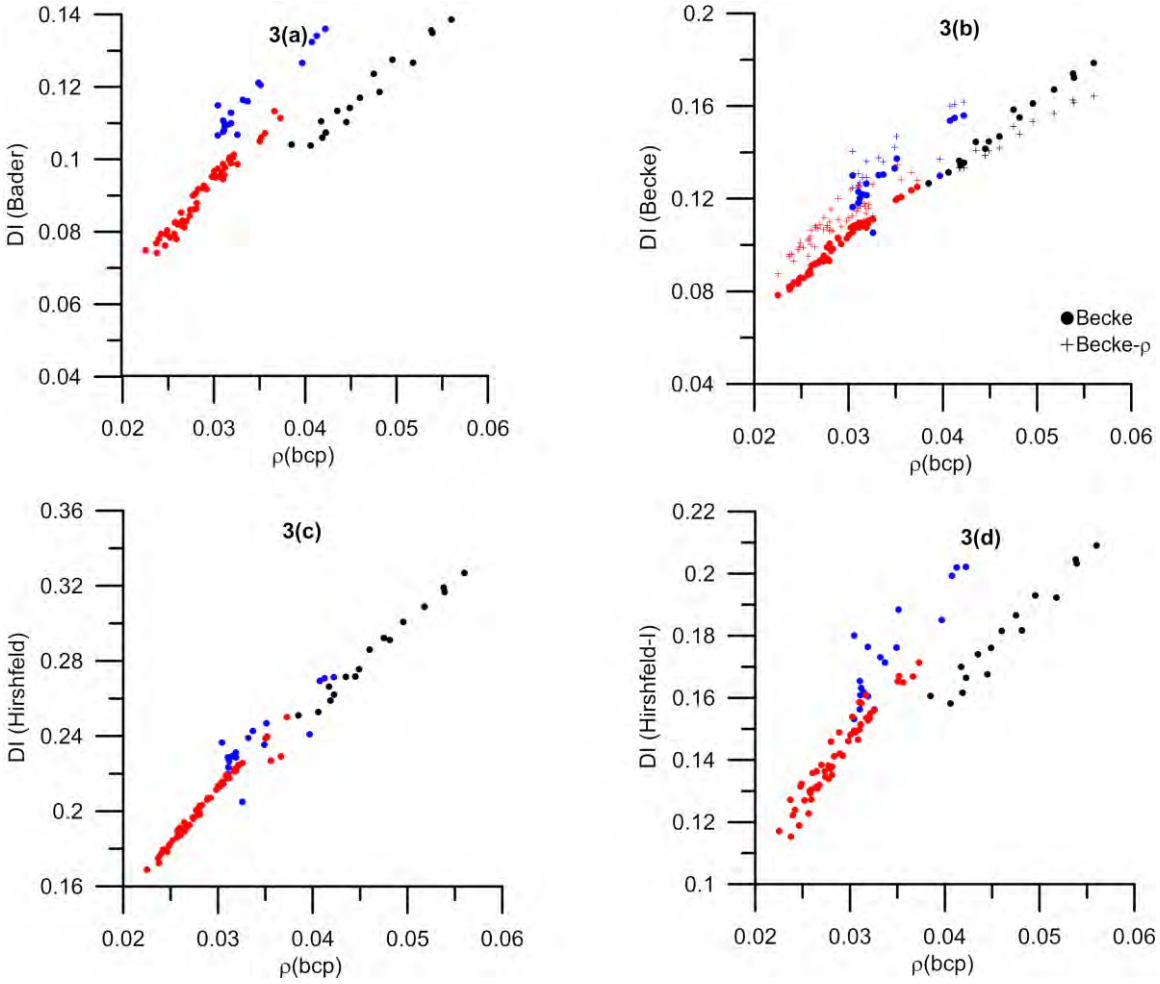

Figure 4.3: DI versus densities at the bcp for QTAIM (a), Becke and Becke-ρ (b), Hirshfeld (c) and Hirshfeld-Iterative (d) atomic definitions. OH···O (black), NH···O (red), and NH···N (blue).

Remarkably, in the Hirshfeld method (Figure 4.3c) the correlation between the DI and the ρ_{bcp} values is essentially the same for all bond types, whereas simplest Becke's (Figure 4.3b) slightly differentiates between proton acceptor atoms. Again, the Becke-ρ method performs very similar to QTAIM.

To conclude this part of the analysis, in Figure 4.4 we depict a direct comparison of the DI values obtained for QTAIM and the different fuzzy-atom approaches.

The same colour code is used to differentiate between HB types. The fuzzy-atom DI values are systematically higher than the QTAIM ones. All data points lie above the *y=x* line represented on Figure 4.4. Similar behaviour was observed for the DI involving atoms not directly bonded in Ref.35.

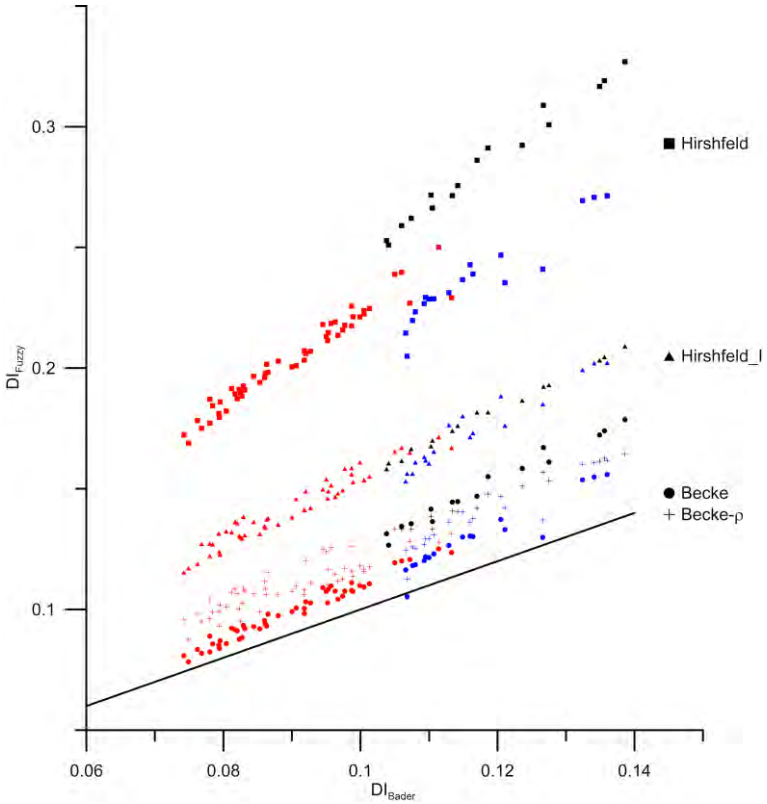

Figure 4.4: Fuzzy-atom versus QTAIM DI for the set of hydrogen bonds. OH···O (black), NH···O (red), and NH···N (blue). The *y=x* line is also represented.

Among all methods, both Becke and Becke-ρ ones exhibit the smaller absolute deviations with respect to the QTAIM values. The correlation between QTAIM and Hirshfeld-Iterative is excellent for all bond types, but the actual DI values are somewhat overestimated. In the case of Hirshfeld, DI are almost twice as large as the QTAIM ones and the correlation significantly depends on the bond-type, meaning that the agreement between the DI values depends upon the nature of the atoms involved. This clearly illustrates fundamental differences between the QTAIM and those fuzzy-atom approaches that cannot properly describe the partial ionic character of the bonds, namely, simplest Becke and especially Hirshfeld.

We have just seen how the DI values obtained with the different fuzzy-atom schemes correlate with other geometrical and topological descriptors that have been used in the past. Equilibrium distances and electron density properties are ultimately governed by electron distribution reorganization upon hydrogen bond formation. The pairwise DI between the atoms involved in the HB are able to capture the essential features of the electronic distribution.

Of course these correlations are only legitimate for equilibrium structures, as in general the DI monotonically decrease with the interatomic distance away from equilibrium (with some singular exceptions).[18,40]

As mentioned above, our test set is based on dimers that are able to form two or more HB between them, so that one or more *quasi*-rings appear upon formation of the complex. It was previously suggested[28] that an enhanced electron delocalization within this new *quasi*-ring may be a signature of

the strength of the interaction in the complex. Since the *quasi*-rings of the different complexes can exhibit different number of π-electrons and different number of atoms involved in the ring, a normalized version of the I_{ring} cyclic delocalization index such as the I_{NG} is preferred.

Heyndrickx *et al.*[35] already found that n-center delocalization indices such as I_{ring} and MCI were more atomic-partitioning dependent than the simplest pairwise DI values between bonded atoms. The main reason is the accumulative effect of small differences on the contributions involving nonbonded atoms in the rather complex expressions such as eq. (4.3). From their study, based on a number of aromatic compounds of different ring sizes, it was concluded that the n-center delocalization indices should be better calculated using atomic domains with minimal or zero overlap, such as QTAIM. In the *quasi*-rings we consider here the distances between the atoms involved are in general larger than in molecular aromatic systems. Thus, one could expect that the deviations of the nonbonded contributions may have a lesser influence on the overall values for these indices.

Figure 4.5 represents the I_{NG} values calculated using QTAIM and the different fuzzy-atom approaches. The *y=x* curve is also plotted for better comparison.

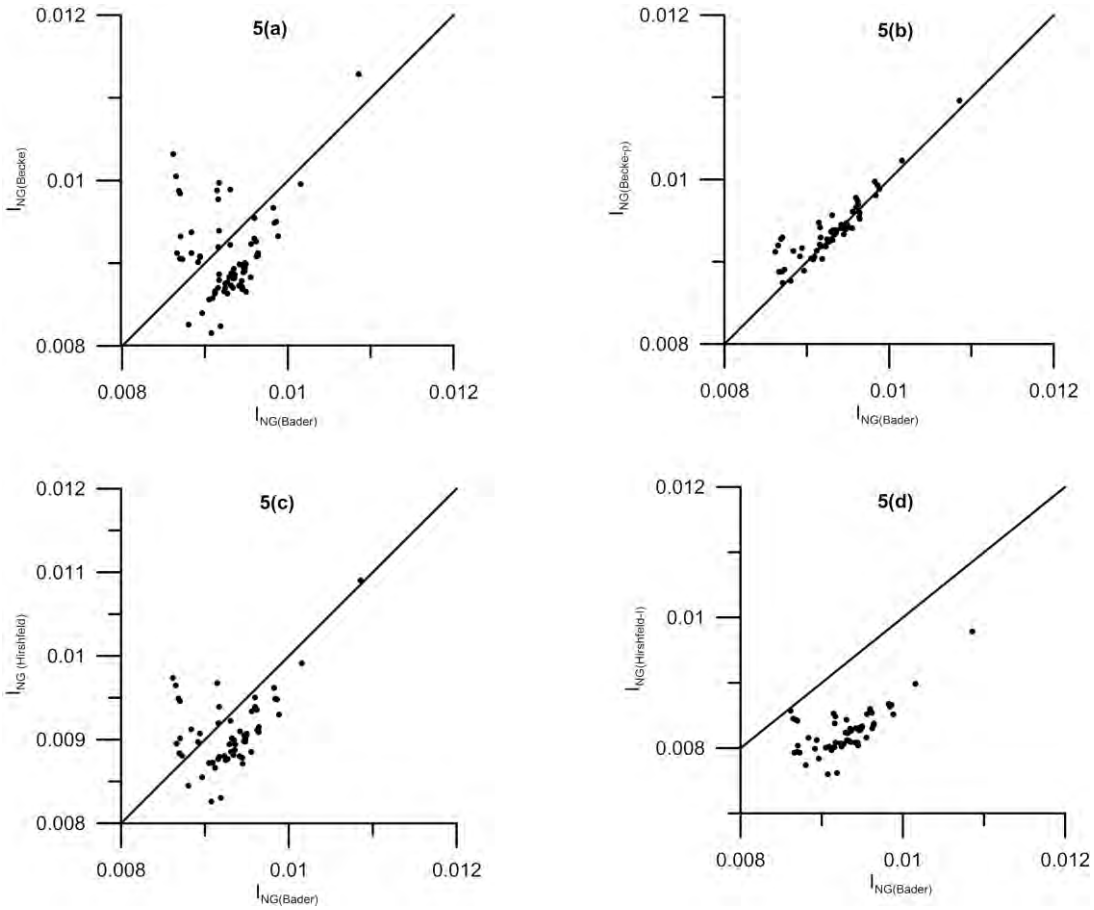

Figure 4.5: Fuzzy-atom versus QTAIM I_{NG} values for the *quasi*-rings.

Contrary to the analysis of the DI values, in the case of the I_{NG} index there is a significant lack of correlation between the QTAIM and fuzzy-atom values, except for Becke-ρ. For Becke and Hirshfeld

schemes, the I_{NG} values can be both underestimated or overestimated with respect to QTAIM, with no significant correlation. With Hirshfeld-Iterative the I_{NG} values are systematically smaller. Moreover, except for the two rightmost data points on Figure 4.5d, the I_{NG} values calculated with this method barely change from one complex to another, which leads to a rather poor correlation coefficient of the data (r^2=0.45). Among all fuzzy-atom schemes, Becke-ρ shows once again much better performance. In some cases, particularly involving formic acid derivatives (FO_X on Figure 4.1), the I_{NG} values obtained with Becke-ρ are slightly overestimated with respect to QTAIM. These are the group of data points with low I_{NG} values that lay over the *y=x* line in Figure 4.5b. There is no straightforward relationship between the I_{NG} values and the DI between the atom pairs involved in the *quasi*-ring. Nevertheless, for these systems we have observed that the QTAIM and Becke-ρ DI values involving the O-H intramolecular bonds differ significantly. In fact, the corresponding bcp between these two atoms appears at a very short distance to the H atom, beyond the maximum shift of the fuzzy interatomic boundary that the Becke-ρ scheme allows.[52] In any case, the data points are still quite close to the *y=x* line, and the overall correlation is also very good (r^2=0.83).

4.5 Conclusions

To summarize, our analysis shows good correlations in general between the DI values obtained in the framework of fuzzy-atom*s* and other geometrical or topological descriptors used in the literature for the particular case of hydrogen bonded complexes. Direct comparison with QTAIM DI values also indicates that the methods that can better accommodate the different partial ionic character of the bonds outperform simpler fuzzy-atom approaches such as Becke's and Hirshfeld. In the case of the I_{NG} index the differences with respect to QTAIM are somewhat larger.

It is straightforward to see that the Becke-ρ method is the best performing scheme at reproducing the QTAIM results for both pairwise DI and especially the I_{NG} n-center indices. Its simplicity and reduced computational cost compared to the more involved QTAIM integrations allow extending studies to larger systems where hydrogen bonds play an important role.

4.6 References

1. Grabowski, S. *Hydrogen Bonding-New Insights*. Springer: Dordrecht, The Netherlands, **2006**.
2. Jeffrey, G. A. *An Introduction to Hydrogen Bonding*. Oxford University Press: New York, **1997**.
3. *Molecular Interactions: From van der Waals to Strongly Bound Complexes.* Scheiner, S., Ed.; Wiley & Sons: Chichester, U.K., **1997**.
4. Steiner, T. *Angew. Chem., Int. Ed.* **2002**, *41*, 48-76.
5. Arunan, E.; Desiraju, G. R.; Klein, R. A.; Sadlej, J.; Scheiner, S.; Alkorta, I.; Clary, D. C.; Crabtree, R. H.; Dannenberg, J. J.; Hobza, P. *Pure Appl. Chem.* **2011**, *83*, 1619.
6. Arunan, E.; Desiraju, G. R.; Klein, R. A.; Sadlej, J.; Scheiner, S.; Alkorta, I.; Clary, D. C.; Crabtree, R. H.; Dannenberg, J. J.; Hobza, P. *Pure Appl. Chem.* **2011**, *83*, 1637-1641.
7. Desiraju, G. R. *Angew. Chem., Int. Ed.* **2011**, *50*, 52-59.

8. Bader, R. F. W. *Atoms in Molecules: A Quantum Theory*. Oxford University Press: New York, **1990**.
9. Espinosa, E.; Alkorta, I.; Elguero, J.; Molins, E. *J. Chem. Phys.* **2002**, *117*, 5529-5542.
10. Grabowski, S. J. *J. Phys. Org. Chem*. **2004**, *17*, 18-31.
11. Grabowski, S. J. *Chem. Phys. Lett*. **2001**, *338*, 361-366.
12. Grabowski, S. J. *Chem. Rev.* **2011**, *111*, 2597-2625.
13. Koch, U.; Popelier, P. L. A. *J. Phys. Chem.* **1995**, *99*, 9747-9754.
14. Weinhold, F.; Klein, R. A. *Mol. Phys.* **2012**, *110*, 565-579.
15. Lane, J. R.; Contreras-García, J.; Piquemal, J. P.; Miller, B. J.; Kjaergaard, H. G. *J. Chem. Theory Comput.* **2013**, *9*, 3263−3266.
16. Poater, J.; Fradera, X.; Solà, M.; Duran, M.; Simon, S. *Chem. Phys. Lett.* **2003**, *369*, 248-255.
17. Fradera, X.; Poater, J.; Simon, S.; Duran, M.; Solà, M. *Theor. Chem. Acc.* **2002**, *108*, 214-224.
18. Garcia-Revilla, M.; Popelier, P. L. A.; Francisco, E.; Pendas, A. M. *J. Chem. Theory Comput.* **2011**, *7*, 1704-1711.
19. Hugas, D.; Guillaumes, L.; Duran, M.; Simon, S. *Comput. Theor. Chem.* **2012**, *998*, 113-119.
20. Gora, R. W.; Maj, M.; Grabowski, S. J. *Phys. Chem. Chem. Phys.* **2013**, *15*, 2514-2522.
21. Fonseca Guerra, C. F.; Bickelhaupt, F. M.; Snijders, J. G.; Baerends, E. J. *Chem. Eur. J.* **1999**, *5*, 3581-3594.
22. Bertolasi, V.; Gilli, P.; Ferretti, V.; Gilli, G. *J. Am. Chem. Soc.* **1991**, *113*, 4917-4925.
23. Gastone Gilli, P. G. *The Nature of the Hydrogen Bond: Outline of a Comprehensive Hydrogen Bond Theory*. Oxford University Press: New York, **2009**; Vol. 23.
24. Gilli, G.; Bellucci, F.; Ferretti, V.; Bertolasi, V. *J. Am. Chem. Soc.* **1989**, *111*, 1023-1028.
25. Sanz, P.; Mó, O.; Yáñez, M.; Elguero, J. *ChemPhysChem* **2007**, *8*, 1950-1958.
26. Sanz, P.; Yáñez, M.; Mó, O. *Chem. Eur. J.* **2003**, *9*, 4548-4555.
27. Palusiak, M.; Simon, S.; Solà, M. *J. Org. Chem*. **2006**, *71*, 5241-5248.
28. Palusiak, M.; Simon, S.; Solà, M. *J. Org. Chem*. **2009**, *74*, 2059-2066.
29. Palusiak, M.; Simon, S.; Solà, M. *Chem. Phys.* **2007**, *342*, 43-54.
30. Cioslowski, J.; Matito, E.; Solà, M. *J. Phys. Chem. A* **2007**, *111*, 6521-6525.
31. Matito, E.; Salvador, P.; Duran, M.; Solà, M. *J. Phys. Chem. A* **2006**, *110*, 5108-5113.
32. Poater, J.; Fradera, X.; Duran, M.; Solà, M. *Chem. Eur. J.* **2003**, *9*, 400-406.
33. Giambiagi, M.; de Giambiagi, M. S.; dos Santos Silva, C. D.; de Figueiredo, A. P. *Phys. Chem. Chem. Phys.* **2000**, *2*, 3381-3392.
34. Bultinck, P.; Ponec, R.; Van Damme, S. *J. Phys. Org. Chem.* **2005**, *18*, 706-718.
35. Heyndrickx, W.; Salvador, P.; Bultinck, P.; Solà, M.; Matito, E. *J. Comput. Chem.* **2011**, *32*, 386-395.
36. Lenain, P.; Mandado, M.; Mosquera, R. A.; Bultinck, P. *J. Phys. Chem. A* **2008**, *112*, 7898-7904.
37. Lenain, P.; Mandado, M.; Mosquera, R. A.; Bultinck, P. *J. Phys. Chem. A* **2008**, *112*, 10689-10696.
38. Becke, A. D. *J. Chem. Phys.* **1988**, *88*, 2547−2553.
39. Mayer, I.; Salvador, P. *Chem. Phys. Lett.* **2004**, *383*, 368-375.
40. Matito, E.; Solà, M.; Salvador, P.; Duran, M. *Faraday Discuss.* **2007**, *135*, 325-345.
41. Hirshfeld, F. L. *Theoret. Chim. Acta* **1977**, *44*, 129-138.
42. Bultinck, P.; Cooper, D. L.; Van Neck, D. *Phys. Chem. Chem. Phys.* **2009**, *11*, 3424-3429.
43. Bultinck, P.; Van Alsenoy, C.; Ayers, P. W.; Carbo-Dorca, R. *J. Chem. Phys.* **2007**, *126*, 144111-144119.
44. Becke, A. D. *J. Chem. Phys.* **1993**, *98*, 5648.
45. Salvador, P.; Paizs, B.; Duran, M.; Suhai, S. *J. Comput. Chem.* **2001**, *22*, 765-786.
46. Frisch, M. J.; Trucks, G. W.; Schlegel, H. B.; Scuseria, G. E.; Robb, M. A.; Cheeseman, J. R.; Zakrzewski, V. G.; Montgomery, J. A.; Stratmann, R. E.; Burant, J. C.; Dapprich, S.; Millam, J. M.; Daniels, A. D.; Kudin, K. N.; Strain, M. C.; Farkas, O.; Tomasi, J.; Barone, V.; Cossi, M.; Cammi, R.; Mennucci, B.; Pomelli, C.; Adamo, C.; Clifford, S.; Ochterski, J.; Petersson, G. A.; Ayala, P. Y.; Cui, Q.; Morokuma, K.; Malick, D. K.; Rabuck, A. D.; Raghavachari, K.; Foresman, J. B.; Cioslowski, J.; Ortiz, J. V.; Stefanov, B. B.; Liu, G.; Liashenko, A.; Piskorz, P.; Komaromi, I.; Gomperts, R.; Martin, L. R.; Fox, D. J.; Keith, T.; Al.-Laham, M. A.; Peng, C. Y.; Nanayakkara, A.; Gonzalez, G.;

Challacombe, M.; Gill, P. M. W.; Johnson, B.; Chen, W.; Wong, M. W.; Andres, J. L.; Gonzalez, C.; Head-Gordon, M.; Replogle, E. S.; Pople, J. A. Gaussian 03, revision C.02; Gaussian, Inc.: Wallingford, CT, **2004**.
47. Biegler-König, F. AIM2000; University of Applied Science: Bielefeld, Germany, **2000**.
48. Salvador, P., Ramos-Cordoba, E. APOST-3D, *Institute of Computational Chemistry and Catalysis*; University of Girona: Catalonia, Spain, **2011**.
49. Matito, E. *ESI-3D: Electron Sharing Indices Program for 3d Molecular Space Partitioning; Institute of Computational Chemistry and Catalysis*, University of Girona: Catalonia, Spain, **2006**; http://iqc.udg.es/~eduard/ESI, IQC-USz-EHU, Girona-Szczecin-Donosti, 2006.
50. Hugas, D.; Simon, S.; Duran, M. *J. Phys. Chem. A* **2007**, *111*, 4506-4512.
51. Mo, Y. *J. Phys. Chem. A* **2012**, *116*, 5240-5246.
52. Salvador, P.; Ramos-Cordoba, E. *J. Chem. Phys.* **2013**, *139*, 071103.

5. Dealing with *Quasi*-Ring Formation by Two Hydrogen Bonds. Cooperativity Analysis with Delocalization Indices

5.1 Abstract

The *quasi*-ring formation between monomers structurally similar to DNA base pairs which interact with more than one hydrogen bond may show an extra stabilization linked with the delocalization of π electrons, commonly known as resonance-assisted hydrogen bonds (RAHB). Our aim is to reach a further understanding of their interaction energy and to find out if π delocalization associated with RAHB is an important contribution to it. Pairwise and n-center electron delocalization indices have been used to study qualitatively the interaction energies. From our results, delocalization indices on hydrogen bonds are helpful to classify their strength and to assess that delocalization within the *quasi*-ring is not the main component in the sense of energetically assisting the formation of the second HB. In addition, this idea is reinforced by considering the π contribution of the n-center delocalization index within the ring, which is not directly related to interaction energy. Regarding our results, ring reorganization energy (E_{RiR}) appearing when going from one HB to the *quasi*-ring formation is mainly due to the electron reorganization within the individual fragments, accounted for by the use of delocalization indices of the main skeleton.

5.2 Introduction

Hydrogen bonds (HB)[1,2] are of utmost importance in chemistry and biology. Many crystals, as well as some biological systems like DNA, show more than one hydrogen bond, which may make them more stable because of the cooperative effects. The presence of π electrons within their structure can increase the strength between the interacting molecules. As Gilli *et al.*[3,4] pointed out, π electrons of one fragment will strengthen the interaction, which leads to an increase in the system π delocalization. This synergic mechanism is known as resonance assisted hydrogen bond (RAHB). Many authors have been studying the role of these π electrons. As an example, Palusiak *et al.* analyzed a series of *o*-hydroxyaryl ketones where an intramolecular RAHB was formed. The stabilization energy upon HB formation was shown to exhibit good correlation with the electron delocalization indices between the proton and the proton-acceptor atoms.[5–7] Thus, the electron delocalization induced when a *quasi*-ring is built is closely related to the strength of this HB. However, there are different interpretations of this effect. In

particular, Becke and Mo[8] claimed that the enhancement of HB interaction is due to dipol-dipol electrostatic interactions. Others, like Sanz and co-workers, argued that RAHB is not the primary cause of the extra stabilization, leading to the conclusion that π electrons are not the main contribution.[9,10]

Many studies can be found about the nature of DNA base pair and the role of RAHB.[11−14] In a relevant paper of Fonseca Guerra *et al.*,[15] hydrogen bonds in DNA were proved not to be only an essentially electrostatic phenomenon, as they have a substantial charge-transfer character caused by donor-acceptor orbital interaction. Hence, both are of the same order of magnitude. One of their main conclusions is that there is no resonance assistance in the sense of synergism between σ charge transfer and π polarization. Kurczab *et al.*[16] studied adenine-thymine hydrogen bond interactions using slightly different orbital interaction decomposition energy. They corroborated the findings of Fonseca Guerra *et al.*[15] saying that some kind of resonance assistance because of π polarization is energetically a minor bonding component. A similar conclusion was published by Mitoraj *et al.*[17] as well as Gora *et al.*[18]

When one is interested in evaluating the cooperativity between HB in a complex with multiple HB, the first thing should be to calculate the individual contribution of each HB to the total energy. Comparing individual HB energies with the total interaction energy will give us the extra stabilization due to the ring formation. Different approximations can be found in the literature. From our group, Hugas *et al.*[19] used quantum theory of atoms in molecules (QTAIM) theory to relate different topological parameters to intermolecular strength. Also, natural bond orbital analyses were used by Szatyłowicz and Sadlej-Sosnowska[20] for DNA bases. Fonseca Guerra *et al.*[15] calculated individual contributions of HB by switching off one of the interactions and removing the appropriate σ or π virtuals. Other approaches are based on atom replacement procedure.[21] Asensio *et al.*[22] switched off one HB by rotating perpendicularly one of the molecules with certain constraints on geometrical parameters.

As it has been said, different topological parameters have been used to quantify the HB strength for inter- and intramolecular interactions. When a *quasi*-ring is formed, not only are we interested in HB strength but also in the electron delocalization within it. Different studies by Palusiak *et al.*[5−7] assess the relationship between HB strength and the electron delocalization within the *quasi*-ring. Also, Lenain *et al.*[23,24] used several n-center delocalization indices to demonstrate the validity of the resonance model for different intra- and intermolecular HB.

The main goal of this paper is to get deeper inside the nature of HB in systems related to DNA base pairs. This objective will be accomplished with the use of electron topological parameters like bond and ring n-center delocalization indices. Individual HB interaction energy will be calculated similar to Asensio *et al.*'s scheme,[22] that is, twisting the systems in order to have two perpendicular molecules. The comparison between the individual contributions with the total interaction energy will give us an extra energy due to the ring formation, the nature of which will be evaluated.

5.3 Methodology

All monomers and dimers considered in this study have been optimized at the nonlocal three-parameter hybrid B3LYP level of theory.[25] The 6-311++G(d,p) basis set was chosen for being one of the most widely used for the study of medium- and large-sized hydrogen-bonded systems and for yielding a very small basis set superposition error (BSSE), with counterpoise (CP)-corrected values comparable to those of the larger 6-311++G(3df,2pd) basis set.[26] Single-point CP correction for all complexes is ranging between 0.5 and 1.0 kcal·mol^{-1}. Vibrational analyses of optimized structures have shown that, in general, the structures are minima of the potential energy surface. Some of them do exhibit imaginary frequencies because of the planarity imposed to the systems (see Table S6 (p. 125) and Table 5.1). All calculations were carried out with the Gaussian 03 package.[27] Electron delocalization indices (DI) and n-center delocalization indices (I_{NG}) have been obtained using APOST-3D[28] and ESI-3D[29] programs, respectively.

DI are among the most popular bonding indicators. The delocalization index between atoms A and B, DI_{AB}, is obtained by double Integration of the exchange-correlation density, $\rho_{XC}(\vec{r}_1,\vec{r}_2)$, over their respective atomic domains Ω_A and Ω_B as

$$DI_{AB} = -2\int_{\Omega_A}\int_{\Omega_B}\rho_{XC}(\vec{r}_1,\vec{r}_2)d\vec{r}_1 d\vec{r}_2 \qquad \textbf{(5.1)}$$

In the particular case of a single-determinant closed-shell wave function, the delocalization index can be expressed solely in terms of the elements of the atomic overlap matrices **S**(A) in the molecular orbital basis

$$DI_{AB} = 4\sum_{i,j}^{occ} S_{ij}(A)S_{ji}(B) \qquad \textbf{(5.2)}$$

where the summation runs over all doubly occupied molecular orbitals.

To account for electron delocalization within the ring, Giambiagi *et al.*[31] proposed the I_{ring}, which measures the n-center electron delocalization among a set of atoms sequentially connected.

$$I_{ring}(R_n) = \sum_{i_1,i_2,\ldots i_n}^{occ} S_{i_1 i_2}(A_1)S_{i_2 i_3}(A_2)\ldots S_{i_n i_1}(A_n) \qquad \textbf{(5.3)}$$

where the summation runs over all occupied molecular orbital (MOs).

A normalization of this index was published by Cioslowski *et al.*,[30] named I_{NG}, which takes into account the number of atoms that built the ring. Thus, the I_{NG} index is defined as

$$I_{NG} = \frac{\pi^2}{4}\frac{1}{nN_\pi} I_{Ring}(R_n)^{1/n} \quad \textbf{(5.4)}$$

where N_π is the number of π electrons of the n-membered ring.

The value of I_{NG} can be split into its π and σ contributions. Therefore, the π contribution of this n-center electron delocalization index ($I_{NG\pi}$) is obtained by only taking into account π orbitals in eq. (5.4). The planarity of the systems is necessary in order to avoid the overlaps between σ and π orbitals.

Numerical integration over atomic domains has been performed in the framework of the fuzzy-atoms, which have no strict boundaries, but they overlap to some extent. This makes the numerical integrations over the atomic domains much more efficient computationally speaking. The results reported here have been obtained by using atomic grids consisting of 60 radial and 266 angular points. Becke-ρ scheme has been chosen, which considers some Bader QTAIM characteristics, showing similar results for both approximations.[32]

To account for each individual contribution of HB, a similar scheme proposed by Asensio *et al.*[22] has been used but without reoptimizing the systems. The difference between total interaction energy and individual HB will give us the reorganization ring energy (E_{RiR}).

$$E_{RiR} = E_{\text{int}} - E_{HB_1(90^\circ)} - E_{HB_2(90^\circ)} \quad \textbf{(5.5)}$$

where E_{int} is the total interaction energy while $E_{HB_1(90^\circ)}$ and $E_{HB_2(90^\circ)}$ are the energies of the complex after rotating 90° monomers with respect to each HB.

5.4 Results

Figure 5.1 collects the monomers that have been used to form different complexes, which are in total 50 (see Figure S1 of the Supporting Information, p.125). The analysis will start with symmetric systems, following the nonsymmetric ones. At the end, a ring formation analysis will be discussed within the framework of extra stabilization energy.

a. Symmetrics. In previous studies,[32] a relationship was found between hydrogen bond distances and delocalization indices of HB (DI_{HB}, which corresponds to the DI_{HX} between H···X), which mainly depends both on donor and acceptor atoms. Symmetric compounds (with two identical HB) give us the possibility of analyzing the relationship between the total interaction energy (with no relaxation of monomers) and local bond indices, being here delocalization indices (DI).

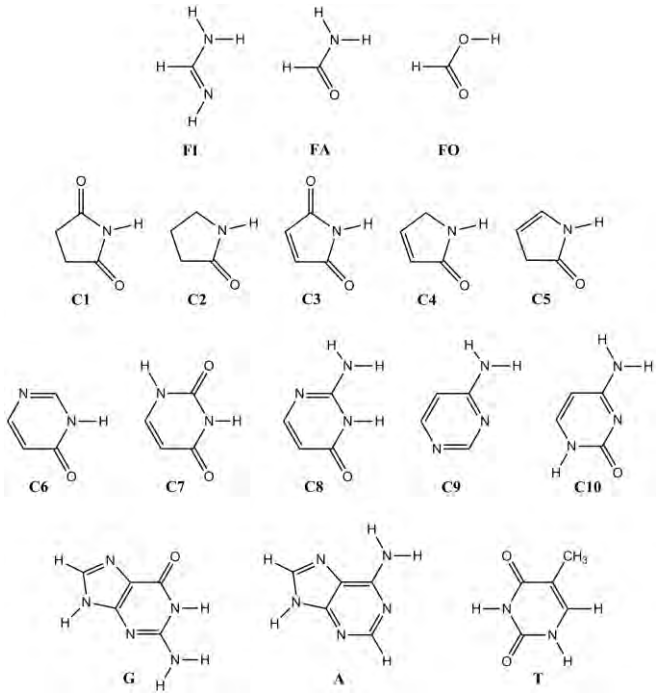

Figure 5.1: All the monomers with the nomenclature used in this work.

Figure 5.2 depicts half of the interaction energy (which can be related to an individual HB and thus to a local bond index) in front of DI_{HB}. All data for these complexes is collected in Table 5.1. It can be observed that, as it was expected, the larger the DI_{HB} the stronger the HB is. This general linear trend is not specially followed by C10-C10, with the same pattern as FI−FI for both donor and acceptor atoms (together with C9-C9). C10-C10, which is much stronger than FI−FI (-20.3 kcal·mol^{-1} compared to -15.0 kcal·mol^{-1}), shows lower DI within the HB (0.1097 vs 0.1308). While delocalization indices in the HB for C9-C9 and C10-C10 are quite similar, their interaction energy is very different, C10-C10 being almost the double of the C9-C9 value. Thus, regarding the nonexpected trends for C10-C10, a deeper insight into complexes with this monomer will be done later in this paper.

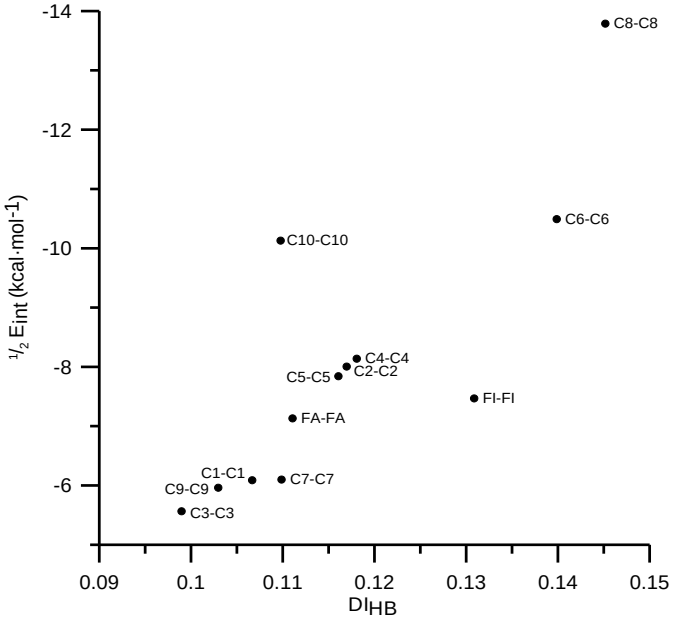

Figure 5.2: Half of the interaction energy (E_{int}) with respect to delocalization indices on HB.

Table 5.1: Interaction Energy (kcal·mol^{-1}), CP-Corrected Interaction Energy (kcal·mol^{-1}), HB Distance (Å), HB Delocalization Index (DI_{HB} for complex and $DI_{HB90°}$ for perpendicular configuration), I_{NG}, and Ring Reorganization Energy (E_{RiR}, kcal·mol^{-1})

Compound	E_{int}[b]	E_{int}+CP	R_{HB}	DI_{HB}[c]	$DI_{HB(90°)}$[d]	$I_{NG}\cdot10^{-3}$	$I_{NG\pi}\cdot10^{-3}$	E_{RiR}
C8-C8[a]	-27.6	-26.9	1.73	0.1451	0.1400	9.443	8.448	-8.8
C6-C6	-21.0	-20.3	1.75	0.1398	0.1356	9.460	8.514	-7.4
C10-C10	-20.3	-19.5	1.92	0.1097	0.1069	8.713	8.218	-8.9
C4-C4	-16.3	-15.7	1.85	0.1180	0.1153	9.382	8.939	-5.6
C5-C5	-16.0	-15.4	1.86	0.1169	0.1145	9.364	8.934	-5.0
C2-C2[a]	-15.7	-15.1	1.86	0.1160	0.1130	9.385	8.984	-5.3
FI-FI[a]	-15.0	-14.5	1.94	0.1308	0.1246	9.597	9.254	-4.8
FA-FA	-14.3	-13.9	1.89	0.1110	0.1087	9.520	9.011	-5.2
C7-C7	-12.2	-11.5	1.85	0.1098	0.1088	9.203	8.415	-3.1
C1-C1	-12.2	-11.5	1.90	0.1066	0.1068	8.890	8.276	-2.8
C9-C9	-11.9	-11.5	2.00	0.1029	0.1003	8.488	7.772	-2.0
C3-C3	-11.2	-10.5	1.93	0.0989	0.0994	8.768	8.156	-2.7

[a]Compounds with imaginary frequency. [b]Interaction energy (E_{int}) has been calculated as the difference between the complex and the sum of both monomers, always in the complex geometry (no relaxation is taken into account). [c]DI_{HB} is the delocalization index between H···X (proton and proton acceptor). [d]$DI_{HB(90°)}$ states for delocalization index of H···X after rotating 90° one of the monomers.

There is still an important discussion about the nature of interaction energy in systems where two HB form a *quasi*-ring, mainly related to the possible existence of resonance-assisted hydrogen bond (RAHB). N-center delocalization indices can be considered as a good indicator of the charge delocalized within a ring. In that case, the I_{NG} has been chosen for this purpose. As it has been explained, its π contribution ($I_{NG\pi}$) can be obtained when working with planar molecules (see Table 5.1). Compared to benzene,[33] the values for the I_{NG} are one order of magnitude smaller. Thus, one could think already beforehand that these contributions will not have a huge influence on the energetic results. However, to check it, the relationship between I_{NG} (in particular its π contribution) and other parameters will be analyzed. $I_{NG\pi}$ and I_{NG} present very similar trends (see Figure S2, Figure S3 and Figure S4 of the Supporting Information for I_{NG} graphic representation, p.125).

Differently from DI, which is linked with an individual HB, I_{NG} can be related to the total interaction energy. Figure 5.3 depicts the interaction energy in front of $I_{NG\pi}$ for all symmetric compounds. Mainly, two sets of compounds can be observed in the graphic. First, there is a set of dimers with similar interaction energy but quite different delocalization within the ring (e.g., C9-C9 with E_{int}=-11.9 kcal·mol^{-1} and $I_{NG\pi}$=7.772·10^{-3} and C7-C7 with E_{int}=-12.2 kcal·mol^{-1} and $I_{NG\pi}$=8.415·10^{-3}). On the other hand, there is a set of dimers that have similar delocalization within the ring but a large range of interaction energies (e.g., FA–FA with E_{int}=-14.3 kcal·mol^{-1} and $I_{NG\pi}$=9.011·10^{-3} and C8-C8 with E_{int}=-27.6 kcal·mol^{-1} and $I_{NG\pi}$=8.448·10^{-3}). These results suggest that there is no direct relationship between interaction energy and the amount of π charge delocalized when a *quasi*-ring is formed. Thus, if synergism due to π

electrons was an important factor between HB, a larger amount of π delocalization inside the ring would stabilize the system, which is not shown in Figure 5.3. This is in agreement with the conclusion published by Fonseca Guerra *et al.*,[15] as they find out that there is no resonance-assistance in terms of synergism between HB in DNA.

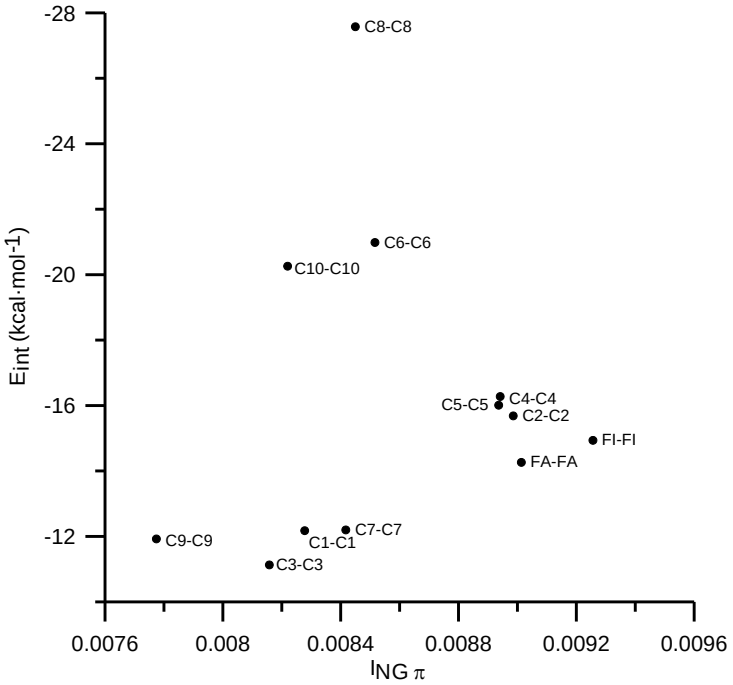

Figure 5.3: Interaction energy (E_{int}) with respect to the π contribution of the n-center delocalization index, $I_{NG\pi}$.

b. Nonsymmetrics. Following the analysis started for symmetric systems, a combination between different monomers will be added to them in this section. In Table S6 of the Supporting Information (p.125), all data corresponding to them can be found.

As it has been explained for symmetric systems, there is a relationship between HB delocalization indices (DI_{HB}) and half of the total interaction energy. However, when one considers nonsymmetric complexes, it is not straightforward to calculate the contribution of each individual hydrogen bond after forming the dimer. Not far from what has been considered above (dividing interaction energies), one can consider as a first approximation for nonsymmetric complexes the addition of both electron delocalization HB indices (which are the same when symmetric complexes are considered). In this section, graphics are done with all symmetric and nonsymmetric compounds.

In Figure 5.4, the addition of both DI_{HB} with respect to the total interaction energy (with no relaxation) is represented. It can be seen that there is a correlation between both parameters. Only some complexes, mostly related to C10 molecule, are slightly not following the general trend. As it has been said before, these systems will receive a detailed treatment in the next section.

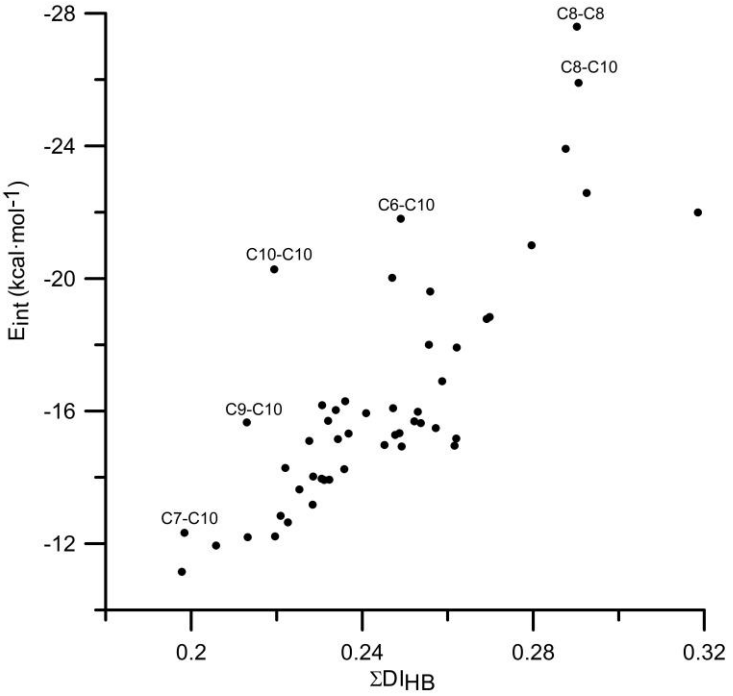

Figure 5.4: Interaction energy with respect to the addition of both DI_{HB}.

As it has been considered above, one could think about a possible π electron delocalization within the ring, commonly related to RAHB.

Figure **5.5** depicts E_{int} in front of $I_{NG\pi}$.

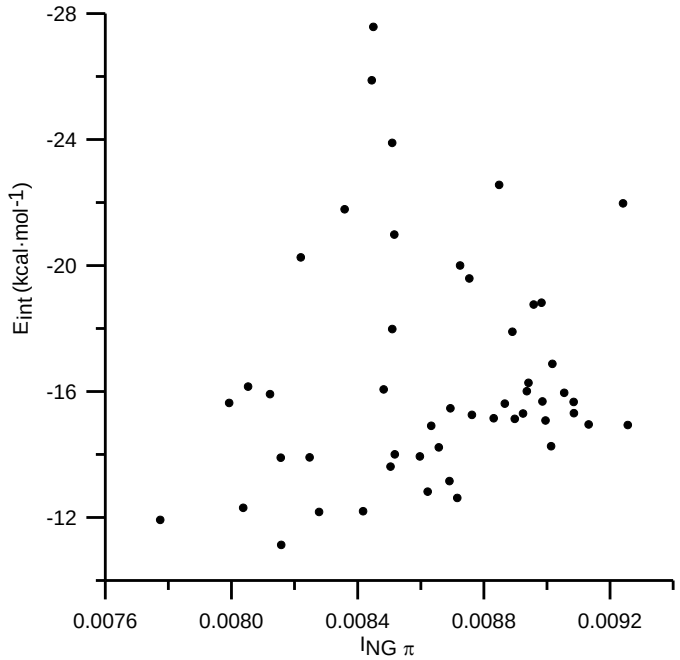

Figure 5.5: Interaction energy (E_{Int}) with respect to the π contribution of the n-center delocalization index, $I_{NG\pi}$.

As shown by the results, there is no general trend, with all data quite scattered, and so one can arrive at the same conclusion as with the symmetric ones. Again, π delocalization within the ring is not directly ruling the interaction energy. Therefore, larger π delocalization does not necessarily imply an increase in the stabilization of the system.

c. Ring Formation Analysis. We will treat now an individual HB and the analysis of a possible synergic energy effect when forming the second HB by analyzing electron delocalization of different bonds. To calculate the energetic contribution of each HB, we used a similar method proposed by Asensio *et al.*,[22] where one monomer was rotated 90°. In that perpendicular position, there is only one HB interacting, and so it allows getting its interaction energy. The difference between the addition of these two individual HB energies and the total complex energy is the stabilization energy when forming the ring (E_{RiR}). It is expected beforehand for this extra stabilization to be due to different contributions. In Figure 5.6, the three different structures considered in the calculation are represented. Figure 5.6a represents the monomer with the geometry in the dimer, Figure 5.6b is the two-HB complex where the *quasi*-ring is formed, and Figure 5.6c is the 90°-rotated structure. The main DI of *quasi*-ring skeleton are written down in the figures.

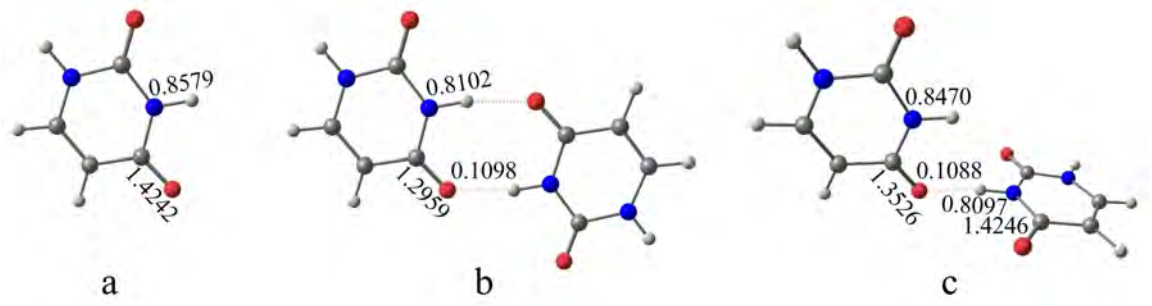

Figure 5.6: C7-C7 complex with corresponding bond DI. (a) Monomer in the dimer geometry, (b) two-HB system, and (c) one-HB complex.

As it was pointed out before, one of our main goals is to get a picture of the nature of the stabilization energy that appears when forming a *quasi*-ring because of two HB. First, we will consider the relationship between E_{RiR} and the π delocalization within the ring, which can be measured with $I_{NG\pi}$ (Figure 5.7).

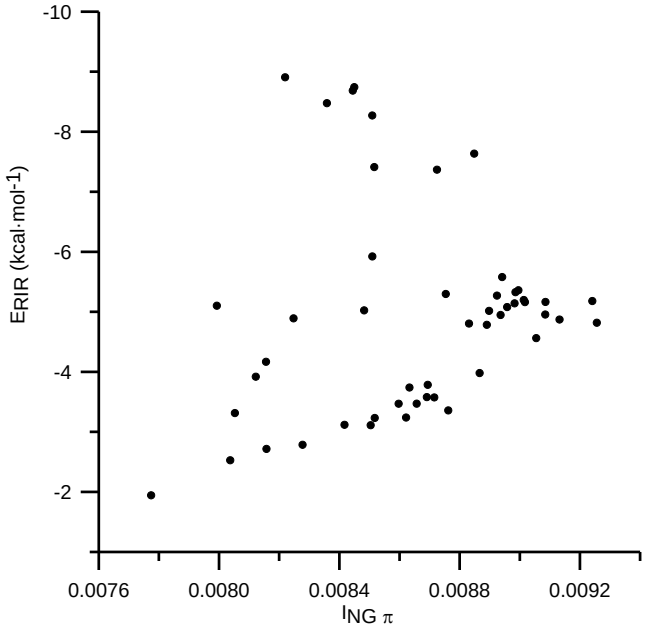

Figure 5.7: E_{RiR} with respect to the π contribution of the n-center delocalization index, $I_{NG\pi}$.

As shown by the represented data, only the E_{RiR} of some systems is, in some way, related to the π delocalization within the *quasi*-ring. Thus, from this data, one can read that in general no connection between the values of π delocalization within the ring and the E_{RiR} is found. Thus, the extra stabilization is not directly due to π delocalization.

To get a further understanding of this extra stabilization when the ring is formed, we will proceed to study how the DI_{HB} (delocalization indices of hydrogen bond) of the rotated complex change when forming the new bond (going from one-HB to two-HB conformers). As shown in Table 5.1, changes between both DI_{HB} are not very large (about a 2% of the value). This small variation reinforces the conclusion that HB interaction is the same although there is a *quasi*-ring formation. The largest change is found within FI-FI compound, which represents almost a 5% of the total DI_{HB}, although this complex is not the one with higher ring stabilization energy. An early first conclusion goes again to the direction that the formation of the second HB does not change the strength of the first one, as DI_{HB} is being kept almost constant when forming the second HB.

To assess the possible interplay between both HB in the ring, now we will also focus on the DI between proton donor and hydrogen (N-H bond) of the formed HB. We need to analyze the change of the hydrogen-bonded NH when forming the second HB, going from one (Figure 5.6c) to two-HB (Figure 5.6b). All data for symmetric compounds are collected in Tables S7 and S8 of the Supporting Information (p.125) (for DI and ΔDI, respectively). In Figure 5.6, we can see that when two monomers interact to form one-HB complex (from Figure 5.6a to Figure 5.6c) DI_{NH} goes from 0.8579 to 0.8097 (decreasing 0.0482), while rotating DI_{NH} (from Figure 5.6c to Figure 5.6b) changes from 0.8097 to 0.8102 (increasing 0.0005). This last number shows that no important difference is found, meaning that delocalization is similar in this bond when forming one-HB or two-HB. Now, we can compare proton acceptor (C=O), where larger variation can be found. For C7-C7 (Figure 5.6), we can see that forming one-HB complex (from Figure 5.6a to Figure 5.6c) DI_{CO} goes from 1.4242 to 1.3526 (decreasing 0.0716), while rotating (from 6c to 6b) DI_{CO} changes from 1.3526 to 1.2959 (decreasing 0.0567).

In general, NH (proton donor) bonds show a small increase in their DI when going from one-HB to two-HB complex, which sometimes can be negligible. However, there is a larger change of DI on the bonds related to the proton acceptor. However, as one goes further from the HB, the changes of DI within the skeleton are larger. This fact can be observed from Figure 5.6, where the NH (not forming HB in one-HB complex) changes from 0.8470 to 0.8102 when forming the second bond. Thus, extra stabilization because of rotating monomers, E_{RiR}, is associated to the electron reorganization within each fragment. On the other hand, it has been demonstrated that there is not synergism between HB because of π delocalization within the *quasi*-ring.

C10-C10 and C8-C8 do not follow the trends of the other compounds. These complexes have the particularity of presenting a large E_{RiR} and also a large delocalization index of the CN bond that not belong directly to the ring, when going from one- to two-HB (-0.0304 and 0.0344, respectively), see

Table S8 of the Supporting Information, p.125. This delocalization is out of the *quasi*-ring and is not directly related to the delocalization within it. As it can be observed in Figure 5.4, other compounds with C10 follow the same behavior. In that sense, special emphasis should be done in systems with skeleton similar to C10, which are the only ones with a C=O near the proton acceptor. Also, C8-C8 shows a special behavior, which could be attributed to the fact of being the only compound with two proton donor groups almost one next to each other. There is a relevant difference on its ΔDI of the interacting NH when going from one to two-HB (-0.0188, see Table S8 of the Supporting Information, p.125), as it is larger than in the case of the other compounds.

To sum up, we can say that π delocalization within the ring is not linearly related to E_{RiR}. While some complexes follow the trend that higher π delocalization ($I_{NG\pi}$) implies larger E_{RiR}, many others do not follow this direct relationship between both parameters.

Delocalization indices can be used, in general, to account for the strength in two-HB systems with a *quasi*-ring formation (Figure 5.2 and Figure 5.4). Evaluation of the DI_{HB} brings to the conclusion that both HB are not connected in the sense of energetic synergy between them. Also, electron reorganization within the fragments is being analyzed in terms of DI changes. Special attention should be paid when two proton donors (C8) or acceptors (C10) are almost one next to each other.

5.5 Conclusions

Similar HB patterns as in DNA bases have been analyzed with the aim of gaining further understanding of the interaction energy. The main goal was to find out if RAHB was ruling the interaction energy between monomers. Pairwise and n-center electron delocalization indices have been used to study qualitatively the different components of interaction energy.

From our calculation, by using delocalization indices, one can conclude that π delocalization within the *quasi*-ring is not the main component in the sense of energetically assisting the formation of the second HB. This contribution can be considered negligible as far as the total interaction is concerned. Regarding our results, the ring reorganization energy (E_{RiR}) found when a *quasi*-ring is formed can be associated to the electron reorganization in fragments, which can be accounted for by DI of the main skeleton.

Delocalization indices on HB in systems with *quasi*-ring formation are helpful to classify the strength of HB. On the other hand, π contribution of the n-center delocalization index ($I_{NG\pi}$) within the *quasi*-ring has small values, and it is not directly related to HB formation, meaning no RAHB is found in the sense of one HB assisting the other. An important aspect to take into account is that the electron donor group C=O is situated almost next to the HB electron donor. In those systems, the interaction energy is larger and there is also a larger electron reorganization within a part of the fragment out of the *quasi*-ring,

which is not reflected on DI_{HB}. Also, having two proton donor groups almost connected (C8) requires a special analysis.

Our results have involved complexes with an interacting skeleton similar to DNA, showing all of them two HB. Further studies are being developed with the aim of extrapolating the conclusions to systems with three or more HB.

5.6 References

1. Jeffrey, G. A. *An Introduction to Hydrogen Bonding*. Oxford University Press: New York, **1997**.
2. Scheiner, S. *Molecular Interactions: From van der Waals to Strongly Bound Complexes*. Wiley & Sons: Oxford, U.K., **1997**.
3. Gilli, G.; Bellucci, F.; Ferretti, V.; Bertolasi, V. *J. Am. Chem. Soc.* **1989***, 111* (3), 1023-1028.
4. Gastone Gilli, P. G. *The Nature of the Hydrogen Bond: Outline of a Comprehensive Hydrogen Bond Theory*. Oxford University Press: New York, **2009**; Vol. 23.
5. Palusiak, M.; Simon, S.; Solà, M. *J. Org. Chem.* **2006**, *71* (14), 5241-5248.
6. Palusiak, M.; Simon, S.; Solà, M. *J. Org. Chem.* **2009**, *74* (5), 2059-2066.
7. Palusiak, M.; Simon, S.; Solà, M. *Chem. Phys.* **2007**, *342* (1−3), 43-54.
8. Beck, J. F.; Mo, Y. *J. Comput. Chem.* **2007**, *28* (1), 455-466.
9. Sanz, P.; Mó, O.; Yáñez, M.; Elguero, J. *ChemPhysChem* **2007**, *8* (13), 1950-1958.
10. Sanz, P.; Yáñez, M.; Mó, O. *Chem. Eur. J.* **2003**, *9* (18), 4548-4555.
11. Mó, Y. R. *J. Mol. Model.* **2006**, *12* (2), 221-228.
12. Jurecka, P.; Sponer, J.; Cerny, J.; Hobza, P. *Phys. Chem. Chem. Phys.* **2006**, *8* (17), 1985-1993.
13. Fonseca Guerra, C.; Bickelhaupt, F. M.; Snijders, J. G.; Baerends, E. J. *J. Am. Chem. Soc.* **2000**, *122* (17), 4117-4128.
14. Fonseca Guerra, C.; Bickelhaupt, F. M. *Angew. Chem., Int*. Ed. **1999**, *38* (19), 2942-2945.
15. Fonseca Guerra, C. F.; Bickelhaupt, F. M.; Snijders, J. G.; Baerends, E. J. *Chem. Eur. J.* **1999**, *5* (12), 3581-3594.
16. Kurczab, R.; Mitoraj, M. P.; Michalak, A.; Ziegler, T. *J. Phys. Chem. A* **2010**, *114* (33), 8581-8590.
17. Mitoraj, M.; Kurczab, R.; Boczar, M.; Michalak, A. *J. Mol. Model.* **2010**, *16* (11), 1789-1795.
18. Gora, R. W.; Maj, M.; Grabowski, S. J. *Phys. Chem. Chem. Phys.* **2013**, *15* (7), 2514−2522.
19. Hugas, D.; Simon, S.; Duran, M. *J. Phys. Chem. A* **2007**, *111* (20), 4506-4512.
20. Szatyłowicz, H.; Sadlej-Sosnowska, N. *J. Chem. Inf. Model.* **2010**, *50* (12), 2151-2161.
21. Dong, H.; Hua, W.; Li, S. *J. Phys. Chem. A* **2007**, *111* (15), 2941-2945.
22. Asensio, A.; Kobko, N.; Dannenberg, J. *J. Phys. Chem. A* **2003**, *107* (33), 6441-6443.
23. Lenain, P.; Mandado, M.; Mosquera, R. A.; Bultinck, P. *J. Phys. Chem. A* **2008**, *112* (34), 7898-7904.
24. Lenain, P.; Mandado, M.; Mosquera, R. A.; Bultinck, P. *J. Phys. Chem. A* **2008**, *112* (42), 10689-10696.
25. Becke, A. D. Density-Functional Thermochemistry. III. *J. Chem. Phys.* **1993**, *98* (7), 5648-5652.
26. Salvador, P.; Paizs, B.; Duran, M.; Suhai, S. *J. Comput. Chem.* **2001**, *22* (7), 765--786.
27. Frisch, M. J.; Trucks, G. W.; Schlegel, H. B.; Scuseria, G. E.; Robb, M. A.; Cheeseman, J. R.; Montgomery, J. A., Jr.; Vreven, T.; Kudin, K. N.; Burant, J. C.; Millam, J. M.; Iyengar, S. S.; Tomasi, J.; Barone, V.; Mennucci, B.; Cossi, M.; Scalmani, G.; Rega, N.; Petersson, G. A.; Nakatsuji, H.; Hada, M.; Ehara, M.; Toyota, K.; Fukuda, R.; Hasegawa, J.; Ishida, M.; Nakajima, T.; Honda, Y.; Kitao, O.; Nakai, H.; Klene, M.; Li, X.; Knox, J. E.; Hratchian, H. P.; Cross, J. B.; Bakken, V.; Adamo, C.; Jaramillo, J.; Gomperts, R.; Stratmann, R. E.; Yazyev, O.; Austin, A. J.; Cammi, R.; Pomelli, C.; Ochterski, J. W.; Ayala, P. Y.; Morokuma, K.; Voth, G. A.; Salvador, P.; Dannenberg, J. J.; Zakrzewski, V. G.; Dapprich, S.; Daniels, A. D.; Strain, M. C.; Farkas, O.; Malick, D. K.; Rabuck, A. D.; Raghavachari, K.; Foresman, J. B.; Ortiz, J. V.; Cui, Q.; Baboul, A. G.; Clifford, S.; Cioslowski, J.; Stefanov, B. B.; Liu, G.; Liashenko, A.; Piskorz, P.; Komaromi, I.; Martin, R. L.; Fox, D. J.; Keith, T.;

Al-Laham, M. A.; Peng, C. Y.; Nanayakkara, A.; Challacombe, M.; Gill, P. M. W.; Johnson, B.; Chen, W.; Wong, M. W.; Gonzalez, C.; Pople, J. A. Gaussian 03, revision C.02; Gaussian, Inc.: Wallingford, CT, **2004**.

28. Salvador, P., Ramos-Cordoba, E. APOST-3D, *Institute of Computational Chemistry and Catalysis*; University of Girona: Catalonia, Spain, **2011**.
29. Matito, E. ESI-3D: *Electron Sharing Indices Program for 3D Molecular Space Partitioning*; Institute of Computational Chemistry and Catalysis, University of Girona: Catalonia, Spain, 2006; http://iqc.udg.es/~eduard/ESI.
30. Cioslowski, J.; Matito, E.; Solà, M. *J. Phys. Chem. A* **2007**, *111* (28), 6521-6525.
31. Giambiagi, M.; de Giambiagi, M. S.; dos Santos Silva, C. D.; de Figueiredo, A. P. *Phys. Chem. Chem. Phys.* **2000**, *2* (15), 3381-3392.
32. Guillaumes, L.; Salvador, P.; Simon, S. *J. Phys. Chem. A* **2014**, *118* (6), 1142-1149.

(33) Feixas, F.; Matito, E.; Poater, J.; Solà, M. *J. Comput. Chem.* **2008**, *29* (10), 1543-1554.

6. The Role of Aromaticity, Hybridization, Electrostatics and Covalency in Resonance-Assisted Hydrogen Bonds of Adenine-Thymine (AT) Base Pair and Their Mimics

6.1 Abstract

Hydrogen bonds play a crucial role in many biochemical processes and in supramolecular chemistry. In this study, we show quantum chemically that neither aromaticity nor other forms of π assistance are responsible for the enhanced stability of the hydrogen bonds in adenine-thymine (AT). This follows from extensive bonding analyses of AT and smaller analogues thereof, based on dispersion-corrected density functional theory (DFT). Removing the aromatic rings of either A or T has no effect on the Watson-Crick bond strength. Only when the smaller mimics become saturated, that is, when the hydrogen-bond acceptor and donor groups go from sp^2 to sp^3, does the stability of the resulting model complexes suddenly drop. Bonding analyses based on quantitative Kohn-Sham molecular orbital theory and corresponding energy decomposition analyses (EDA) show that the stronger hydrogen bonds in the unsaturated model complexes and in AT stem from stronger electrostatic interactions as well as enhanced donor-acceptor interactions in the σ-electron system, with the covalency being responsible for shortening the hydrogen bonds in these dimers.

6.2 Introduction

Hydrogen bonds play a crucial role in many biochemical processes and supermolecular chemistry.[1] After observing the X-ray diffraction images of DNA obtained by Rosalind Franklin, Watson and Crick proposed in 1953 that hydrogen bonds are essential for the working of the genetic code.[2] In DNA, the two helical strands of nucleotides are held together by the hydrogen bonds that arise between a purine- and a pyrimidine-derived nucleic base, that is, adenine-thymine (AT) or guanine-cytosine (GC).

Gilli *et al.*[3] proposed that the hydrogen bonds in DNA base pairs are reinforced by π assistance, the so-called resonance-assisted hydrogen bonding (RAHB). The resonance of the conjugated double bonds assists the hydrogen bonds by charge delocalization, which results in a shortening of the distance between proton donor and proton acceptor. They proposed that the RAHB interaction occurs for inter- and intramolecular systems. Numerous theoretical studies have been devoted to study these inter- and

intramolecular RAHBs.[4,5a] For the DNA base pair, the resonance assistance, as proposed by Gilli *et al.*, is presented in Scheme 6.1 with the upper Lewis structure.

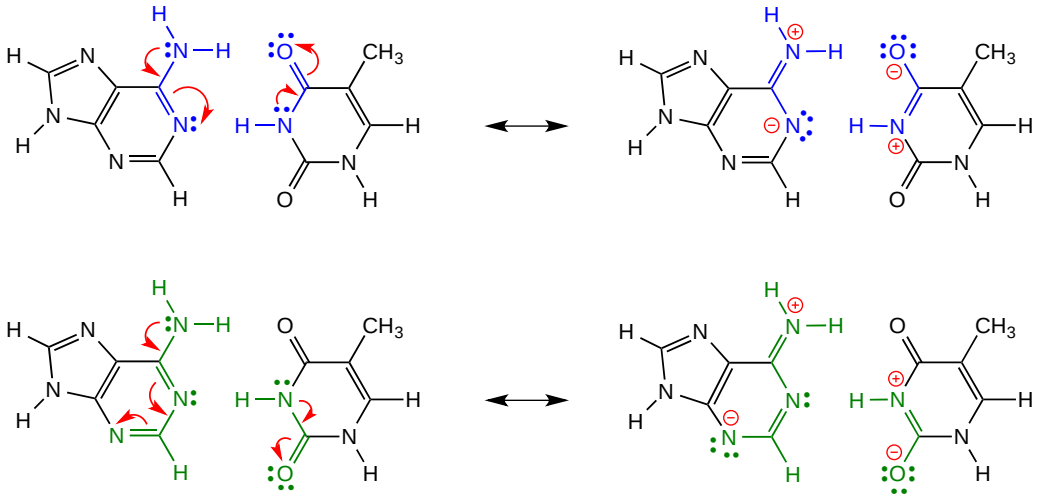

Scheme 6.1. Resonance-assisted hydrogen bonding in adenine-thymine (AT).

In previous work,[5] we established theoretically that, for the hydrogen bonds in DNA base pairs, the electrostatic interactions and orbital interactions are of equal importance and that, indeed, the π electrons provide an additional stabilizing component. This finding was reconfirmed by others.[4g,4j] However, our work[5] also showed computationally that the synergetic interplay between the delocalization in the π-electron system and the donor-acceptor interactions in the σ-electron system was small, that is, the simultaneous occurrence of the π and σ interactions is only slightly stronger than the sum of each of these interactions occurring individually. Recently, we showed that the intriguing cooperativity in guanine quartets, which can occur in the telomeric part of the chromosome, originates from the charge separation that goes with donor-acceptor orbital interactions in the σ-electron system, and not from the strengthening caused by resonance in the π-electron system.[4i] Also in this case the π delocalization provides only an extra stabilisation to the hydrogen bonds.

In the present paper, we study the resonance assistance to the hydrogen bonds of AT and its smaller analogues (see Scheme 6.2), because the Lewis structure of AT in Scheme 6.1 as proposed by Gilli *et al.*[3] suggests that the smaller mimic can also give the same resonance assistance. Also, our previous work on the Watson-Crick base pairs based on high level DFT computations,[5a] showed that the hydrogen bonds affected mainly the atomic charges of the blue part in Scheme 6.1. However, the resonance of the π electrons encompasses a larger part of the of the adenine nucleobase as can be seen in the lower (green) part of Scheme 6.1, suggesting that we can remove the 5-membered ring of the purine base, but we cannot remove the 6-membered ring. For the pyrimidine base, the resonance structures suggest that we need to incorporate all frontier atoms.

To validate the charge rearrangements suggested by resonance structures, the number of π electrons will be made smaller in the monomers by going from A, to A' and A" and from T to T' and T".

All the possible pairing combinations will be taken into account (AT, AT', AT", A'T, A'T', A'T", A"T, A"T' and A"T", see Scheme 6.2). This computational investigation determines if the π assistance is exclusively due to aromaticity,[6,4f] or if the sp^2-hybridization of the proton-donor and acceptor atoms already accounts for the π charge delocalization. The logical follow up question is to address the importance of hybridization by comparison of sp^2 and sp^3 hybridized dimers. The latter hydrogen bonds are known to be longer when the difference is only the saturation of the molecules, but the complex has the same front atoms participating in the hydrogen bonds.

The computational analyses of DNA base pair AT and its smaller mimics are based on dispersion-corrected density functional theory (DFT-D3).[7] The small geometrical and bonding differences computed for the hydrogen bonds of AT and its mimics are explained with our quantitative Kohn-Sham molecular orbital (MO) and corresponding energy decomposition analyses (EDA).[8] They reveal that the π assistance is independent of the number of π electrons of the monomers but it is essential that the proton donor and acceptor atoms have π electrons.

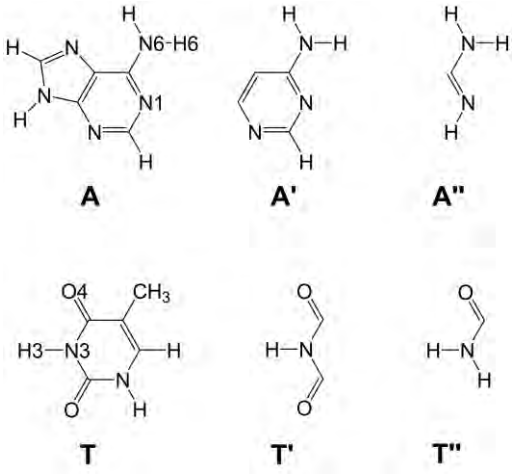

Scheme 6.2: Adenine (A) and its smaller analogues (A' and A") and thymine (T) and its smaller analogues (T' and T").

6.3 Computational Methods

6.3.1 General Procedure

All calculations were performed using the Amsterdam Density Functional (ADF) program (2013) developed by Baerends, Ziegler, and others.[9,10] The MOs were expanded in a large uncontracted set of Slater-type orbitals (STOs) containing diffuse functions: TZ2P (no Gaussian functions are involved).[10i] The basis set is of triple-ζ quality for all atoms and has been augmented with two sets of polarization functions, i.e., 2*p* and 3*d* on H and 3*d* and 4*f* on C, N and O. The 1*s* core shells of carbon, nitrogen and oxygen were treated by the frozen-core approximation.[10c] An auxiliary set of *s*, *p*, *d*, *f* and *g* STOs was used to fit the molecular density and to represent the Coulomb and exchange potentials accurately in each self-consistent field cycle.[10a,b]

The calculations were done with density functional theory (DFT) using the BLYP functional[11,12] with dispersion corrections as developed by Grimme,[7e] BLYP-D3(BJ). Dispersion corrections are applied using the DFT-D3(BJ) method, developed by Grimme,[7f] which contains the damping function proposed by Becke and Johnson.[13] In this approach, the density functional is augmented with an empirical term correcting for long-range dispersion effects, described by a sum of damped interatomic potentials of the form $C_6/(R^6+c)$ added to the usual DFT energy.[7] Equilibrium structures were optimized using analytical gradient techniques.[10k]

Geometries were optimized in the gas phase with Cs symmetry. All stationary points were verified to be minima through vibrational analysis. For the dispersion-corrected functional, the basis set superposition error (BSSE) on the bond energy was not calculated because the dispersion correction[7e] has been developed such that the small BSSE effects[5c] are absorbed into the empirical potential.

6.3.2 Bonding Energy Analysis

The hydrogen bond energy ΔE of the dimer is defined as:

$$\Delta E = E_{\text{dimer}} - E_{\text{monomer1}} - E_{\text{monomer2}} \quad \textbf{(6.1)}$$

where E_{dimer} is the energy of the dimer, optimized in C_s symmetry, and E_{monomer1} or E_{monomer2} are the energies of the monomers adenine, thymine or one of their smaller analogues, optimized in C_1 symmetry, i.e., without any geometrical constraint. The overall bond energy ΔE is made up of two major components:

$$\Delta E = \Delta E_{\text{prep}} + \Delta E_{\text{int}} \quad \textbf{(6.2)}$$

In this formula, the preparation energy ΔE_{prep} is the amount of energy required to deform the monomers from their equilibrium structure to the geometry that they acquire in the dimer. The interaction energy ΔE_{int} corresponds to the actual energy change when the prepared monomers are combined to form the pair.

The interaction energy is examined in the hydrogen-bonded model systems in the framework of the Kohn-Sham MO model using a quantitative energy decomposition analysis (EDA) into electrostatic interaction, Pauli repulsive orbital interactions, and attractive orbital interactions:[8,14-15,19]

$$\Delta E_{\text{int}} = \Delta V_{\text{elstat}} + \Delta E_{\text{Pauli}} + \Delta E_{\text{oi}} + \Delta E_{\text{disp}} \quad \textbf{(6.3)}$$

The term ΔV_{elstat} corresponds to the classical electrostatic interaction between the unperturbed charge distributions of the prepared (i.e. deformed) bases and is usually attractive. The Pauli-repulsion ΔE_{Pauli} comprises the destabilizing interactions between occupied orbitals and is responsible for any steric repulsion. The orbital interaction ΔE_{oi} in any MO model, and therefore also in Kohn-Sham theory, accounts for charge transfer (i.e., donor–acceptor interactions between occupied orbitals on one moiety

with unoccupied orbitals of the other, including the HOMO-LUMO interactions) and polarization (empty/occupied orbital mixing on one fragment due to the presence of another fragment). The term ΔE_{disp} accounts for the dispersion corrections as introduced by Grimme and coworkers.[7e,7f]

The orbital interaction energy can be further decomposed into the contributions from each irreducible representation Γ of the interacting system (eq. (6.4)) using the extended transition state (ETS) scheme developed by Ziegler and Rauk.[14] Our approach differs in this respect from the Morokuma scheme[15] which instead attempts a decomposition of the orbital interactions into polarization and charge transfer. In systems with a clear σ/π separation (such as our planar DNA base pair AT and its equivalents), the symmetry partitioning in our approach proves to be most informative.

$$\Delta E_{oi} = \Delta E_{\sigma} + \Delta E_{\pi} \qquad \textbf{(6.4)}$$

6.3.3 Analysis of the Charge Distribution

The electron density distribution is analyzed using the Voronoi deformation density (VDD) method introduced in Ref.16. The VDD charge Q_A is computed as the (numerical) integral of the deformation density $\Delta\rho(\mathbf{r}) = \rho(\mathbf{r}) - \sum_B \rho_B(\mathbf{r})$ associated with the formation of the molecule from its atoms in the volume of the Voronoi cell of atom A (eq. (6.5)).

The Voronoi cell of an atom A is defined as the compartment of space bounded by the bond midplanes on and perpendicular to all bond axes between nucleus A and its neighboring nuclei (cf. the Wigner-Seitz cells in crystals).[10h,17]

$$Q_A = -\int_{Voronoi\ cell\ of\ A} \left(\rho(\vec{r}) - \sum_B \rho_B(\vec{r})\right) d\vec{r} \qquad \textbf{(6.5)}$$

Here, $\rho(\mathbf{r})$ is the electron density of the molecule and $\sum_B \rho_B(\mathbf{r})$ the superposition of atomic densities ρ_B of a fictitious promolecule without chemical interactions that is associated with the situation in which all atoms are neutral. The interpretation of the VDD charge Q_A is rather straightforward and transparent. Instead of measuring the amount of charge associated with a particular atom A, Q_A directly monitors how much charge flows, due to chemical interactions, out of ($Q_A > 0$) or into ($Q_A < 0$) the Voronoi cell of atom A, that is, the region of space that is closer to nucleus A than to any other nucleus.

The chemical bond between two molecular fragments can be analyzed by examining how the VDD atomic charges of the fragments change due to the chemical interactions. In Ref.5a, however, we have shown that eq. (6.5) leads to small artifacts that prohibit an accurate description of the subtle changes in atomic charges that occur in case of weak chemical interactions, such as hydrogen bonds. This is due to the so-called front-atom problem that, in fact, all atomic-charge methods suffer from. To resolve this

problem and, thus, enabling a correct treatment of even subtle changes in the electron density, the change in VDD atomic charges ΔQ_A is defined by eq. (6.6), which relates this quantity directly to the deformation density $\rho_{dimer}(\mathbf{r}) - \rho_1(\mathbf{r}) - \rho_2(\mathbf{r})$ associated with forming the overall molecule (i.e., the base pair) from the joining of monomer 1 and 2.[5a]

$$\Delta Q_A = -\int_{Voronoi\ cell\ of\ A} \left(\rho_{dimer}(\vec{r}) - \rho_1(\vec{r}) - \rho_2(\vec{r})\right) d\vec{r} \qquad \textbf{(6.6)}$$

Again, ΔQ_A has a simple and transparent interpretation: it directly monitors how much charge flows out of ($\Delta Q_A > 0$) or into ($\Delta Q_A < 0$) the Voronoi cell of atom A as a result of the chemical interactions between monomer 1 and 2 in the dimer.

This functionality is extended to also enable a decomposition of the charge redistribution per atom ΔQ_A into a component associated with the Pauli repulsion ΔE_{Pauli} and a component associated with the bonding orbital interactions ΔE_{oi}:

$$\Delta Q_A = \Delta Q_{A,Pauli} + \Delta Q_{A,oi} \qquad \textbf{(6.7)}$$

This charge decomposition constitutes a complete bond analysis tool that mirrors the ΔE_{Pauli} and ΔE_{oi} terms occurring in the bond energy decomposition of eq. (6.3) described in Section 6.3.2 (note that ΔV_{elstat} is not associated with any charge redistribution nor the empirical ΔE_{disp}).

The Pauli repulsion ΔE_{Pauli} is the energy change associated with going from the superposition of unperturbed monomer densities $\rho_1 + \rho_2$ to the wave function $\Psi^0_{dimer}=N\hat{A}[\Psi_1\Psi_2]$ that properly obeys the Pauli principle through explicit anti-symmetrization ($\hat{A}$ operator) and renormalization (N constant) of the product of monomer wave functions.[18] The deformation density $\Delta\rho(\mathbf{r}) = \rho_{dimer} - \rho_1 - \rho_2$ associated with the formation of the dimer from the monomers is now divided into two components (eq. (6.8)):

$$\Delta\rho(\vec{r}) = \Delta\rho_{Pauli}(\vec{r}) + \Delta\rho_{oi}(\vec{r}) \qquad \textbf{(6.8)}$$

Here, $\Delta\rho_{Pauli} = \rho^0_{dimer} - \rho_1 - \rho_2$ is associated with the Pauli repulsive orbital interactions and $\Delta\rho_{oi} = \rho_{dimer} - \rho^0_{dimer}$ is associated with the bonding orbital interactions; ρ^0_{dimer} is the density belonging to Ψ^0_{dimer}.

Thus, the change in atomic charge caused by Pauli repulsion between the monomers in the complex is defined by eq. (6.9) and the corresponding change caused by charge transfer and polarization is given by eq. (6.10).

$$\Delta Q_{A,\,Pauli} = -\int_{\substack{Voronoi\ cell\ of\ A \\ in\ dimer}} \left(\rho^0{}_{dimer}(\vec{r}) - \rho_1(\vec{r}) - \rho_2(\vec{r})\right) d\vec{r} \qquad \textbf{(6.9)}$$

$$\Delta Q_{A,\,oi} = -\int_{\substack{Voronoi\ cell\ of\ A \\ in\ \mathrm{dimer}}} \left(\rho_{\mathrm{dimer}}(\vec{r}) - \rho^{0}_{\mathrm{dimer}}(\vec{r})\right) d\vec{r} \qquad \textbf{(6.10)}$$

With eqs. (6.9) and (6.10), we are able to measure quantitatively and separately the charge redistributions associated with the energy component $\Delta E_{\mathrm{Pauli}}$ and with the orbital interaction component ΔE_{oi}.

The $\Delta Q_{\mathrm{A,Pauli}}$ and $\Delta Q_{\mathrm{A,oi}}$ can be further decomposed into contributions from the various irreducible representations Γ of the dimer, e.g., the σ and the π component (for the planar, C_s symmetric dimers):

$$\Delta Q^{\Gamma}_{A,\,Pauli} = -\int_{\substack{Voronoi\ cell\ of\ A \\ in\ \mathrm{dimer}}} \left(\rho^{0,\Gamma}{}_{\mathrm{dimer}}(\vec{r}) - \rho^{\Gamma}_{1}(\vec{r}) - \rho^{\Gamma}_{2}(\vec{r})\right) d\vec{r} \qquad \textbf{(6.11)}$$

$$\Delta Q^{\Gamma}_{A,\,oi} = -\int_{\substack{Voronoi\ cell\ of\ A \\ in\ \mathrm{dimer}}} \left(\rho^{\Gamma}{}_{\mathrm{dimer}}(\vec{r}) - \rho^{0,\Gamma}_{\mathrm{dimer}}(\vec{r})\right) d\vec{r} \qquad \textbf{(6.12)}$$

Here, the density ρ^{Γ} is obtained as the sum of orbital densities of the occupied molecular orbitals belonging to the irreducible representation Γ (eq. (6.3)):

$$\rho^{\Gamma} = \sum_{i\in\Gamma}^{occ} \left|\psi_i^{\Gamma}\right|^2 \qquad \textbf{(6.13)}$$

It appears that in particular the decomposition of $\Delta Q_{\mathrm{A}}{}^{\sigma}$ into a Pauli repulsion and a bonding orbital interaction component makes it possible to reveal small charge-transfer effects that are otherwise masked by the charge redistribution caused by Pauli repulsion (see Section 6.4.3).

6.4 Results and Discussion

6.4.1 Structure and Stability of AT and its analogues

To study the importance of the π electrons and aromaticity on the hydrogen bonds of the DNA base pair AT, we have investigated computationally all the possible dimers of A and its smaller mimics A' and A" with T and its smaller mimics T' and T". The hydrogen bond distances and energies calculated at the BLYP-D3(BJ)/TZ2P level of theory for the possible dimers (AT, AT', AT", A'T, A'T', A'T", A"T, A"T' and A"T") are shown in Figure 6.1. The optimal structures of these dimers have been obtained in C_S symmetry and monomers in C_1 symmetry.

From this computational investigation it can be deduced that the hydrogen bond energy changes slightly from -16.8 kcal·mol^{-1} to -15.2 kcal·mol^{-1}, when the size of the aromatic system or the number of π electrons is varied. However, the difference in energy between the largest system AT and the smallest

dimer A"T" is only 0.6 kcal·mol^{-1}. The geometrical changes in the hydrogen bond distances are more pronounced (> 0.1Å) when the number of π electrons is modified. From A to A' and A", the N6(H)···O4 and N1···(H)N3 distances are approximately similar when pairing with T, T' or T". However, when we keep A (or A', A") the same and pair it with T, T' and T", the pattern in the hydrogen bond distances changes: for T and T' the N6–O4 distance is larger (by 0.05–0.08Å) than the N1–N3 distance whereas for T" the N6–O4 distance is shorter (by 0.2–0.6Å) than the N1–N3 distance.

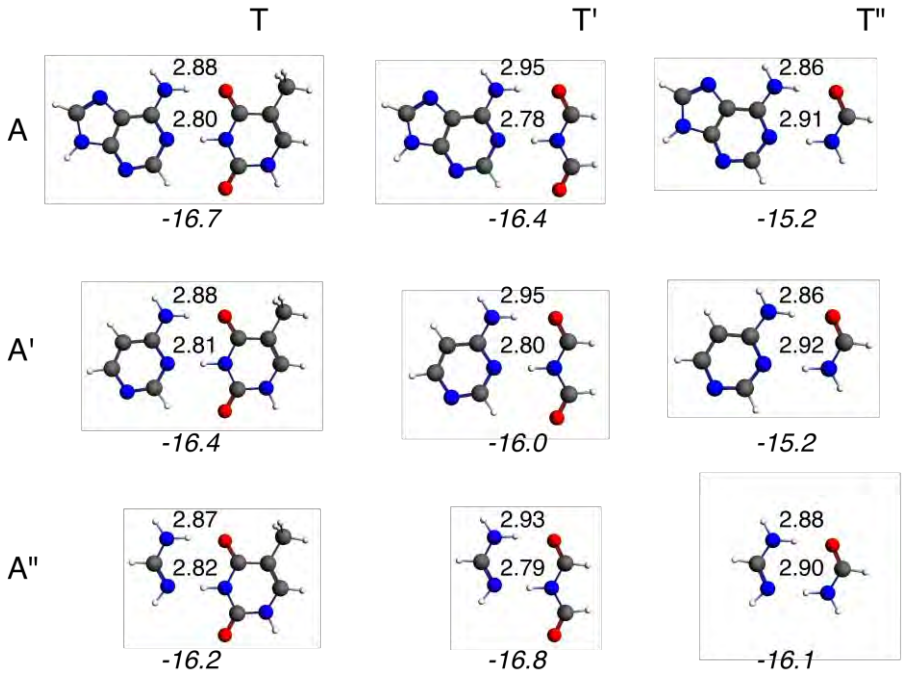

Figure 6.1: Hydrogen bond distances (in Å) and energies (in kcal·mol^{-1}) for adenine-thymine AT and its smaller analogues at the BLYP-D3(BJ)/TZ2P level of theory.

6.4.2 Nature of the hydrogen bond interaction

In the next part, we will discuss the nature of the hydrogen bonds in AT and its smaller mimics. Previous work,[5a] on the nature of the Watson-Crick base pairs AT and GC revealed the importance of electrostatic and covalent interactions in the bonding mechanism.

Electronic structure of A versus A' and A" and of T versus T' and T"

Previously, we showed that A and T are electronically complementary, that is, the proton-acceptor atoms have a negative charge whereas the corresponding protons they face are all positively charged. This is also the case for the smaller mimics of A and T (as can be seen in Figure 6.2). The differences in charge of the atoms N1 and H6 for A, A' and A", and of H3 and O4 for T, T' and T" are small as expected from the small differences in hydrogen bond energies and lengths.

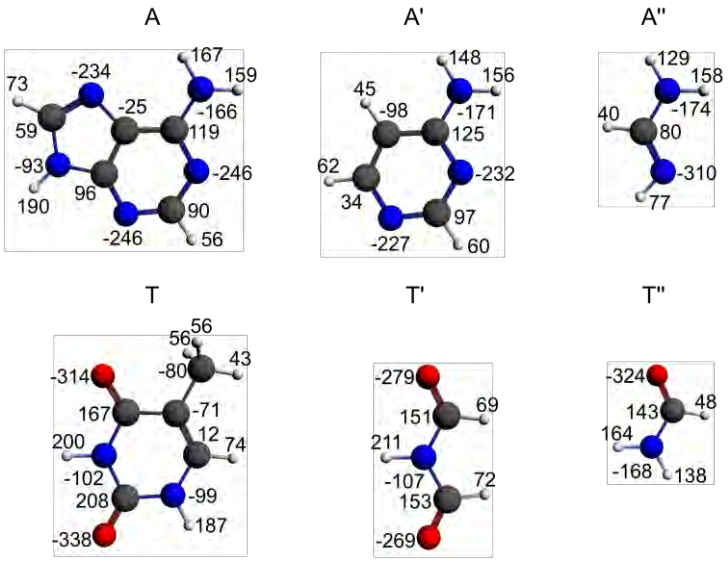

Figure 6.2: VDD atomic charges (in mili-electrons) of the prepared monomers (see eq. (6.5)).

Next, we consider the possibility of charge-transfer interactions in the σ-electron system. Figure 6.3 displays the basic features in the electronic structures of the DNA bases A and T that lead to the donor-acceptor orbital interactions: a lone pair on a proton-acceptor nitrogen or oxygen atom pointing toward and donating charge into the unoccupied σ* orbital of an N–H group of the other base. This leads to the formation of a weak covalent bond which is $\sigma_{LP} + \sigma^*_{N-H}$ bond. For a complete description of the covalent component in the hydrogen bonds of AT, see Ref.5a.

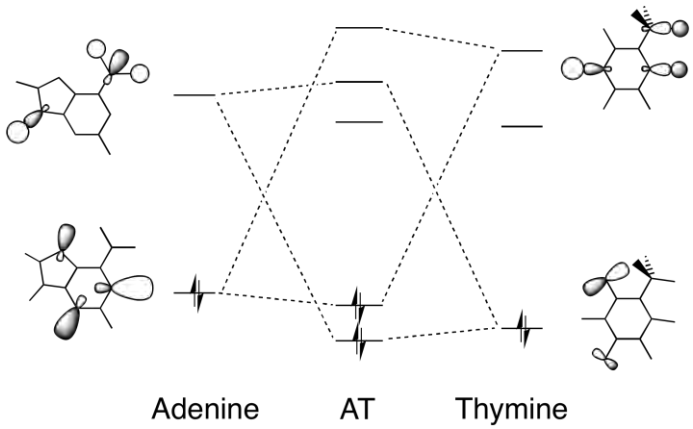

Figure 6.3: Molecular orbital diagram with the most pronounced donor-acceptor interactions in the N6(H)···O4 and N1···(H)N3 hydrogen bonds between adenine and thymine.

For the same donor-acceptor interactions to occur in the different dimers, the smaller mimics of A and T need to possess similar frontier orbitals in the σ electronic system. In Figure 6.4, the frontier orbitals of A, A', A", T, T' and T" are depicted.

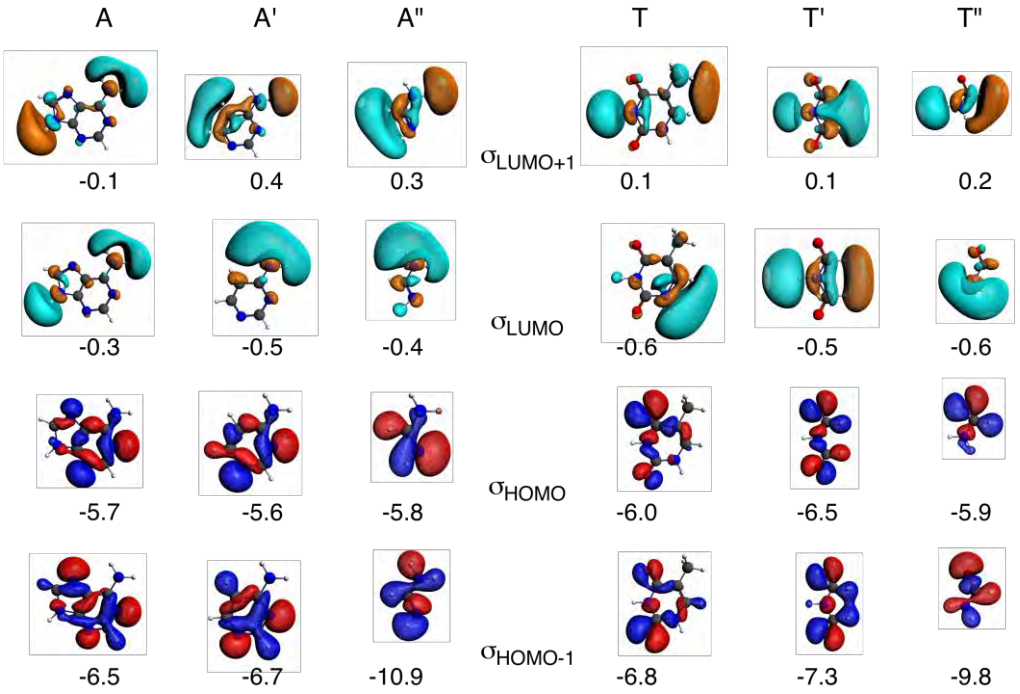

Figure 6.4: Frontier orbitals of the monomers (HOMO-1, HOMO, LUMO and LUMO+1) in the σ electronic system, with the corresponding energies (eV).

The orbitals are very similar except for the σ_{HOMO-1} of A" and T", which have only one proton-acceptor nitrogen or oxygen atom, respectively, and therefore, also have only one lone-pair character orbital. The donor-acceptor interactions occur between the σ_{HOMO-1} and σ_{HOMO} of A (or A', A") and the σ_{LUMO} or σ_{LUMO+1} of T (or T', T") for the N···(H)N hydrogen bond. For the other hydrogen bond, N(H)···O, the interaction occurs between the σ_{HOMO-1} and σ_{HOMO} of T (or T', T") and the σ_{LUMO} or σ_{LUMO+1} of A (or A', A"). Note that for A", the donor-acceptor interactions occur only between the σ_{HOMO} of A" and the σ_{LUMO} or σ_{LUMO+1} of T, T' or T" for the N···(H)N hydrogen bond, and for T", the donor-acceptor interactions occur between the σ_{HOMO} of T" and the σ_{LUMO} or σ_{LUMO+1} of A, A' or A" for the N(H)···O hydrogen bond.

The donor-acceptor interactions in the σ electronic system lead to small depopulations of the occupied σ-orbitals and small populations of the unoccupied σ-orbitals of the monomers when they form the complex. In Table 6.1, the values of Gross populations for the σ_{HOMO-1}, σ_{HOMO}, σ_{LUMO} and σ_{LUMO+1} of the different monomers are given. The Gross populations are obtained from the calculation where the prepared monomers (that is in the geometry that they acquire in the dimer) are combined together to form the dimer. The values of the Gross populations are small (mostly less than 0.10 electrons) which is in line with previous work on hydrogen bonds.[5a] Other orbitals such as the σ_{HOMO-3} or σ_{HOMO-2} can also be slightly depopulated or such as the σ_{LUMO+2} or σ_{LUMO+3} slightly populated, but as these are not the main interactions, we have left them out of Table 6.1.

Quantitative decomposition of the hydrogen bond energy

In the previous part, we established that the mimics of A and T have suitable charge distributions for electrostatically attracting each other and after having established the occurrence of σ charge transfer and π polarization (see also previous work[5a]), we want to quantitatively assess the importance of the various components of the dimerization energy as we did for the Watson-Crick base pair AT. Thus, we have carried out the bond energy decomposition for the different dimers (see Table 6.1).

The bond energy is first decomposed into a preparation energy ΔE_{prep} for the deformation of the monomers and the interaction energy between the monomers, ΔE_{int}. The former is small (1.4 to 2.5 kcal·mol^{-1}) as the monomers are only slightly deformed due to the hydrogen bonds. The trend of the bond energy is followed by the interaction energy. The values of the interaction energy deviate somewhat more and are between -16.7 kcal·mol^{-1} and -19.4 kcal·mol^{-1}.

Further decomposition of the interaction energy shows that, in all cases, the electrostatic interaction ΔV_{elstat} is not capable of providing a net bonding interaction as it only compensates partly the Pauli-repulsive orbital interactions ΔE_{Pauli}. Without the bonding orbital interactions, ΔE_{oi}, the monomers would repel each other. The orbital interaction is divided into a σ component and a π component. ΔE_{σ} consists mainly of the electron donor-acceptor interactions mentioned above. The π component (ΔE_{π}) accounts basically for the polarization in the π system, which turns out to partly compensate the local build-up of charge caused by the charge-transfer interactions in the σ system (see section 6.4.3 on charge redistribution). The dispersion term comprises the correction for dispersion interactions and lies between -3.8 kcal·mol^{-1} and -5.4 kcal·mol^{-1}.

The σ orbital interaction term ΔE_{σ} is the sum of the donor-acceptor interactions in both hydrogen bonds. To get a quantitative estimate of how large each donor-acceptor interaction is in the individual N(H)···O and N···(H)N bond, we used the same technique as in Ref.5a where we removed σ and π virtuals for the AT base pairs. In this previous work,[5a] we removed the π virtuals of both bases to switch off the polarization in the π electronic system. Furthermore, we removed the σ virtuals from one base to switch off the donor-acceptor interactions of one of the hydrogen bonds. The same procedure was followed for the A, T and its analogues. The σ interactions of the hydrogen bonds, $\Delta E_{\sigma}(\sigma,–;\sigma,–)$, were analyzed without occurrence of the π polarization (that is the π virtuals were removed in the calculation from both monomers). Comparison of ΔE_{σ} from Table 6.1 and $\Delta E_{\sigma}(\sigma,–;\sigma,–)$ from Figure 6.5 shows that when the π polarization is allowed, the donor-acceptor interactions are only 0.3 kcal·mol^{-1} lower. Therefore, we can conclude that also for the smaller mimics of A and T the synergy between σ and π is small. Figure 6.5 also displays the donor-acceptor interactions in the individual hydrogen bonds $\Delta E_{\sigma}(\sigma,–;–,–)$ for N(H)···O with the σ virtuals removed from T, T' or T" and $\Delta E_{\sigma}(–,–;\sigma,–)$ for N···(H)N with the σ virtuals removed from A, A' or A".

Table 6.1: Bonding analyses (in kcal·mol^{-1}) and populations (in electrons) for AT and its smaller analogues.[a]

	AT	AT’	AT’’	A’T	A’T’	A’T”	A”T	A”T’	A”T”
Bond Energy									
ΔE	-16.7	-16.4	-15.2	-16.4	-16.0	-15.2	-16.2	-16.8	-16.1
ΔE_{prep}	1.8	2.0	1.4	1.8	1.9	1.5	2.3	2.5	1.8
ΔE_{int}	-18.5	-18.4	-16.7	-18.3	-17.9	-16.7	-18.5	-19.4	-17.9
Bond Energy Decomposition									
ΔE_{Pauli}	39.9	39.4	32.0	38.6	37.9	31.3	38.2	38.2	32.3
ΔV_{elstat}	-31.9	-31.2	-27.3	-31.0	-30.0	-26.8	-31.2	-31.5	-28.4
ΔE_{disp}	-5.4	-5.0	-3.9	-5.3	-4.9	-3.9	-4.1	-3.8	-3.4
ΔE_{oi}	-21.1	-21.6	-17.5	-20.5	-20.8	-17.2	-21.5	-22.2	-18.5
ΔE_{σ}	-19.5	-20.0	-15.9	-19.0	-19.3	-15.6	-19.7	-20.4	-16.6
ΔE_{π}	-1.6	-1.6	-1.6	-1.5	-1.6	-1.6	-1.8	-1.9	-1.9
Gross populations of A									
σ_{LUMO+1}	0.01	0.01	0.01	0.01	0.01	0.02	0.02	0.02	0.02
σ_{LUMO}	0.01	0.01	0.02	0.02	0.01	0.02	0.01	0.01	0.01
σ_{HOMO}	1.95	1.95	1.97	1.96	1.95	1.97	1.88	1.87	1.91
$\sigma_{HOMO–1}$	1.97	1.97	1.98	1.96	1.96	1.98	2.00	2.00	2.00
Gross populations of T									
σ_{LUMO+1}	0.04	0.00	0.03	0.03	0.01	0.03	0.06	0.01	0.04
σ_{LUMO}	0.01	0.08	0.02	0.01	0.08	0.02	0.01	0.10	0.03
σ_{HOMO}	1.97	1.98	1.95	1.97	1.98	1.95	1.97	1.98	1.95
$\sigma_{HOMO–1}$	1.99	1.97	2.00	1.99	1.97	2.00	1.99	1.98	2.00

[a] Energies and geometries computed at BLYP-D3(BJ)/TZ2P in C_s symmetry for base pair and C_1 for monomer.

The synergism within the σ system between charge transfer from one base to the other through one hydrogen bond and back through the other hydrogen bond can be investigated by comparison of ΔE_{σ}(σ,–;σ,–) with the sum of ΔE_{σ}(σ,–;–,–) and ΔE_{σ}(–,–;σ,–). In accordance with our previous work, the values show that the hydrogen bonds donating charge in opposite directions operate independently. Furthermore, the N···(H)N hydrogen bond is twice as strong as the N(H)···O hydrogen bond for the dimers with T and T’, but for the dimers with T” the hydrogen bonds are of equal strength.

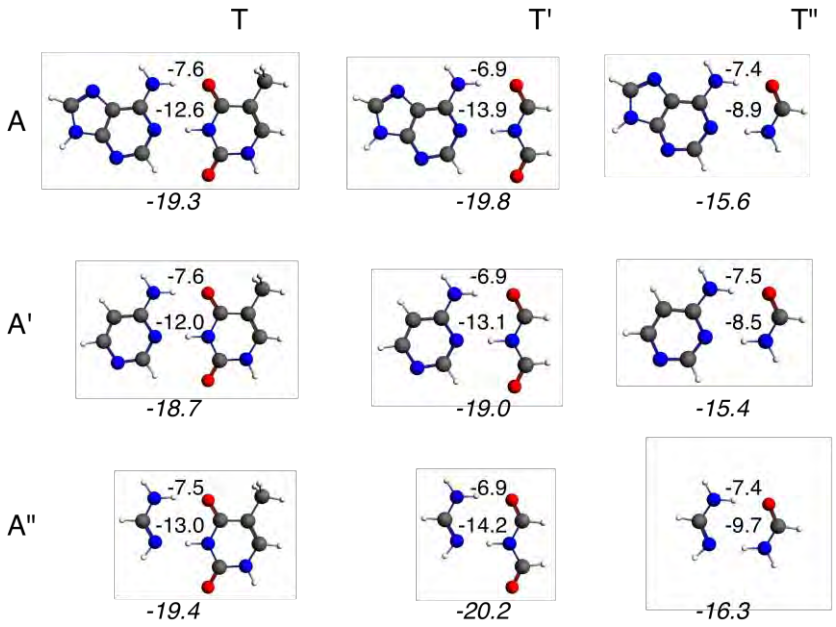

Figure 6.5: ΔE_{σ}(σ,–; σ,–) of both hydrogen bonds and ΔE_{σ}(σ,–;–,–) for the N(H)···O hydrogen bond, and ΔE_{σ}(–,–;σ,–) for the N···(H)N hydrogen bond (see main text).

6.4.3 Charge redistribution due to hydrogen bonding

Up till now, our investigation showed that the smaller mimics of A and T have the same bonding characteristics as the dimer AT, which implies that for these hydrogen bonds the atoms participating in the hydrogen bonds do not need to be connected to an aromatic ring to achieve this strength of hydrogen bonding. In this part, we want to investigate the electronic rearrangements in the σ and π electronic system due to the formation of the hydrogen bonds. For this purpose, we use the partioning of the VDD atomic charges into σ and π components, see Section 6.3.3, eq. (6.11) and (6.12). (For the charge rearrangements due to the Pauli repulsive interaction see Figures S5 and S6, p.135).

The σ and π charge rearrangements for the nine dimers are depicted in Figure 6.6 and Figure 6.7 respectively. The $\Delta Q^{\sigma}_{A,oi}$ values reveal a clear charge-transfer picture for AT and its mimics: negative charge is lost on the electron-donor atoms whereas there is a significant accumulation of negative charge on the nitrogen atoms of the electron-accepting N–H bonds (see Figure 6.6).

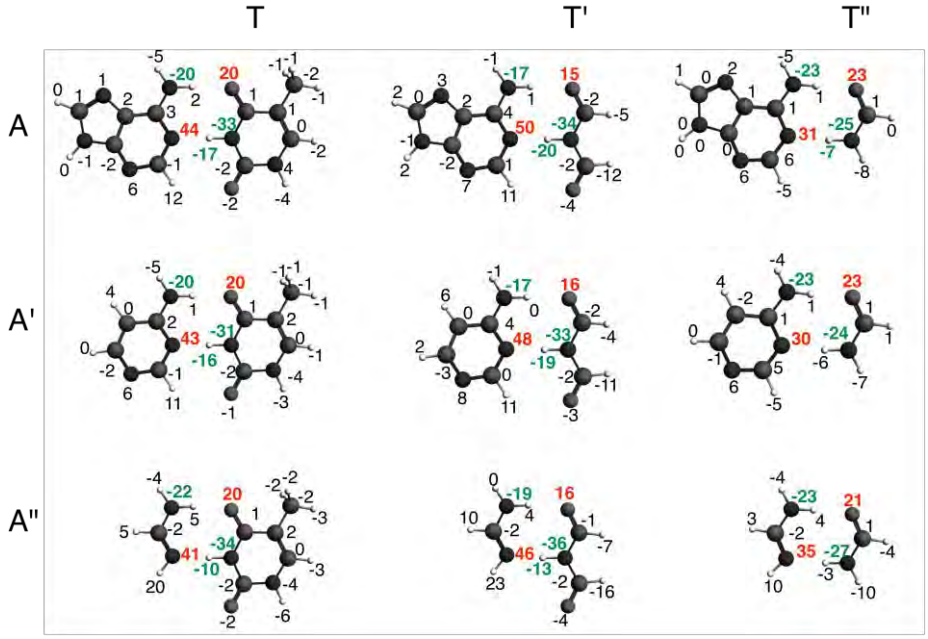

Figure 6.6: Voronoi deformation density (VDD) atomic charges ($\Delta Q^{\sigma}_{A,oi}$, in milli-electrons) associated with the formation of the different dimers. The contributions stemming from the σ electrons are given.

The π-electron density of the bases is polarized in such a way that the build-up of charge arising from charge-transfer interactions in the σ system is counteracted and compensated: the electron-donor atoms gain π density and the nitrogen atoms of the electron-accepting N–H bonds lose π density (compare $\Delta Q^{\sigma}_{A,oi}$ and $\Delta Q^{\pi}_{A,oi}$ in Figure 6.6 and Figure 6.7). This π charge rearrangement is in agreement with the Lewis structure proposed by Gilli *et al.*[3] (see Scheme 6.1). The charge rearrangements for T" are somewhat smaller than for T and T', which is in line with the weaker orbital interactions for T". Furthermore, we see that the charge rearrangements in σ and π electronic systems do not depend on the aromatic ring.

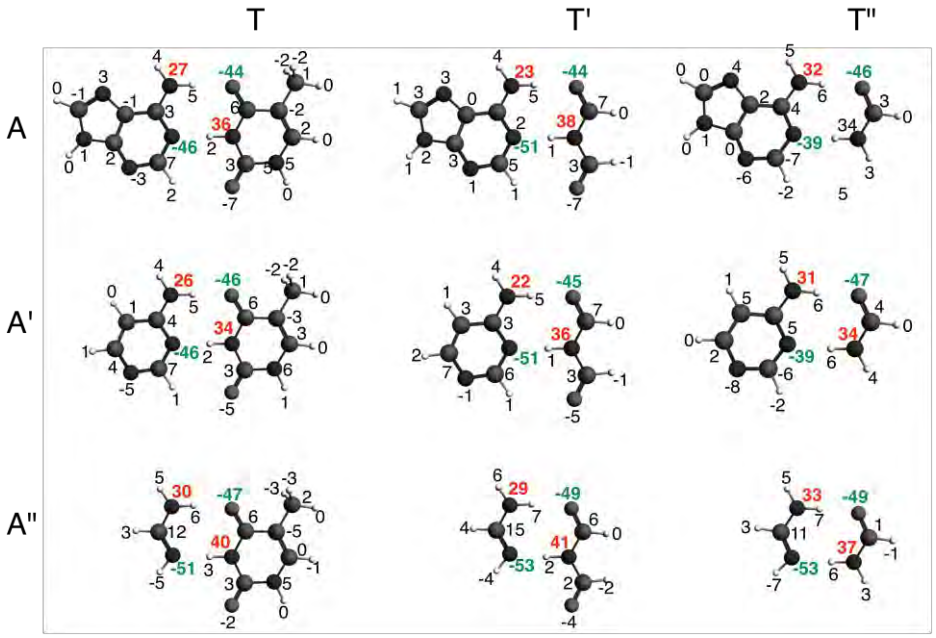

Figure 6.7: Voronoi deformation density (VDD) atomic charges ($\Delta Q^{\pi}_{A,oi}$, in milli-electrons) associated with the formation of the different dimers. The contributions stemming from the π electrons are given.

6.4.4 *sp*² versus *sp*³ hybridization

In the previous section, we established that the number of π electrons does not influence the hydrogen bond energy: that is the strength of the hydrogen bonds of AT and its smaller analogues deviate less than 1.6 kcal·mol^{-1} from each other. This leads us to conclude that the hydrogen donor and acceptor atoms do not need to be part of an aromatic ring to establish this strong hydrogen bonding, but do they need to be *sp*^{2} hybridized? If so, how then does the *sp*^{2} hybridization assist the hydrogen bonds, which results in a shortening of the distance between proton donor and proton acceptor?[3]

This part will address this question if the hydrogen donor and acceptor atoms need to be *sp*^{2}-hybridized atoms by comparing A"T" (*sp*^{2}) to a"t" (*sp*^{3}), see Figure 6.8. The latter exists in the chair and boat conformation and in analogy to cyclohexane, the chair conformation is 4.8 kcal·mol^{-1} lower in energy (see SI, p.135). The hydrogen bond energy of the *sp*^{2}-hybridized A"T" is 7.9 kcal·mol^{-1} stronger bound than its saturated equivalent (see Table 6.2). This cannot be attributed to the π electrons as the π polarisation in the *sp*^{2}-hybridized A"T" amounts only to –1.9 kcal·mol^{-1} (see Table 6.1). At the equilibrium structures, all the bonding components of the interaction energy ΔE_{oi} and ΔV_{elstat} are smaller for a"t", than for A"T", but also the Pauli repulsion is smaller in the case of a"t".

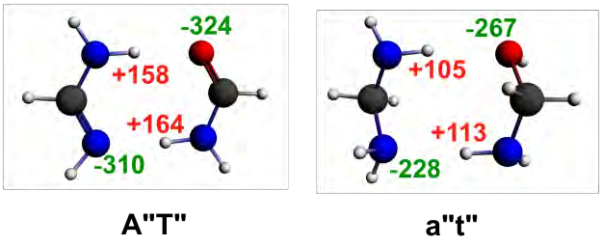

Figure 6.8: Atomic Voronoi deformation density (VDD) charges (in mili-electrons) for front atoms in A''T'' and a''t''.

To analyze where the difference due to hybridization comes from, we compressed a”t” to the distance R(sp^2): that is the hydrogen bond distances of A”T”. We also expanded A”T” to the distances of R(sp^3): that is the hydrogen bond distances of a”t”. At R(sp^2) the interaction energy of A”T” amounts to -17.9 kcal·mol^{-1} and of a”t” to -7.4 kcal·mol^{-1}. Comparison of the components of the interaction energy at the R(sp^2) distance for both dimers reveals that the stronger interaction energy of A”T” can be ascribed to the stronger electrostatic interaction as well as the larger orbital interaction. We see that both dimers have almost the same Pauli interaction (32.3 for A”T” and 34.3 for a”t”). The electrostatic interaction and the orbital interaction are both stronger (by 4.6 kcal·mol^{-1} and 4.8 kcal·mol^{-1}, respectively) for A’’T’’ than for a’’t’’ at the distance R(sp^2). The π resonance only amounts to –1.9 kcal·mol^{-1} (see Table 6.2). The smaller ΔV_{elstat} for a”t” compared with A”T”, at the same R(sp^2) distance, can be understood with the atomic Voronoi deformation density charges depicted in Figure 6.8. The absolute values of the VDD charges of the front atoms in a”t” are smaller than in the A”T”.

The decomposition of the interaction energy is presented in graphical form in Figure 6.9 at the R(sp^2) and R(sp^3) distances.

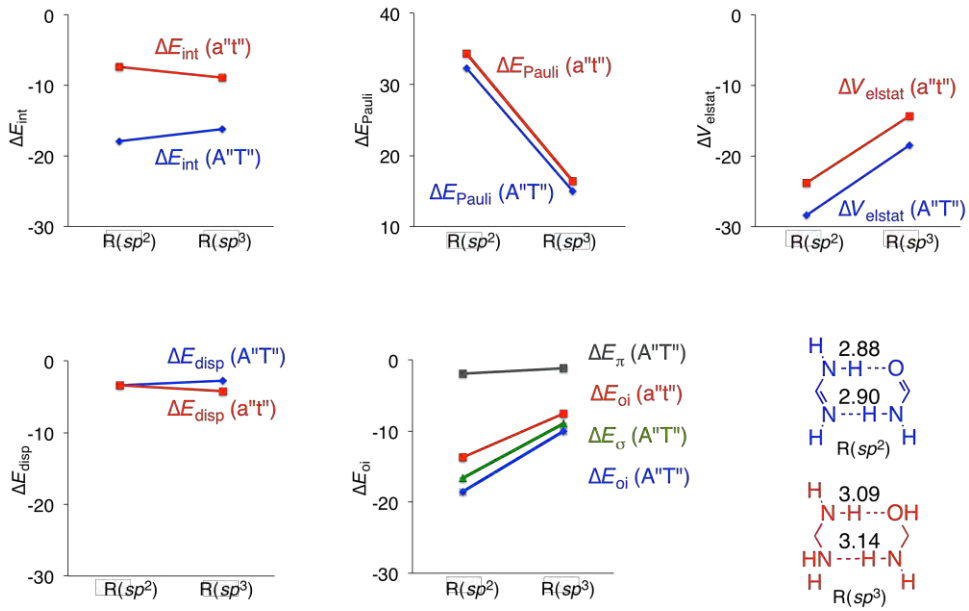

Figure 6.9: Energy decomposition analysis for A”T” and a”t” at the equilibrium distance R(sp^2) of A”T” and at the equilibrium distance R(sp^3) of a”t”.

The augmentation of Pauli repulsion by compressing the dimers A”T” and a”t” from R(sp^3) to the R(sp^2) distance has to be overcome by the attractive contributions to the bonding energy. The electrostatic interaction gains for both dimers equally and the dispersion correction does not change much by the compression. The largest difference due to the shortening is seen in the orbital interaction: A”T” gains more rapidly (blue line in ΔE_{oi}) than a”t” (red line in ΔE_{oi}). Decomposition of ΔE_{oi} of A”T” into ΔE_{σ} and ΔE_{π} of A”T” shows that it is the σ component in the orbital interaction (green line) that is responsible for strengthening the hydrogen bonds for the sp^2-hybridized dimers, as it increases more rapidly. This results in an equilibrium structure of A”T” with shorter hydrogen bonds than for a’’t’’.

We are left with the question why the σ-component of the orbital interaction is much more favorable for sp^2 than sp^3. To understand this, we performed Kohn-Sham MO analysis on the hydrogen bonds in A"T" and a"t" at the R(sp^2) and R(sp^3) distances (see Table 6.2).

Table 6.2: Bonding analyses (in kcal·mol^{-1}), populations (in electrons), orbital energies (in eV) and distances (in Å) for adenine-thymine analogues A"T" and a"t".[a]

	A"T"	A"T" at R(sp^3)[b]		a"t''	a"t'' at R(sp^2)[b]
Distances					
N(H)···O	2.88	3.09		3.09	2.88
N···(H)N	2.90	3.14		3.14	2.90
Bond energy					
ΔE	-16.1	-14.4		-8.2	-6.7
ΔE_{prep}	1.8	1.8		0.7	0.7
ΔE_{int}	-17.9	-16.2		-8.9	-7.4
ΔE_{Pauli}	32.3	15.0		16.4	34.3
ΔV_{elstat}	-28.4	-18.5		-14.4	-23.8
ΔE_{disp}	-3.4	-2.7		-3.4	-4.2
ΔE_{oi}	-18.5	-10.0		-7.5	-13.7
ΔE_{σ}	-16.6	-8.9			
ΔE_{π}	-1.9	-1.1			
Gross populations: N(H)···O			***Gross populations: N(H)···O***		
σ_{LUMO+1} of A"	0.02	0.02	LUMO+1 of a"	0.01	0.01
σ_{LUMO} of A"	0.01	0.01	LUMO of a"	0.01	0.02
σ_{HOMO} of T"	**1.95**	**1.97**	HOMO of t"	2.00	2.00
σ_{HOMO-1} of T"	2.00	2.00	HOMO-1 of t"	**1.98**	**1.96**
Gross populations: N···(H)N			***Gross populations: N···(H)N***		
σ_{LUMO+1} of T"	0.04	0.03	LUMO+1 of t"	0.02	0.02
σ_{LUMO} of T"	0.03	0.02	LUMO of t"	0.01	0.01
σ_{HOMO} of A"	**1.91**	**1.94**	HOMO of a"	**1.95**	**1.93**
σ_{HOMO-1} of A"	2.00	2.00	HOMO-1 of a"	1.99	1.99
Orbital energies of A"			***Orbital energies of a"***		
σ_{LUMO+1}	0.29		LUMO+1	0.30	
σ_{LUMO}	-0.39		LUMO	-0.24	
σ_{HOMO}	**-5.80**		HOMO	**-5.31**	
σ_{HOMO-1}	-10.86		HOMO-1	-5.60	
Orbital energies of T"			***Orbital energies of t"***		
σ_{LUMO+1}	0.18		LUMO+1	0.41	
σ_{LUMO}	-0.64		LUMO	-0.49	
σ_{HOMO}	**-5.85**		HOMO	-5.77	
σ_{HOMO-1}	-9.80		HOMO-1	**-6.54**	
Overlap <A"|T"> for N(H)···O			***Overlap <a"|t"> for N(H)···O***		
$< \sigma_{LUMO+1} \mid \sigma_{HOMO} >$	0.11	-0.10	< LUMO+1 | HOMO–1 >	-0.08	-0.08
$< \sigma_{LUMO} \mid \sigma_{HOMO} >$	0.09	-0.08	< LUMO | HOMO–1 >	-0.12	-0.11
Overlap <A"|T"> for N···(H)N			***Overlap <a"|t"> for N···(H)N***		
$< \sigma_{HOMO} \mid \sigma_{LUMO+1} >$	0.27	0.26	< HOMO | LUMO+1 >	-0.15	0.14
$< \sigma_{HOMO} \mid \sigma_{LUMO} >$	0.23	0.21	< HOMO | LUMO >	0.10	-0.10

[a] Energies and geometries computed at BLYP-D3(BJ)/TZ2P level of theory: A"T" in C_s symmetry and a"t" in C1 symmetry (chair conformation).
[b] A"T" has been elongated to the distance of a"t", R(sp^3) and a"t" compressed to the distance of A"T", R(sp^2).

The Gross populations and the energies of the frontier orbitals are given, together with the overlap between the frontier orbitals in Table 6.2. The N(H)···O hydrogen bond in A"T" is explained by a charge–

transfer interaction of 0.05 electrons from the σ_{HOMO} of T" to the σ_{LUMO} and σ_{LUMO+1} of A" (respectively 0.02 and 0.01 electrons). For a"t" this charge transfer is smaller: 0.02 electrons from the HOMO–1 of t" to the LUMO and LUMO+1 of a" (both 0.01 electrons). The electron donation and acceptation within one hydrogen bond of the dimers are not exactly of the same magnitude because there is also polarization (mixing between occupied and unoccupied) on the same monomer due to the presence of the other monomer. The smaller charge-transfer interaction in a"t" has its origin in the lower lying electron donor orbital (HOMO–1 at –6.54 eV for t" and HOMO at –5.85 eV for T"). The accepting orbitals of A" and a" do not differ so much in energy and also the overlap between the frontier orbitals is of the same size in the N(H)···O hydrogen bond of A"T" and a"t".

The charge transfer in the N···(H)N hydrogen bond is also larger in A"T" than in a"t". The σ_{HOMO} of A" donates 0.09 electrons into the accepting orbitals of T" whereas the HOMO of a" donates only 0.05 electrons in the accepting orbitals of t". In this case, the HOMO-LUMO gap between frontier orbitals cannot be held responsible for this difference as it amounts to 5.2 eV for A"T" and 4.8 eV for a"t" (nor the HOMO-LUMO+1 gap which amounts to respectively 6.0 eV and 5.7eV). However, the overlap between the frontier orbitals in A"T" is twice as large than for a"t": $\langle\sigma_{HOMO}|\sigma_{LUMO}\rangle$ amounts to 0.23 and <HOMO|LUMO> to 0.10, respectively (see Table 6.2). This is merely the consequence of the σ_{HOMO} of A" and σ_{LUMO} of T" being somewhat better directed towards each other due to the sp^2-hybridization (see Figure S7, SI p.135).

Thus, the sp^2-hybridized dimer has stronger hydrogen bonds for two different reasons: 1) because of the smaller HOMO-LUMO gap in the σ electronic system for one hydrogen bond and 2) because the overlap between the frontier orbitals in the σ system is better than in the sp^3 system for the other hydrogen bond.

6.5 Conclusions

In the present paper, we studied the π assistance to the hydrogen bonds of AT and its analogues. This investigation determined that the π assistance is not exclusively due to aromaticity, but that the sp^2-hybridization of the proton-donor and acceptor atoms already accounts for the π charge delocalization. This follows from extensive computational analyses of DNA base pair AT and its smaller mimics (AT', AT", A'T, A'T', A'T", A"T, A"T' and A"T", see Scheme 6.1) based on dispersion-corrected density functional theory (DFT-D3). The pair A"T", which is the smallest equivalent, lacks the aromatic rings of AT, but the hydrogen bond energy is very similar to the bonding energy of AT. The small geometrical and bonding differences computed for the hydrogen bonds of A"T" and the other equivalents of AT are explained with our quantitative Kohn-Sham molecular orbital (MO) and corresponding energy decomposition analyses (EDA). They reveal that the π assistance is independent of the number of π

electrons of the monomers but it is essential that the proton donor and acceptor atoms have π electrons to arrive at similar hydrogen bond energies for all mimics of AT.

Thus, the small sp^2-hybridized dimer was compared to its sp^3 mimic and subjected to a Kohn Sham MO analysis to understand where the strengthening ans shortening comes from. The hydrogen bond energy of the sp^2 system (A"T") amounts to -16.1 kcal·mol^{-1} and of the equivalent sp^3 dimer (a"t") to -8.2 kcal·mol^{-1}. This could not be explained with the assistance by the π electronic system, because the polarization in the π electronic system is only 2 kcal·mol^{-1}. The MO analysis revealed that the stronger hydrogen bonds in the sp^2 systems can be ascribed to enhanced electrostatic interactions and also better covalent interactions. The shorter hydrogen bonds in the sp^2-hybridized dimer are ascribed to two different reasons: for the N(H)···O hydrogen bond it can be explained with the smaller HOMO-LUMO gap in the σ electronic system of A"T" and for the N···(H)N hydrogen bond the reason can be found in the larger overlap between the frontier orbitals in the σ system of the sp^2 system than in the sp^3 system. Thus, it is not the assistance by the π electrons; rather, the stronger covalent interaction in the hydrogen bonds of unsaturated dimers compared with the covalency in saturated dimers is the reason for the experimental finding of smaller hydrogen bond distances for resonance-assisted AT and its smaller analogues.

6.6 References

1. G. A. Jeffrey; W. Saenger. *Hydrogen Bonding in Biological Structures*. Springer-Verlag, Berlin, **1991**; b) G. A. Jeffrey. *An Introduction to Hydrogen Bonding*. Oxford University Press, New York, Oxford, **1997**, Chapter 10; c) W. Saenger. *Principles of Nucleic Acid Structure*. Springer-Verlag, New York, Berlin, Heidelberg, Tokyo, **1984**.
2. a) J. D. Watson; F. H. C. Crick. *Nature* **1953**, *171*, 737; b) M. H. F. Wilkins, A. R. Stokes; H. R. Wilson. *Nature* **1953**, *171*, 738; c) R. E.Franklin; R. G. Gosling. *Nature* **1953**, *171*, 740.
3. G. Gilli; F. Belluci; V. Ferretti; V. Bertolasi. *J. Am. Chem. Soc.* **1989**, *111*, 1023.
4. a) P. Gilli; V. Bertolasi; V. Ferretti; G. Gilli. *J. Am. Chem. Soc.* **2000**, *122*, 10405; b) J. F. Beck; Y. Mo. *J. Comp. Chem*. **2007**, *28*, 455; c) P. Sanz; O. Mó; M. Yáñez; J. Elguero. *ChemPhysChem* **2007**, *8*, 1950; d) P. Sanz; O. Mó; M. Yáñez; J. Elguero. *J. Phys. Chem. A* **2007**, *111*, 3585; e) P. Sanz; O. Mó; M. Yáñez; J. Elguero. *Chem. Eur. J.*, **2008**, *14*, 4225; f) M. Palusiak; S. Simon; M. Solà. *J. Org. Chem.* **2006**, *71*, 5241; g) R. Kurczab; M. P. Mitoraj; A. Michalak; T. Ziegler. *J. Phys. Chem. A* **2010**, *114*, 8581; h) T. M. Krygowski; J. E. Zachara-Horeglad; M. Palusiak; S. Pelloni; P. Lazzeretti. *J. Org. Chem*. **2008**, *73*, 2138; i) C. Fonseca Guerra; H. Zijlstra; G. Paragi; F. M. Bickelhaupt. *Chem. Eur. J*. **2011**, *17*, 12612 ; j) Y. Mo. *J. Mol. Model* **2006**, *12*, 665.
5. a) C. Fonseca Guerra; F. M. Bickelhaupt; J. G. Snijders; E. J. Baerends. *Chem. Eur. J.* **1999**, *5*, 3581; b) C. Fonseca Guerra; F. M. Bickelhaupt. *Angew. Chem.* **1999**, *111*, 3120; *Angew. Chem., Int. Ed.* **1999**, *38*, 2942; c) C. Fonseca Guerra; F. M. Bickelhaupt; J. G. Snijders; E. J. Baerends. *J. Am. Chem. Soc.* **2000**, *122*, 4117; d) C. Fonseca Guerra; F. M. Bickelhaupt; E. J. Baerends. *Cryst. Growth Des.* **2002**, *2*, 239; e) C. Fonseca Guerra; Z. Szekeres; F. M. Bickelhaupt. *Chem. Eur. J*. **2011**, *17*, 8816.
6. S.C.A.H. Pierrefixe; F.M. Bickelhaupt. *Chem. Eur. J.* **2007**, *13*, 6321.
7. a) S. Grimme. *J. Comput. Chem.* **2004**, *25*, 1463; b) S. Grimme. *J. Comput. Chem.* **2006**, *27*, 1787; c) C. Fonseca Guerra; T. van der Wijst; J. Poater; M. Swart; F. M. Bickelhaupt. *Theor. Chem. Acc.* **2010**, *125*, 245; d) T. van der Wijst; C. Fonseca Guerra; M. Swart; F. M. Bickelhaupt; B. Lippert. *Angew. Chem.* **2009**, *121*, 3335; *Angew. Chem., Int. Ed*. **2009**, *48*, 3285; e) S. Grimme; S. Ehrlich;

L. Goerigk. *J. Compu. Chem.* **2011**, *32*, 1456; f) S. Grimme; J. Antony; S. Ehrlich; H. Krieg. *J. Chem. Phys.* **2010**, *132*, 154104.

8. F. M. Bickelhaupt; E. J. Baerends. *Rev. Comput. Chem.* **2000**, *15*, 1.
9. *Computer code ADF2013*: E. J. Baerends; T. Ziegler; J. Autschbach; D. Bashford; A. Bérces; F. M. Bickelhaupt; C. Bo; P. M. Boerrigter; L. Cavallo; D. P. Chong; L. Deng; R. M. Dickson; D. E. Ellis; M. van Faassen; L. Fan; T. H. Fischer; C. Fonseca Guerra; A. Ghysels; A. Giammona; S. J. A. van Gisbergen; A. W. Götz; J. A. Groeneveld; O. V. Gritsenko; M. Grüning; S. Gusarov; F. E. Harris; P. van den Hoek; C. R. Jacob; H. Jacobsen; L. Jensen; J. W. Kaminski; G. van Kessel; F. Kootstra; A. Kovalenko; M. V. Krykunov; E. van Lenthe; D. A. McCormack; A. Michalak; M. Mitoraj; J. Neugebauer; V. P. Nicu; L. Noodleman; V. P. Osinga; S. Patchkovskii; P. H. T. Philipsen; D. Post; C. C. Pye; W. Ravenek; J. I. Rodríguez; P. Ros; P. R. T. Schipper; G. Schreckenbach; J. S. Seldenthuis; M. Seth; J. G.Snijders; M. Solà; M. Swart; D. Swerhone; G. te Velde; P. Vernooijs; L. Versluis; L. Visscher; O. Visser; F. Wang; T. A. Wesolowski; E. M. van Wezenbeek; G. Wiesenekker; S. K. Wolff; T. K. Woo; A. L. Yakovlev. SCM, Theoretical Chemistry, Vrije Universiteit, Amsterdam, The Netherlands, http://www.scm.com.
10. a) G. te Velde; F. M. Bickelhaupt; E. J. Baerends; C. Fonseca Guerra; S. J. A. van Gisbergen; J. G. Snijders; T. Ziegler. *J. Comput. Chem.* **2001**, *22*, 931; b) C. Fonseca Guerra; O. Visser; J. G. Snijders; G. Te Velde; E. J. Baerends in *Methods and Techniques for Computational Chemistry* (Eds.: E. Clementi, G. Corongiu), STEF, Cagliari, **1995**, pp. 305-395; c) E. J. Baerends; D. E. Ellis; P. Ros. *Chem. Phys.* **1973**, *2*, 41; d) E. J. Baerends; P. Ros; *Chem. Phys.* **1975**, 8, 412; e) E. J. Baerends; P. Ros. *Int. J. Quantum Chem. Symp.* **1978**, 14 (S*12)*, 169; f) C. Fonseca Guerra; J. G. Snijders; G. te Velde; E. J. Baerends. *Theor. Chem. Acc.* **1998**, *99*, 391; g) P. M. Boerrigter; G. te Velde; E. J. Baerends. *Int. J. Quantum Chem.* **1988**, *33*, 87; h) G. te Velde; E. J. Baerends. *J. Comp. Phys.* **1992**, *99*, 84; i) J. G. Snijders; P. Vernooijs; E. J. Baerends. *At. Data Nucl. Data Tables* **1981**, *26*, 483; j) L. Versluis; T. Ziegler. *J. Chem. Phys.* **1988**, *88*, 322.
11. A.D. Becke. *Phys. Rev. A* **1988**, *38*, 3098.
12. C. Lee; W. Yang; R. G. Parr. *Phys. Rev. B* **1988**, *37*, 785.
13. a) A.D. Becke; E.R. Johnson. *J .Chem. Phys.* **2005**, *122*, 154101; b) E.R. Johnson; A.D. Becke. *J. Chem. Phys.* **2005**, *123*, 024101; c) E.R. Johnson; A.D. Becke. *J. Chem. Phys.* **2006**, *124*, 174104.
14. a) T. Ziegler; A. Rauk. *Inorg. Chem*. **1979**, *18*, 1755; b) T. Ziegler; A. Rauk. *Inorg. Chem*. **1979**, *18*, 1558; c) T. Ziegler; A. Rauk. *Theor. Chim. Acta* **1977**, *46*, 1.
15. a) K. Morokuma. *J. Chem. Phys.* **1971**, *55*, 1236; b) K. Kitaura ; K. Morokuma. *Int. J. Quantum Chem.* **1976**, *10*, 325.
16. a) C. Fonseca Guerra; J. W. Handgraaf; E. J. Baerends; F. M. Bickelhaupt. *J. Comput. Chem.* **2004**, *25*, 189; b) F. M. Bickelhaupt; N. J. R. van Eikema Hommes; C. Fonseca Guerra. E. J. Baerends, *Organometallics* **1996**, *15*, 2923.
17. C. Kittel. *Introduction to Solid State Physics*. 6th ed., Wiley, New York, **1986**.
18. F. M. Bickelhaupt and E. J. Baerends. *Rev. Comput. Chem.* edited by K. B. Lipkowitz and D. B. Boyd (Wiley-VCH, New York, **2000**), Vol. *15*, pp. 1-86.
19. C. Fonseca Guerra; F. M. Bickelhaupt. *J. Chem. Phys.* **2003**, *119*, 4262.

7. Theoretical Study on the Resonance-Assisted Hydrogen Bonding of DNA Base Pair Guanine-Cytosine (GC) and Mimics

7.1 Abstract

Computational analyses based on dispersion-corrected density functional theory (DFT-D3) on the hydrogen bond interaction of guanine-cytosine (GC) base pair and its smaller analogues have been performed to investigate the influence of aromaticity. We show that the 6-membered ring of guanine is needed to achieve a similar bonding energy as GC. The small geometrical and bonding differences computed for the hydrogen bonds of GC and its analogues are explained with the quantitative Kohn-Sham molecular orbital theory (MO) and a corresponding energy decomposition analysis (EDA).

7.2 Introduction

Hydrogen bonds play a crucial role in many biochemical processes and supermolecular chemistry.[1] After observing the X-ray diffraction images of DNA obtained by Rosalind Franklin, Watson and Crick proposed in 1953 that hydrogen bonds are essential for the working of the genetic code.[2] In DNA, the two helical strands of nucleotides are held together by the hydrogen bonds that arise between a purine- and a pyrimidine-derived nucleic base.

Gilli *et al.*[3] proposed that the hydrogen bonds in DNA base pairs are reinforced by π assistance, the so-called resonance-assisted hydrogen bonding (RAHB). The resonance of the conjugated double bonds assists the hydrogen bonds by charge delocalization, which results in a shortening of the distance between proton donor and proton acceptor. They proposed that the RAHB interaction occurs for inter- and intramolecular systems. Numerous theoretical studies have been devoted to study these inter- and intramolecular RAHB's.[4,5a] For the GC base pair, different Lewis structures can be drawn to explain the resonance assistance (see Scheme 7.1). The lower line in Scheme 7.1 has been proposed by Gilli *et al*. to explain RAHB.

In previous work,[5] we established theoretically that, for the hydrogen bonds in DNA base pairs, the electrostatic interactions and orbital interactions are of equal importance and that indeed the π electrons provide an additional stabilizing component. This finding was reconfirmed by others.[4g,4j] However, our work[5] also showed computationally that the synergetic interplay between the delocalization in the π-electron system and the donor-acceptor interactions in the σ-electron system

Embargoed until publication

Guillaumes, L.; Simon, S; Fonseca Guerra, C. “Theoretical Study on the Resonance-Assisted Hydrogen Bonding of DNA Base Pair Guanine-Cytosine (CG) and Mimics”. In preparation, 2015

8. Results and discussion

The main object of study of this thesis is the well-known concept of Resonance-Assisted Hydrogen Bonds (RAHB), proposed by Gilli *et al.*[26] The presence of π electrons within the skeleton of a molecule is usually linked with the appearance of an extra stabilization due to resonance when forming HB.

This thesis deals with systems based on two molecules that interact thanks to intermolecular hydrogen bonds. The role of the π electrons within these structures has been analyzed and questioned mainly from two points of view. On one hand, it is developed through the calculation of delocalization indices (DI) between the proton and the proton acceptor atom, and also I_{NG}, which is an n-center index, within the *quasi*-ring. On the other hand, the tools used are energetic decompositions of the hydrogen bonding energy and also Voronoi Deformation Density charges. The main results for both approaches are outlined below.

8.1 Atomic division schemes

The first part of this thesis wants to calculate delocalization indices (DI) between the proton and the proton-acceptor atom of hydrogen bonds by using different atomic divisions. The aim is to find a fuzzy-atom scheme (Becke,[88] Becke-ρ,[89] Hirshfeld[92] and Hirshfeld-iterative[93-94]) with similar DI and I_{NG} values to QTAIM[84] when dealing with hydrogen bonds, but with less computational cost. Then, working with larger systems would be more feasible.

The initial property to analyze is the relationship between DI on HB at equilibrium structures and their respective HB distances. Different correlations are obtained for all schemes depending on the nature of the proton donor and acceptor atoms. These linear separations are mainly seen in QTAIM DI (see Figure 8.1).

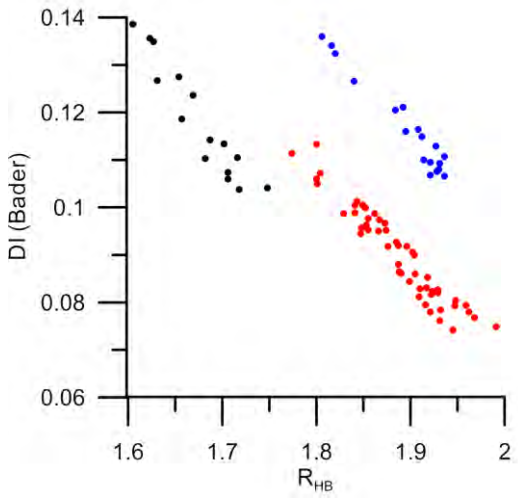

Figure 8.1: DI versus HB distances R_{HB} (Å) for QTAIM. OH···O (black), NH···O (red), and NH···N (blue).

Looking at the fuzzy atomic divisions, Becke-ρ and Hirshfeld-iterative are the ones that show similar trends to QTAIM, while both Hirshfeld and Becke DI are not affected by the nature of the proton donor (OH···O and NH···O bond types are situated almost lineally). Neither Becke nor Hirshfeld approach take into account the partial ionic character of the bonds, as they treat atoms of an element in the same way regardless of the chemical environment.

The observed differences between bond-types in QTAIM essentially lie on the different relative atomic sizes of the atoms, and this is best captured by Hirshfeld-Iterative or Becke-ρ schemes. When dealing with the representation of DI associated to the HB in front of the respective densities on bond critical point, ρ_{bcp}, QTAIM shows also three linear trends depending on the atoms involved in the HB, a thing that happens also with Becke-ρ and Hirshfeld-Iterative. However, the correlation of the latter is significantly worst, particularly for the NH···N bonds.

Another parameter that has been analyzed by using the same different atomic division schemes is I_{NG}. A *quasi*-ring appears when there is the formation of two hydrogen bonds of the complex, and I_{NG} is a normalized index that gives information about the delocalization of electrons within this *quasi*-ring. There is not a good correlation between the I_{NG} QTAIM and fuzzy-atom values, as the numbers are overestimated or underestimated, but it improves for the case of Becke-ρ.

So, after studying some features of hydrogen bonds by using different ways of dividing the 3D space, Becke-ρ has resulted to be the most similar method to QTAIM.

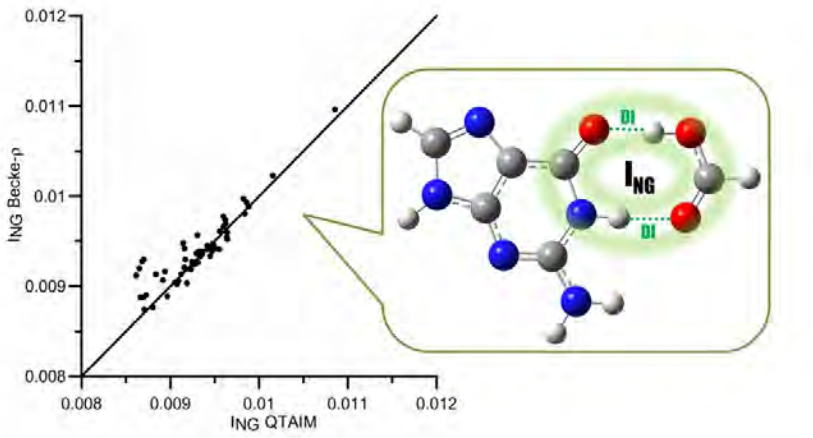

Figure 8.2: QTAIM versus Becke-ρ I_{NG} values for the *quasi*-rings.[86]

8.2 Delocalization indices and I_{NG} to study RAHB

Once having seen which fuzzy method is the most similar one to QTAIM when it comes to describing the hydrogen bonds, Becke-ρ delocalization indices and I_{NG} indices are used to develop a ring formation analysis within the framework of extra stabilization energy. The methodology developed consists on going from having one HB (one monomer is perpendicular to the other) to the formation of the *quasi*-

ring. By doing this, an extra energy (E_{RiR}) appears, as the addition of the two HB energies is less stable than the total E_{int} (Figure 8.3). The aim is to study the nature of this extra energy, to analyze whether it has to do with the presence of π electrons within the skeleton.

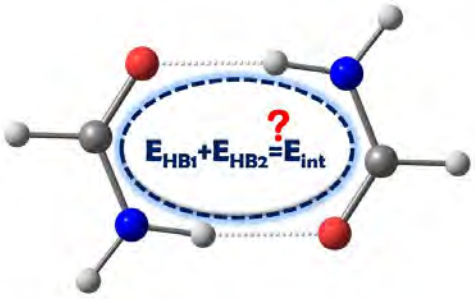

Figure 8.3: Is the addition of both HB energies equal to the total interaction energy?[100]

Among all the complexes of the study, some are symmetric (two equal monomers form the dimer, so two identical HB) and others nonsymmetric (interacting monomers are different). The first step is to relate the total energy of the HB formation (E_{int}) with their delocalization indices (DI). For the symmetric ones the half of the total E_{int} is used (Figure 5.2) to consider it as the energy of one of the HB, so it includes the possible extra energy for each HB. For both symmetric and nonsymmetric compounds, the E_{int} and DI of HB (DI_{HB}) have almost a linear relationship. Thus, the larger the DI_{HB} are the stronger the HB are.

The nature of the extra interaction energy in systems where two HB form a *quasi*-ring is usually related to the existence of resonance-assisted hydrogen bonds (RAHB). Here, n-center delocalization indices, and specially their π contribution ($I_{NG\pi}$), are calculated to study the π charge delocalized within a ring and its possible relationship with an extra stabilization energy. No trend is found when representing this $I_{NG\pi}$ with E_{int} or with the extra energy when forming the two HB (E_{RiR}). So results say that larger π delocalization does not necessarily imply an increase in the stabilization of the system, neither for symmetric nor for nonsymmetric systems.

Another aspect reinforces this idea, as DI_{HB} are being kept almost constant when forming the second HB. The strength of HB does not change due to the formation of the *quasi*-ring and so there is no synergism between them. However, DI when going further from the interacting HB show more relevant changes when rotating one monomer and the second HB takes place, which can be associated to the E_{RiR}. It happens especially for some bonds directly joined to the *quasi*-ring in compounds that have in their interacting structure two proton donors or acceptors almost one next to each other. Special attention should be paid to them, which also correspond to the ones with larger $E_{RiR.}$

8.3 RAHB for the DNA base pairs

The concept of RAHB has also been analyzed by studying computationally the base pairs adenine-thymine (AT) and guanine-cytosine (GC) through an energy decomposition analysis (EDA, see Figure 8.4)

and Voronoi Deformation Density (VDD) charges. These tools are useful to understand the appearance of stabilization due to the presence of π electrons within the structure of the compounds.

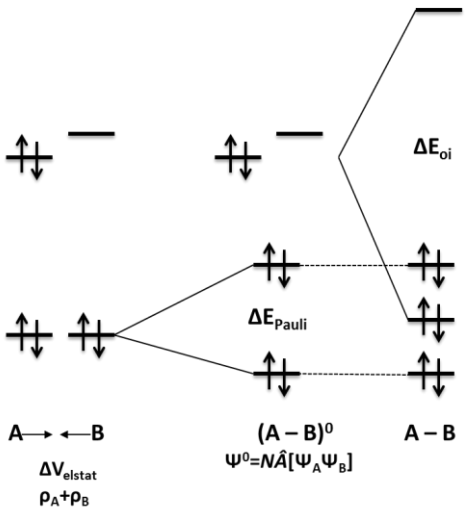

Figure 8.4: Terms of EDA: ΔV_{elstat}, ΔE_{Pauli} and ΔE_{oi} (see eq. (6.3)) for the case of having HB between molecule A and molecule B.

For both base pairs AT and GC the procedure has been the same: molecules are reduced in size, so with less π electrons, but by maintaining the interacting sp^2 character of the frontier atoms. Then, we analyze the changes in HB energies and in VDD charges.

8.3.1 Adenine-thymine

In this section, adenine-thymine base pair and its smaller mimics (A', A'' and T', T'') are considered (Figure 8.5). The latter lack the aromatic rings, but include the same sp^2 frontier atoms. The objective is to know whether resonance assistance (RAHB) is a characteristic exclusively of aromaticity or if sp^2-hybridization plays a role.

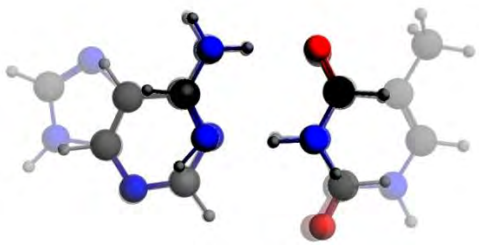

Figure 8.5: AT and its smaller mimics, reducing the number of π electrons: A, A', A'' and T, T', T''.

The total energy corresponding to the formation of the two HB changes only slightly (0.6 kcal·mol^{-1}) from AT to its smallest mimic A''T''. In contrast, the geometrical variations in the hydrogen bond distances are more pronounced (> 0.1Å) when the size of the molecules is reduced.

Looking at the VDD charges of the monomers in the geometry of the dimer (before interaction) it is seen that adenine and thymine, but also its smaller analogues, are electronically complementary. That

is, the proton-acceptor atoms have a negative charge while the corresponding protons they face are all positively charged. There are only slight differences among the mimics of A or among the mimics of T.

Another aspect to study is the charge-transfer interactions in the σ-electron system. The σ frontier orbitals need to be similar for the smaller molecules to have the same donor-acceptor interaction as AT, which consist of a lone pair on a proton-acceptor nitrogen or oxygen atom pointing toward and donating charge into the unoccupied σ* orbital of an N–H group of the other base. It is the case, as they are alike except for the σ_{HOMO-1} of A" and T", which have only one proton-acceptor nitrogen or oxygen atom, respectively, and so they have only one lone-pair character orbital. So, similar σ interactions take place in the HB of the analogues of AT, regardless of the size of the molecules and their number of π electrons.

Once having seen that the conditions for the HB are favorable and almost do not change when we do the molecules smaller, the nature of the binding energy is examined by decomposing it. A relevant energetic term is the orbital interaction ΔE_{oi}, which is divided into a σ component ΔE_{σ} (the sum of the donor-acceptor interactions in both hydrogen bonds) and a π component ΔE_{π} (basically the π polarization). When comparing ΔE_{σ}(σ,–; σ,–), where the π virtuals have been removed, with ΔE_{σ}, donor-acceptor interactions are only 0.3 kcal·mol^{-1} lower in the latter case. So the synergy between σ and π is very small. Furthermore, by removing the σ virtuals from one base to switch off the donor-acceptor interactions of one of the hydrogen bonds, we obtain ΔE_{σ}(σ,–;–,–) and ΔE_{σ}(–,–;σ,–), respectively for N(H)···O and N···(H)N bonds. The sum of these two terms in comparison to the ΔE_{σ}(σ,–; σ,–), where both HB are included, results in saying that there is no synergism within the σ system.

The bonding characteristics for A or T and their analogues are therefore the same, so no aromatic rings are needed to achieve the strength of hydrogen bonds. We can also make an analysis with the changes of VDD charges due to the formation of HB, which states that σ and π charge rearrangements do not depend on the aromatic ring.

Comparison between sp^2 and sp^3 hybridization

Until now we have seen that π electrons of the aromatic ring do not influence the hydrogen bond energy, but there is still a question related to the need of the donor and acceptor atoms to be sp^2 hybridized. It is studied by comparison of sp^2 (A''T'') and its analogous sp^3-hybridized dimers (a''t'').

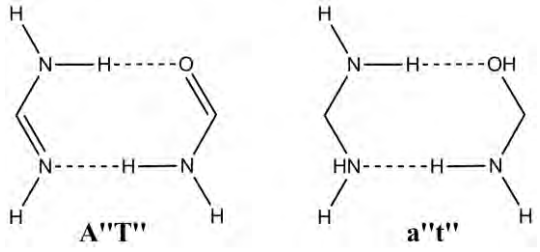

Figure 8.6: sp^3 (A''T'', Cs) and sp^2 (a''t'', chair conformation) hybridized dimers.

It is true that the hydrogen bond of the sp^2-hybridized is stronger bound than its saturated mimic, but the π polarization in the sp^2-hybridized A"T" is a small value, so this stabilization cannot be attributed to the π electrons.

When comparing A''T'' with a''t'' compressed to sp^2 distance, the first is 10.5 kcal·mol^{-1} more stable although its π polarization is only –1.9 kcal·mol^{-1}. The stronger interaction energy of A"T" can be ascribed to the stronger electrostatic interaction as well as the larger orbital interaction. Linked with this idea, we see that the absolute values of the VDD charges of the frontier atoms (prepared monomers) in the sp^3 system are smaller than in the sp^2-hybridized dimer.

The differences in the strength of hydrogen bonds for A''T'' and a''t'' can be explained with the σ-component of the orbital interaction. When A''T'' and a''t'' go from sp^3 to sp^2 distances, the orbital interaction component of A''T'' becomes stable more rapidly than for a''t''. The σ term of the orbital interaction is the one responsible for this trend.

The charge transfer in the formation of both N(H)···O and N···(H)N hydrogen bonds is larger in A"T" than in a"t". For the N(H)···O HB, the smaller charge-transfer interaction in a"t" has its origin in the lower lying electron donor orbital, so there is a larger gap between the two interacting orbitals. For the N···(H)N, the overlap between the frontier orbitals in A"T" is twice as large than for a"t", as they are somewhat better directed towards each other due to the sp^2-hybridization. So, in conclusion, we can state that covalency is the major factor responsible for the shorter resonance-assisted hydrogen bonds and that the sp^2-hybridization of the hydrogen bond acceptors and donors appears to be essential to achieve the same bonding interaction as AT.

8.3.2 Guanine-cytosine

In order to study the importance of the π electrons and aromaticity on the hydrogen bonds of the DNA base pair GC, we have investigated computationally possible dimers of G^{I} and its smaller analogues G^{II}, G^{III} and G^{IV} with C^{I} and its smaller analog C^{II} (see Figure 8.7).

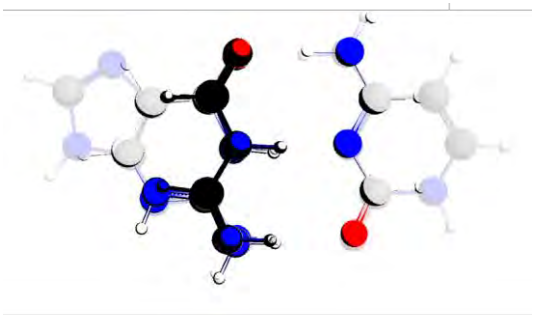

Figure 8.7: $G^{I}C^{I}$ and its smaller mimics, reducing the number of π electrons: G^{II}, G^{III}, G^{IV} and C^{II}.

The results indicate that the difference in the hydrogen bond energies between the largest system $G^{I}C^{II}$ and the smallest dimer $G^{IV}C^{II}$ is 8.9 kcal·mol^{-1}. When making G^{I} and C^{I} smaller, it is seen that the 5-

membered ring of guanine can be removed and also the 6-membered ring of cytosine can be made smaller without having much effect on the bonding capacities of the bases. But when the 6-membered ring of guanine is also reduced (G^{III} and G^{IV}) and therefore aromaticity is reduced, the hydrogen bond energies become weaker.

Moreover, although G^{I} and C^{I} and their analogues are electronically complementary, some differences among the VDD charges on the frontier atoms are found. However, analogues of $G^{I}C^{I}$ show similar bonding characteristics as $G^{I}C^{I}$ itself. In the σ-electron system of the hydrogen bonds in $G^{I}C^{I}$ and its equivalents, similar (but not equal in size) donor-acceptor orbital interactions occur.

From the analysis for the bond energy decomposition for the different dimers it is extracted by the comparison of $\Delta E_{\sigma}(\sigma,–;\ \sigma,–)$, where the π virtuals have been removed, with ΔE_{σ}, that the donor-acceptor interactions are only 0.5 kcal·mol^{-1} lower in the latter case. Therefore, we can conclude that also for the smaller equivalents of G^{I} and C^{I} that the synergy between σ and π is small.

Also the rearrangements of the orbital interaction σ and π charges are in agreement for all equivalents with what is expected. In the first case, negative charge is lost on the electron-donor atoms whereas there is a significant accumulation of negative charge on the nitrogen atoms of the electron-accepting N–H bonds. It is compensated by the π charges, as the electron-donor atoms gain π density and the nitrogen atoms of the electron-accepting N–H bonds lose it.

So, in conclusion, we have seen that all the analogues of $G^{I}C^{I}$ have similar characteristics for the formation of hydrogen bonds. However, reduction of the 6-membered ring of guanine leads to a slight non-planarity of the base and smaller hydrogen bond energies.

8.4 Conclusion from results

To sum up we can say that, although the studies have been done with two different methods, the conclusions follow the same direction. They both show that the π electrons are not responsible for the enhanced stability of the RAHB. Morever, molecular orbital theory with the corresponding energy decomposition analyses demonstrate that the enhanced stability of the hydrogen bonded sp^2-hybridized dimers compared to sp^3-hybridized dimers is due to a better covalent interaction in the sp^2-hybridized ones.

9. General conclusions

The conclusions for chapters 4-7 are outlined below.

In chapter 4, direct comparison between DI values obtained with fuzzy-atoms schemes and QTAIM indicates that the methods that can better accommodate the different partial ionic character of the bonds (Becke-ρ and Hirshfeld-it) outperform the simpler fuzzy-atom approaches, such as Becke's and Hirshfeld's. Specifically, when dealing with HB, Becke-ρ is the best performing method at reproducing the QTAIM results for both pairwise DI and especially for the I_{NG} n-center indices. This study could be extended to larger systems where hydrogen bonds play an important role, as fuzzy-atoms schemes show a reduced computacional cost.

In chapter 5, delocalization indices (DI) lead to conclude that π delocalization within the *quasi*-ring is not the main component in the sense of energetically assisting the formation of the second HB. This contribution can be considered negligible as far as the total interaction is concerned. Moreover, ring reorganization energy (E_{RiR}), found with the formation of the *quasi*-ring, is associated to the electron reorganization, which can be accounted for by DI of the main skeleton.

The π contribution of the n-center delocalization index ($I_{NG\pi}$) within the *quasi*-ring has small values, and it is not directly related energetically to HB formation. In addition, it has been seen that having in the monomer one electron donor or acceptor group situated almost next to the HB electron donor or acceptor atom requires a special analysis.

By working with AT and some mimics, in chapter 6, we see that π assistance is not exclusively due to aromaticity, but that the sp^2-hybridization of the proton-donor and acceptor atoms already accounts for the π charge delocalization. A sp^2-hybridized dimer (A''T'') was compared to its sp^3 mimic (a''t'') and subjected to a Kohn Sham MO analysis to understand where the stability of the first one comes from, which could not be explained with the assistance by the π electronic system. In reference to this, when comparing A''T'' with a''t'' compressed to sp^2 distance, A''T'' has a larger orbital interaction and electrostatic interaction, which explains its stability compared do a''t''.

The better covalent component in the hydrogen bonds of unsaturated dimers compared to the covalency in saturated dimers has been found to be the reason for the experimental finding of the shorter hydrogen bonds, and not solely the assistance by the π electrons.

With the computational study on GC and some mimics, in chapter 7, we show that the 5-membered ring of guanine and the 6-membered ring of cytosine can be reduced without affecting the hydrogen bond energy. However, when the 6-membered ring of guanine is reduced to just sp^2 front atoms in the analog of guanine, the analog is not planar and shows a smaller bonding energy.

Bibliography

1. Grabowski, S. J. *Hydrogen bonding: new insights*. Springer: **2006**, Vol. 3.
2. Jeffrey, G. A.; Jeffrey, G. A. *An introduction to hydrogen bonding*. Oxford University Press New York: **1997**, Vol. 12.
3. Sobczyk, L.; Grabowski, S. J.; Krygowski, T. M. *Chem. Rev.* **2005**, *105* (10), 3513-3560.
4. Werner, A. *Justus Liebigs Ann. Chem.* **1902**, *322* (3), 261-296.
5. Hantzsch, A. *Ber. Dtsch. Chem. Ges.* **1910**, *43* (3), 3049-3076.
6. Pfeiffer, P. *Ber. Dtsch. Chem. Ges.* **1914**, *47* (2), 1580-1596.
7. Moore, T. S.; Winmill, T. F. *J. Chem. Soc., Trans.* **1912**, *101*, 1635-1676.
8. Huggins, M. L. *Angew. Chem. Int. Edit. Engl.* **1971**, *10* (3), 147-152.
9. Latimer, W. M.; Rodebush, W. H. *J. Am. Chem. Soc.* **1920**, *42* (7), 1419-1433.
10. Pauling, L. *J. Am. Chem. Soc.* **1931**, *53* (4), 1367-1400.
11. Huggins, M. L. *J. Am. Chem. Soc.* **1931**, *53* (8), 3190-3191.
12. Pauling, L. *The Nature of the Chemical Bond and the Structure of Molecules and Crystals: An Introduction to Modern Structural Chemistry*. First edition published in 1939. Cornell University Press: **1960**, Vol. 18.
13. Gilli, G.; Gilli, P. *The Nature of the Hydrogen Bond: Outline of a Comprehensive Hydrogen Bond Theory*. International Union of Crystallography Monographs on Crystallography. Oxford University Press New York.: **2009**.
14. Pimentel, G. C.; McClellan, A. *The Hydrogen Bond.* **1960**, San Francisco, CA: Freeman.
15. Arunan, E.; Desiraju, G. R.; Klein, R. A.; Sadlej, J.; Scheiner, S.; Alkorta, I.; Clary, D. C.; Crabtree, R. H.; Dannenberg, J. J.; Hobza, P. *Pure Appl. Chem.* **2011**, *83* (8), 1637-1641.
16. Arunan, E.; Desiraju, G. R.; Klein, R. A.; Sadlej, J.; Scheiner, S.; Alkorta, I.; Clary, D. C.; Crabtree, R. H.; Dannenberg, J. J.; Hobza, P. *Pure Appl. Chem.* **2011**, *83* (8), 1619-1636.
17. *IUPAC. Compendium of Chemical Terminology, 2nd ed. (the "Gold Book").* Compiled by A. D. McNaught and A. Wilkinson. Blackwell Scientific Publications, Oxford (1997). XML on-line corrected version: http://goldbook.iupac.org (2006-) created by M. Nic, J. Jirat, B. Kosata; updates compiled by A. Jenkins. ISBN 0-9678550-9-8. doi:10.1351/goldbook.
18. Kollman, P. A.; Allen, L. C. *Chem. Rev.* **1972**, *72* (3), 283-303.
19. Desiraju, G. R. S., T. *The weak hydrogen bond: in structural chemistry and biology*. Oxford University Press: **1999**.
20. Emsley, J. *Chem. Soc. Rev.* **1980**, *9* (1), 91-124.
21. Zhang, J.; Chen, P.; Yuan, B.; Ji, W.; Cheng, Z.; Qiu, X. *Science.* **2013**, *342* (6158), 611-614.
22. Hobza, P.; Havlas, Z. *Chem. Rev.* **2000**, *100* (11), 4253-4264.
23. Scheiner, S.; Kar, T. *J. Phys. Chem. A.* **2002**, *106* (9), 1784-1789.
24. Heisenberg, W. *Z. Phys.* **1926**, *39* (7-8), 499-518.
25. Huggins, M. L. *J. Org. Chem.* **1936**, *1* (5), 407-456.
26. Gilli, G.; Bellucci, F.; Ferretti, V.; Bertolasi, V. *J. Am. Chem. Soc.* **1989**, *111* (3), 1023-1028.
27. Bertolasi, V.; Gilli, P.; Ferretti, V.; Gilli, G. *J. Am. Chem. Soc.* **1991**, *113* (13), 4917-4925.
28. Bertolasi, V.; Gilli, P.; Ferretti, V.; Gilli, G. *Chem. Eur. J.* **1996**, *2* (8), 925-934.
29. Gilli, P.; Bertolasi, V.; Ferretti, V.; Gilli, G. *J. Am. Chem. Soc.* **2000**, *122* (42), 10405-10417.
30. Krygowski, T. M.; Zachara-Horeglad, J. E.; Palusiak, M.; Pelloni, S.; Lazzeretti, P. *J. Org. Chem.* **2008**, *73* (6), 2138-2145.
31. Janusz Grabowski, S. *J. Phys. Org. Chem.* **2003**, *16* (10), 797-802.
32. Grabowski, S. J. *Croat. Chem. Acta.* **2009**, *82* (1), 185-192.
33. Lenain, P.; Mandado, M.; Mosquera, R. A.; Bultinck, P. *J. Phys. Chem. A.* **2008**, *112* (34), 7898-7904.
34. Palusiak, M.; Simon, S.; Solà, M. *J. Org. Chem.* **2006**, *71* (14), 5241-5248.
35. Palusiak, M.; Simon, S.; Solà, M. *J. Org. Chem.* **2009**, *74* (5), 2059-2066.

36. Raczyńska, E. D.; Krygowski, T. M.; Zachara, J. E.; Ośmiałowski, B.; Gawinecki, R. *J. Phys. Org. Chem.* **2005**, *18* (8), 892-897.
37. Beck, J. F.; Mo, Y. *J. Comput. Chem.* **2007**, *28* (1), 455-466.
38. Fonseca Guerra, C.; Bickelhaupt, F. M.; Snijders, J. G.; Baerends, E. J. *Chem. Eur. J.* **1999**, *5*, 3581.
39. Kurczab, R.; Mitoraj, M. P.; Michalak, A.; Ziegler, T. *J. Phys. Chem. A.* **2010**, *114* (33), 8581-8590.
40. Sanz, P.; Mó, O.; Yáñez, M.; Elguero, J. *Chem. Eur. J.* **2008**, *14* (14), 4225-4232.
41. Sanz, P.; Mó, O.; Yáñez, M.; Elguero, J. *ChemPhysChem.* **2007**, *8* (13), 1950-1958.
42. Sanz, P.; Mó, O.; Yáñez, M.; Elguero, J. *J. Phys. Chem. A.* **2007**, *111* (18), 3585-3591.
43. Watson, J. D.; Crick, F. H. *Nature.* **1953**, *171* (4356), 737-738.
44. Fonseca Guerra, C.; Bickelhaupt, F. M.; Baerends, E. J. *ChemPhysChem.* **2004**, *5* (4), 481-487.
45. Fonseca Guerra, C.; Zijlstra, H.; Paragi, G.; Bickelhaupt, F. M. *Chem. Eur. J.* **2011**, *17* (45), 12612-12622.
46. Otero, R.; Schöck, M.; Molina, L. M.; Lægsgaard, E.; Stensgaard, I.; Hammer, B.; Besenbacher, F. *Angew. Chem. Int. Ed.* **2005**, *44* (15), 2270-2275.
47. Mitoraj, M. P.; Michalak, A.; Ziegler, T. *J. Chem. Theory Comput.* **2009**, *5* (4), 962-975.
48. Mo, Y. *J. Mol. Model.* **2006**, *12* (5), 665-672.
49. Fonseca Guerra, C.; van der Wijst, T.; Bickelhaupt, F. M. *Chem. Eur. J.* **2006**, *12* (11), 3032-3042.
50. Thomas, L. H. *The calculation of atomic fields*. Cambridge Univ Press: **1927**, Vol. 23, p 542-548.
51. Fermi, E. *Rend. Accad. Naz. Lincei.* **1927**, *6* (602-607), 32.
52. Fermi, E. *Z. Phys.* **1928**, *48* (1-2), 73-79.
53. Hohenberg, P.; Kohn, W. *Phys. Rev.* **1964**, *136* (3B), B864.
54. Kohn, W.; Sham, L. J. *Phys. Rev.* **1965**, *140* (4A), A1133.
55. Bickelhaupt, F. M.; Baerends, E. J. *Rev. Comput. Chem.* **2000**, *15*, 1-86.
56. Parr, R. G.; Yang, W. *Density-functional theory of atoms and molecules*. Oxford university press: **1989**, Vol. 16.
57. Andrés, J.; Bertran, J. *Theoretical and Computational Chemistry: Foundations, Methods and Techniques*. Publications de la Universitat Jaume I, Castelló de la Plana: Spain, **2007**.
58. Levy, M. *Phys. Rev. A.* **1982**, *26* (3), 1200-1208.
59. Becke, A. D. *Phys. Rev. A.* **1988**, *38* (6), 3098-3100.
60. Perdew, J. P. *Phys. Rev. B.* **1986**, *33* (12), 8822-8824.
61. Perdew, J. P.; Yue, W. *Phys. Rev. B.* **1986**, *33* (12), 8800-8802.
62. Lee, C.; Yang, W.; Parr, R. G. *Phys. Rev. B.* **1988**, *37* (2), 785-789.
63. Becke, A. D. *J. Chem. Phys.* **1993**, *98* (2), 1372-1377.
64. Becke, A. D. *J. Chem. Phys.* **1993**, *98* (7), 5648-5652.
65. Grimme, S.; Ehrlich, S.; Goerigk, L. *J. Comput. Chem.* **2011**, *32* (7), 1456-1465.
66. Grimme, S.; Antony, J.; Ehrlich, S.; Krieg, H. *J. Chem. Phys.* **2010**, *132* (15), 154104.
67. Johnson, E. R.; Becke, A. D. *J. Chem. Phys.* **2006**, *124* (17), 174104.
68. Johnson, E. R.; Becke, A. D. *J. Chem. Phys.* **2005**, *123* (2), 024101.
69. Becke, A. D.; Johnson, E. R. *J. Chem. Phys.* **2005**, *123* (15), 154101.
70. Te Velde, G.; Bickelhaupt, F. M.; Baerends, E. J.; Fonseca Guerra, C.; van Gisbergen, S. J.; Snijders, J. G.; Ziegler, T. *J. Comput. Chem.* **2001**, *22* (9), 931-967.
71. Ziegler, T.; Rauk, A. *Inorg. Chem.* **1979**, *18* (6), 1558-1565.
72. Ziegler, T.; Rauk, A. *Theor. Chim. Acta.* **1977**, *46* (1), 1-10.
73. Ziegler, T.; Rauk, A. *Inorg. Chem.* **1979**, *18* (7), 1755-1759.
74. Kitaura, K.; Morokuma, K. *Int. J. Quantum Chem.* **1976**, *10* (2), 325-340.
75. Morokuma, K. *J. Chem. Phys.* **1971**, *55* (3), 1236-1244.
76. Grimme, S. *J. Comput. Chem.* **2006**, *27* (15), 1787-1799.
77. Grimme, S. *J. Comput. Chem.* **2004**, *25* (12), 1463-1473.
78. Fonseca Guerra, C.; van der Wijst, T.; Poater, J.; Swart, M.; Bickelhaupt, F. M. *Theor. Chem. Acc.* **2010**, *125* (3-6), 245-252.
79. van der Wijst, T.; Fonseca Guerra, C.; Swart, M.; Bickelhaupt, F. M.; Lippert, B. *Angew. Chem. Int. Ed.* **2009**, *48* (18), 3285-3287.

80. Fonseca Guerra, C.; Handgraaf, J. W.; Baerends, E. J.; Bickelhaupt, F. M. *J. Comput. Chem.* **2004**, *25* (2), 189-210.
81. Bickelhaupt, F. M.; van Eikema Hommes, N. J.; Fonseca Guerra, C.; Baerends, E. J. *Organometallics.* **1996**, *15* (13), 2923-2931.
82. Te Velde, G.; Baerends, E. *J. Comput. Phys.* **1992**, *99* (1), 84-98.
83. Voronoï, G. *J. Reine Angew. Math.* **1908**, *134*, 198-287.
84. Bader, R. F. *Atoms in molecules*. Wiley Online Library: **1990**.
85. Grabowski, S. J. *J. Phys. Org. Chem.* **2004**, *17* (1), 18-31.
86. Guillaumes, L.; Salvador, P.; Simon, S. *J. Phys. Chem. A.* **2014**, *118*, 1142 -1149.
87. Mo, Y. *J. Phys. Chem. A.* **2012**, *116* (21), 5240-5246.
88. Becke, a. A. *J. Chem. Phys.* **1988**, *88* (4), 2547-2553.
89. Matito, E.; Solà, M.; Salvador, P.; Duran, M. *Faraday Discuss.* **2007**, *135*, 325-345.
90. Mayer, I.; Salvador, P. *Chem. Phys. Lett.* **2004**, *383* (3), 368-375.
91. Salvador, P.; Ramos-Cordoba, E. *J. Chem. Phys.* **2013**, *139*, 071103.
92. Hirshfeld, F. *Theor. Chim. Acta.* **1977**, *44* (2), 129-138.
93. Bultinck, P.; Van Alsenoy, C.; Ayers, P. W.; Carbó-Dorca, R. *J. Chem. Phys.* **2007**, *126* (14), 144111.
94. Bultinck, P.; Cooper, D. L.; Van Neck, D. *PCCP.* **2009**, *11* (18), 3424-3429.
95. Fradera, X.; Austen, M. A.; Bader, R. F. *J. Phys. Chem. A.* **1999**, *103* (2), 304-314.
96. Giambiagi, M.; de Giambiagi, M. S.; dos Santos Silva, C. D.; de Figueiredo, A. P. *PCCP.* **2000**, *2* (15), 3381-3392.
97. Cioslowski, J.; Matito, E.; Solà, M. *J. Phys. Chem. A.* **2007**, *111* (28), 6521-6525.
98. Heyndrickx, W.; Salvador, P.; Bultinck, P.; Solà, M.; Matito, E. *J. Comput. Chem.* **2011**, *32* (3), 386-395.
99. Gutman, I.; Milun, M.; Trinajstic, N. *J. Am. Chem. Soc.* **1977**, *99* (6), 1692-1704.
100. Guillaumes, L.; Simon, S. *J. Phys. Chem. A.* **2014**, *118*, 9727−9733.

Appendices

Appendix A

Supporting information for CHAPTER 4

Table S1: Delocalization indices (DI) using different atomic definitions, electron density at the bond critical point (au) and hydrogen bond distances (Å). Different HB are NH···N (type 1), NH···O (type 2) and OH···O (type 3).

		DI						
HB-type	**Compound**	**QTAIM**	**Becke**	**Hirshfeld**	**Hirshfeld-Iterative**	**Becke-ρ**	**ρ bcp**	**R_{HB} (Å)**
1	A-T	0.1266	0.1299	0.2410	0.1851	0.1371	0.03967	1.840
1	C1-FI	0.1341	0.1549	0.2708	0.2020	0.1607	0.04125	1.816
1	C2-FI[(2)]	0.1129	0.1265	0.2313	0.1764	0.1361	0.03187	1.927
1	C3-FI	0.1324	0.1537	0.2694	0.1993	0.1601	0.04075	1.820
1	C4-FI	0.1149	0.1300	0.2366	0.1801	0.1405	0.03042	1.912
1	C5-FI	0.1205	0.1373	0.2468	0.1884	0.1469	0.03511	1.884
1	DiFI-Br[(1)]	0.1066	0.1164	0.2145	0.1532	0.1246	0.03042	1.936
1	DiFI-CCH[(1)]	0.1093	0.1202	0.2267	0.1632	0.1269	0.03117	1.931
1	DiFI-Cl[(1)]	0.1076	0.1182	0.2197	0.1563	0.1259	0.03102	1.928
1	DiFI-CN	0.1080	0.1185	0.2233	0.1609	0.1252	0.03109	1.930
1	DiFI-F[(1)]	0.1100	0.1215	0.2286	0.1605	0.1292	0.03189	1.914
1	DiFI-NH_2[(1)]	0.1160	0.1304	0.2428	0.1714	0.1360	0.03368	1.895
1	DiFI-OH[(1)]	0.1095	0.1218	0.2293	0.1617	0.1292	0.03147	1.921
1	FA-FI	0.1164	0.1302	0.2390	0.1731	0.1377	0.03318	1.908
1	FI-FI[(1)]	0.1107	0.1230	0.2287	0.1654	0.1308	0.03103	1.936
1	G-C	0.1068	0.1053	0.2049	0.1563	0.1126	0.03257	1.921
1	G-C	0.1068	0.1053	0.2049	0.1563	0.1126	0.03257	1.921
1	G-FI[(1)]	0.1211	0.1331	0.2354	0.1762	0.1422	0.03488	1.892
1	T-FI	0.1360	0.1559	0.2714	0.2022	0.1617	0.04221	1.806
2	A-T	0.0825	0.0879	0.1896	0.1300	0.0952	0.02572	1.928
2	C1-C1	0.0844	0.0929	0.1966	0.1363	0.1066	0.02733	1.899
2	C1-C2[(2)]	0.1060	0.1201	0.2397	0.1670	0.1347	0.03518	1.800
2	C1-C2[(2)]	0.0804	0.0859	0.1822	0.1324	0.1011	0.02488	1.948
2	C1-FA	0.0957	0.1097	0.2185	0.1515	0.1257	0.03113	1.848
2	C1-FA	0.0827	0.0884	0.1884	0.1294	0.1027	0.02579	1.929
2	C1-FI	0.0794	0.0839	0.1796	0.1239	0.0930	0.02419	1.959
2	C1-FO	0.0812	0.0922	0.1915	0.1320	0.1071	0.02675	1.909
2	C2-C2[(2)]	0.0987	0.1079	0.2175	0.1586	0.1160	0.03098	1.862
2	C2-FA[(2)]	0.0906	0.1006	0.2010	0.1459	0.1099	0.02798	1.902

Table S1 – cont.

2	C2-FA$^{(2)}$	0.1013	0.1107	0.2247	0.1551	0.1177	0.03215	1.843
2	C2-FI$^{(2)}$	0.0974	0.1055	0.2158	0.1494	0.1126	0.03042	1.867
2	C2-FO$^{(2)}$	0.0820	0.0911	0.1873	0.1358	0.1065	0.02605	1.929
2	C3-C3	0.0784	0.0857	0.1844	0.1270	0.0989	0.02519	1.932
2	C3-C4	0.1050	0.1194	0.2389	0.1653	0.1334	0.03501	1.801
2	C3-C4	0.0768	0.0818	0.1751	0.1272	0.0951	0.02369	1.968
2	C3-FA	0.0945	0.1090	0.2181	0.1498	0.1248	0.03099	1.847
2	C3-FA	0.0780	0.0824	0.1772	0.1222	0.0961	0.02395	1.962
2	C3-FI	0.0749	0.0783	0.1689	0.1171	0.0876	0.02250	1.991
2	C3-FO	0.0780	0.0889	0.1871	0.1273	0.1036	0.02589	1.921
2	C4-C4	0.0999	0.1099	0.2212	0.1609	0.1180	0.03165	1.852
2	C4-FA	0.0920	0.1032	0.2060	0.1489	0.1201	0.02886	1.887
2	C4-FA	0.1005	0.1094	0.2224	0.1536	0.1167	0.03172	1.849
2	C4-FI	0.0967	0.1043	0.2136	0.1481	0.1117	0.03003	1.873
2	C4-FO	0.0817	0.0916	0.1893	0.1363	0.1084	0.02647	1.922
2	C5-C3	0.0987	0.1111	0.2256	0.1560	0.1262	0.03257	1.829
2	C5-C3	0.0793	0.0852	0.1812	0.1315	0.0991	0.02477	1.947
2	C5-C5	0.0977	0.1076	0.2177	0.1583	0.1169	0.03120	1.855
2	C5-FA	0.0950	0.1075	0.2131	0.1539	0.1240	0.03023	1.866
2	C5-FA	0.0952	0.1028	0.2114	0.1461	0.1103	0.02980	1.874
2	C5-FI	0.0918	0.0983	0.2033	0.1412	0.1061	0.02831	1.896
2	C5-FO	0.0829	0.0934	0.1926	0.1384	0.1088	0.02698	1.910
2	DiFA-Br	0.0742	0.0808	0.1724	0.1153	0.0959	0.02375	1.945
2	DiFA-CCH	0.0918	0.1004	0.2072	0.1414	0.1081	0.02921	1.876
2	DiFA-Cl	0.0762	0.0834	0.1783	0.1189	0.0981	0.02463	1.931
2	DiFA-CN	0.0861	0.0941	0.1977	0.1339	0.1084	0.02775	1.890
2	DiFA-F	0.0795	0.0870	0.1860	0.1227	0.1019	0.02564	1.916
2	DiFA-$NH_2$$^{(1)}$	0.0963	0.1076	0.2191	0.1466	0.1147	0.03084	1.853
2	DiFA-OH	0.0880	0.0974	0.2029	0.1352	0.1062	0.02811	1.887
2	FA-FA	0.0927	0.1027	0.2070	0.1421	0.1110	0.02891	1.885
2	FA-FI	0.0900	0.0991	0.2005	0.1382	0.1075	0.02769	1.904
2	FA-FO	0.0831	0.0921	0.1910	0.1308	0.1076	0.02655	1.917
2	FO-FI	0.0860	0.0954	0.1960	0.1346	0.1117	0.02739	1.905
2	G-C	0.0853	0.0920	0.1941	0.1313	0.0991	0.02641	1.918
2	G-C	0.1114	0.1251	0.2501	0.1714	0.1279	0.03727	1.774
2	G-FA$^{(1)}$	0.1133	0.1236	0.2292	0.1669	0.1312	0.03663	1.800
2	G-FA$^{(1)}$	0.1005	0.1093	0.2238	0.1535	0.1158	0.03208	1.841
2	G-FI$^{(1)}$	0.0989	0.1075	0.2213	0.1528	0.1137	0.03186	1.841

Table S1 – cont.

2	G-FO[(1)]	0.1072	0.1207	0.2269	0.1650	0.1282	0.03557	1.804
2	T-FA	0.0953	0.1084	0.2147	0.1489	0.1165	0.03057	1.855
2	T-FA	0.0863	0.0931	0.2016	0.1373	0.1061	0.02794	1.889
2	T-FI	0.0823	0.0877	0.1912	0.1305	0.1003	0.02595	1.923
2	T-FO	0.0865	0.0981	0.1983	0.1378	0.1153	0.02810	1.888
3	C1-FO	0.1105	0.1364	0.2663	0.1700	0.1332	0.04173	1.716
3	C2-FO[(2)]	0.1356	0.1740	0.3191	0.2046	0.1626	0.05381	1.623
3	C3-FO	0.1041	0.1266	0.2510	0.1606	0.1269	0.03849	1.748
3	C4-FO	0.1349	0.1723	0.3167	0.2033	0.1614	0.05392	1.627
3	C5-FO	0.1275	0.1611	0.3008	0.1930	0.1533	0.04955	1.654
3	DIFO-Br	0.1038	0.1314	0.2528	0.1582	0.1317	0.04059	1.718
3	DIFO-CCH	0.1142	0.1447	0.2756	0.1761	0.1406	0.04487	1.687
3	DIFO-Cl	0.1060	0.1344	0.2590	0.1616	0.1333	0.04187	1.706
3	DIFO-CN	0.1074	0.1355	0.2621	0.1665	0.1333	0.04225	1.706
3	DIFO-F	0.1103	0.1416	0.2717	0.1676	0.1386	0.04449	1.682
3	DIFO-NH_2	0.1267	0.1671	0.3089	0.1923	0.1568	0.05179	1.631
3	DIFO-OH	0.1186	0.1550	0.2912	0.1817	0.1478	0.04813	1.657
3	FA-FO	0.1236	0.1584	0.2923	0.1866	0.1511	0.0475	1.669
3	FO-FO	0.1134	0.1445	0.2715	0.1740	0.1408	0.0435	1.702
3	G-FO[(1)]	0.1386	0.1786	0.3269	0.2091	0.1643	0.0560	1.605
3	T-FO	0.1170	0.1469	0.2861	0.1816	0.1419	0.0460	1.675

(1) Negative frequency corresponding to NH_2 out-of-plane bending.
(2) Negative frequency corresponding to C2 ring out-of-plane bending.

Table S2: I_{NG} for the *quasi*-rings using different atomic definitions.

Compound	QTAIM	Becke	Hirshfeld	Hirshfeld-iterative	Becke-ρ
C1-FI	0.009338	0.008705	0.008816	0.008109	0.009332
C2-FI	0.009482	0.008933	0.009005	0.008296	0.009452
C3-FI	0.009270	0.008635	0.008768	0.008064	0.009242
C4-FI	0.009479	0.008903	0.008976	0.008280	0.009472
C5-FI	0.009462	0.008891	0.008979	0.008273	0.009446
DiFI-Br	0.009305	0.009891	0.009224	0.008433	0.009566
DiFI-CCH	0.009245	0.008702	0.008754	0.008022	0.009273
DiFI-Cl	0.009160	0.009774	0.009196	0.008379	0.009418
DiFI-CN	0.009120	0.008636	0.008662	0.007966	0.009134
DiFI-F	0.009168	0.009974	0.009393	0.008484	0.009296
DiFI-NH_2	0.008939	0.009086	0.009073	0.008124	0.009165
DiFI-OH	0.008837	0.009375	0.009124	0.008156	0.009132

Table S2 – cont.

FA-FI	0.009637	0.009103	0.009115	0.008359	0.009545
FI-FI	0.009640	0.009096	0.009090	0.008352	0.009597
G-FI	0.009449	0.008687	0.008712	0.008040	0.009334
T-FI	0.009443	0.008719	0.008786	0.008081	0.009443
C1-C2	0.009170	0.008867	0.008796	0.008085	0.009186
C1-FA	0.009311	0.008734	0.008855	0.008122	0.009265
C1-FO	0.009417	0.008987	0.009098	0.008304	0.009449
C2-FA	0.009497	0.008987	0.009072	0.008334	0.009435
C2-FO	0.009596	0.009299	0.009392	0.008564	0.009659
C3-C3	0.008802	0.008258	0.008450	0.007739	0.008768
C3-C4	0.009092	0.008578	0.008725	0.008023	0.009060
C3-FA	0.009230	0.008662	0.008802	0.008072	0.009186
C3-FO	0.009319	0.008882	0.009017	0.008229	0.009383
C4-C4	0.009360	0.008863	0.008943	0.008264	0.009382
C4-FA	0.009497	0.008655	0.009051	0.008323	0.009413
C4-FO	0.009617	0.009265	0.009356	0.008540	0.009739
C5-C3	0.009050	0.008561	0.008722	0.008007	0.009041
C5-C5	0.009293	0.008831	0.008945	0.008238	0.009364
C5-FA	0.009467	0.008950	0.009049	0.008312	0.009392
C5-FO	0.009557	0.009233	0.009338	0.008518	0.009608
C1-C1	0.008966	0.008399	0.008551	0.007841	0.008890
C2-C2	0.009348	0.008934	0.008994	0.008297	0.009385
DiFA-Br	0.008728	0.009048	0.008807	0.007928	0.008904
DiFA-CCH	0.009356	0.008820	0.008878	0.008092	0.009351
DiFA-Cl	0.008696	0.009056	0.008836	0.007942	0.008878
DiFA-CN	0.009157	0.008703	0.008769	0.008015	0.009209
DiFA-F	0.008705	0.009324	0.009015	0.008038	0.008744
DiFA-NH_2	0.008916	0.009014	0.008971	0.007991	0.009068
DiFA-OH	0.008662	0.009125	0.008953	0.007929	0.008879
FA-FA	0.009641	0.009122	0.009149	0.008377	0.009520
FA-FO	0.009837	0.009488	0.009488	0.008636	0.009809
FO-FI	0.009860	0.009502	0.009481	0.008661	0.009931
G-FA	0.009551	0.008832	0.008852	0.008161	0.009408
G-FO	0.009882	0.009327	0.009300	0.008517	0.009887
T-FA	0.009413	0.008729	0.008801	0.008083	0.009407
T-FO	0.009623	0.009083	0.009113	0.008303	0.009696
DiFO-Br	0.008701	0.009842	0.009461	0.008418	0.009296
DiFO-CCH	0.009824	0.009671	0.009618	0.008676	0.009974

Table S2 – cont.

DiFO-Cl	0.008685	0.009876	0.009492	0.008429	0.009276
DiFO-CN	0.009596	0.009548	0.009503	0.008600	0.009779
DiFO-F	0.008616	0.010320	0.009739	0.008573	0.009120
DiFO-NH_2	0.009146	0.009881	0.009677	0.008529	0.009477
DiFO-OH	0.008650	0.010052	0.009649	0.008451	0.009198
FO-FO	0.010155	0.009957	0.009912	0.008983	0.010230
G-C	0.010856	0.011285	0.010903	0.009787	0.010961
G-C	0.009187	0.008240	0.008305	0.007619	0.009035
A-T	0.009075	0.008156	0.008260	0.007601	0.009026

Table S3: Linear regression parameters for all correlations of Figure 4.2.

	QTAIM	**Becke**	**Hirshfeld**	**Hirshfeld-iterative**	**Becke-ρ**
			NH···N		
slope	-0.219	-0.291	-0.395	-0.336	-0.278
y-intercept	0.531	0.681	0.983	0.811	0.663
R^2	0.940	0.748	0.763	0.815	0.705
			NH···O		
slope	-0.197	-0.243	-0.386	-0.275	-0.214
y-intercept	0.463	0.558	0.931	0.662	0.514
R^2	0.914	0.955	0.962	0.878	0.873
			OH···O		
slope	-0.273	-0.399	-0.594	-0.385	-0.293
y-intercept	0.575	0.819	1.280	0.825	0.636
R^2	0.900	0.954	0.954	0.893	0.950

Table S4: Linear regression parameters for all correlations of Figure 4.3.

	QTAIM	**Becke**	**Hirshfeld**	**Hirshfeld -iterative**	**Becke-ρ**
			NH···N		
slope	2.351	3.025	4.088	3.549	2.863
y-intercept	0.036	0.025	0.096	0.052	0.038
R^2	0.905	0.671	0.683	0.756	0.624
			NH···O		
slope	2.770	3.365	5.272	3.869	2.910
y-intercept	0.011	0.003	0.052	0.031	0.027
R^2	0.965	0.980	0.964	0.929	0.868
			OH···O		
slope	2.155	3.104	4.624	3.039	2.281
y-intercept	0.018	0.006	0.069	0.039	0.039
R^2	0.959	0.985	0.986	0.951	0.980

Table S5: Linear regression parameters for all correlations of Figure 4.4.

	Becke	**Hirshfeld**	**Hirshfeld -iterative**	**Becke-ρ**
		NH···N		
slope	1.405	1.874	1.592	1.362
y-intercept	-0.035	0.017	-0.012	-0.023
R^2	0.884	0.877	0.930	0.862
		NH···O		
slope	1.185	1.853	1.378	0.985
y-intercept	-0.008	0.037	0.018	0.022
R^2	0.968	0.949	0.938	0.792
		OH···O		
slope	1.404	2.093	1.410	1.032
y-intercept	-0.016	0.037	0.014	0.023
R^2	0.979	0.981	0.994	0.974
		Global		
slope	1.401	2.000	1.337	1.081
y-intercept	-0.026	0.024	0.021	0.013
R^2	0.917	0.831	0.970	0.920

Appendix B

Supporting information for CHAPTER 5

Table S6: Interaction energy (kcal·mol^{-1}), CP-corrected Interaction energy (kcal·mol^{-1}), HB distance (Å), HB delocalization index, I_{NG} (total and π contribution) and Ring Reorganization Energy (E_{RiR}, kcal·mol^{-1}).

Compound	E_{int} (kcal·mol^{-1})	E_{int} BSSE (kcal·mol^{-1})	RHB (Å)	DI Becke-ρ	I_{NG}·10^{-3}	$I_{NG\pi}$ ·10^{-3}	E_{RiR} (kcal·mol^{-1})
C8-C10[(a)]	-25.9	-25.2	1.76 1.70	0.140 0.151	9.165	8.443	-8.7
C6-C8 [(a)]	-23.9	-23.2	1.72 1.75	0.149 0.139	9.473	8.507	-8.3
G-FO[(a)]	-22.6	-21.9	1.80 1.60	0.128 0.164	9.887	8.846	-7.6
FO-FI	-22.0	-21.4	1.91 1.62	0.112 0.207	9.931	9.239	-5.2
C6-C10	-21.8	-21.1	1.82 1.83	0.133 0.116	9.086	8.357	-8.5
G-FA[(a)]	-20.0	-19.4	1.80 1.84	0.131 0.116	9.408	8.723	-7.4
G-FI[(a)]	-19.6	-19.0	1.89 1.84	0.142 0.114	9.334	8.752	-5.3
C4-FO	-18.8	-18.2	1.92 1.63	0.108 0.161	9.739	8.981	-5.2
C2-FO[(a	-18.8	-18.1	1.93 1.62	0.107 0.163	9.659	8.956	-5.1
C7-C8[(a)]	-18.0	-17.3	1.79 1.78	0.128 0.128	9.385	8.508	-5.9
C5-FO	-17.9	-17.3	1.91 1.65	0.109 0.153	9.608	8.888	-4.8
FA-FO	-16.9	-16.4	1.92 1.67	0.108 0.151	9.809	9.015	-5.2
C8-C9[(a)]	-16.2	-15.6	1.99 1.81	0.109 0.121	8.901	8.051	-3.3
C6-C7	-16.1	-15.4	1.79 1.82	0.127 0.120	9.338	8.480	-5.0

Table S6 – cont.

C5-FI	-16.0	-15.5	1.88 1.90	0.147 0.106	9.446	9.053	-4.6
C6-C9	-15.9	-15.4	1.89 1.85	0.129 0.112	8.966	8.120	-3.9
C4-FI	-15.7	-15.2	1.91 1.87	0.141 0.112	9.472	9.083	-5.0
C9-C10	-15.7	-15.1	1.97 1.94	0.108 0.105	8.618	7.991	-5.1
C1-FI	-15.6	-15.0	1.82 1.96	0.161 0.093	9.332	8.864	-4.0
T-FO	-15.5	-14.8	1.89 1.67	0.115 0.142	9.696	8.692	-3.8
C2-FI(a)	-15.3	-14.8	1.93 1.87	0.136 0.113	9.452	9.083	-5.2
C4-FA	-15.3	-14.8	1.89 1.85	0.120 0.117	9.413	8.922	-5.3
C3-FI	-15.3	-14.7	1.82 1.99	0.160 0.088	9.242	8.760	-3.4
T-FI	-15.2	-14.6	1.81 1.92	0.162 0.100	9.443	8.829	-4.8
C5-FA	-15.2	-14.7	1.87 1.87	0.124 0.110	9.392	8.896	-5.0
C2-FA[(a)]	-15.1	-14.6	1.90 1.84	0.110 0.118	9.435	8.993	-5.4
FA-FI	-15.0	-14.5	1.91 1.90	0.138 0.108	9.545	9.130	-4.9
C1-FO	-14.9	-14.3	1.91 1.72	0.107 0.133	9.449	8.631	-3.7
C1-C2(a)	-14.2	-13.6	1.80 1.95	0.135 0.101	9.186	8.655	-3.5
C3-C4	-14.0	-13.4	1.80 1.97	0.133 0.095	9.060	8.516	-3.2
C3-FO	-14.0	-13.4	1.92 1.75	0.104 0.127	9.383	8.595	-3.5
A-T	-13.9	-13.2	1.84 1.93	0.137 0.095	9.026	8.246	-4.9
C7-C9	-13.9	-13.3	1.85 1.92	0.134 0.097	8.942	8.154	-4.2

Table S6 – cont.

C5-C3	-13.6	-13.0	1.83	0.126	9.041	8.502	-3.1
			1.95	0.099			
C1-FA	-13.2	-12.6	1.85	0.126	9.265	8.689	-3.6
			1.93	0.103			
C3-FA	-12.8	-12.3	1.85	0.125	9.186	8.620	-3.3
			1.96	0.096			
T-FA	-12.6	-12.1	1.86	0.117	9.407	8.714	-3.6
			1.89	0.106			
C7-C10[(a)]	-12.3	-11.7	2.10	0.085	8.768	8.035	-2.5
			1.82	0.113			

[(a)] Compounds with Imaginary frequencies.

Table S7: Delocalization indices for the main bonds in the skeleton. In bold the values for HB formation in one-HB complex (HB formed between NH[(a)] from monomer 1 and C=O[(b)] from monomer 2 (or CN)).

				DI			
		E_{int}	E_{RiR}	Monomer[(c)]	Two-HB complex [(d)]	One-HB complex[(e)]	
						Monomer 1	Monomer 2
FI-FI	NH[(a)]	-15.0	-4.8	0.8998	0.8090	**0.8078**	0.8791
	NC			1.0776	1.1408	1.1294	1.1222
	CN[(b)]			1.5455	1.5557	1.5904	**1.6292**
FA-FA	NH[(a)]	-14.3	-5.2	0.8987	0.8246	**0.8215**	0.8722
	CN			1.0837	1.1188	1.1118	1.1097
	CO[(b)]			1.3757	1.3919	1.4264	**1.4248**
C1-C1	NH[(a)]	-12.2	-2.8	0.8479	0.7708	**0.7714**	0.8422
	CN			1.0147	1.0579	1.0665	1.0706
	CO[(b)]			1.4388	1.3642	1.4653	**1.4216**
C2-C2	NH[(a)]	-15.7	-5.3	0.8807	0.7992	**0.7978**	0.8584
	CN			1.0929	1.1397	1.1676	1.1442
	CO[(b)]			1.3398	1.3016	1.3909	**1.3813**
C3-C3	NH[(a)]	-11.1	-2.7	0.8523	0.7839	**0.7829**	0.8484
	CN			1.0555	1.0431	1.0576	1.0618
	CO[(b)]			1.4113	1.4333	1.4520	**1.4261**
C4-C4	NH(a)	-16.3	-5.6	0.8811	0.8034	**0.8056**	0.8605
	CN			1.0488	1.1068	1.1185	1.1144
	CO[(b)]			1.3305	1.2968	1.3505	**1.3346**
C5-C5	NH[(a)]	-16.0	-5.0	0.8738	0.8143	**0.8137**	0.8623
	CN			1.1012	1.0927	1.1153	1.1051
	CO[(b)]			1.3811	1.3303	1.4229	**1.4013**

Table S7 – cont.

	NH[(a)]			0.8704	0.7643	**0.7637**	0.8566
C6-C6	NC	-21.0	-7.4	0.9351	0.9962	0.9719	0.9616
	CO[(b)]			1.3226	1.2555	1.3852	**1.3312**
	CO			1.2731	1.2768	1.3920	1.3352
	CN			0.9534	0.9681	0.9984	0.9896
C7-C7	NH[(a)]	-12.2	-3.1	0.8579	0.8102	**0.8097**	0.8470
	NC			0.9538	0.9615	1.0062	0.9825
	CO[(b)]			1.4242	1.2959	1.4246	**1.3526**
	CN			1.0133	1.0183	1.0231	1.0119
	CN			1.0247	1.0638	1.0775	1.0294
C8-C8	NH[(a)]	-27.6	-8.7	0.8600	0.7478	**0.7666**	0.8415
	NC			0.9220	0.9388	0.9288	0.9190
	CO[(b)]			1.3360	1.2228	1.4200	**1.2683**
	NH[(a)]			0.8862	0.8177	**0.8192**	0.8731
	NC			1.0745	1.1216	1.1582	1.0919
C9-C9	CN[(b)]	-11.9	-1.9	1.2800	1.2282	1.2984	**1.2653**
	NC			1.2601	1.3022	1.3230	1.2942
	NH[(a)]			0.8852	0.7887	**0.7894**	0.8732
	NC			1.0949	1.1542	1.1983	1.1368
C10-C10	CN[(b)]	-20.3	-8.9	1.3434	1.2810	1.3593	**1.3399**
	NC			1.0896	1.1061	1.1365	1.0941
	CO			1.2685	1.2555	1.3075	1.3339

[(a)] Proton donor; [(b)] Proton acceptor ; [(c)] Figure 6a; [(d)] Figure 6b; [(e)] Figure 6c

Table S8: Change in delocalization indices for the main bonds in the skeleton. In bold values that correspond to the hydrogen bond formation in one-HB complex. (HB formed between NH[(a)] from monomer 1 and C=O[(b)] from monomer 2 (or CN)).

				ΔDI			
				One-HB formation		From one to two-HB (rotation)	
		E_{int}	E_{RiR}	Monomer 1	Monomer 2	Monomer 1	Monomer 2
	NH[(a)]			**-0.0920**	-0.0207	0.0012	-0.0701
FI-FI	NC	-15.0	-4.8	0.0518	0.0446	0.0114	0.0186
	CN[(b)]			0.0449	**0.0837**	-0.0347	-0.0735
	NH[(a)]			**-0.0772**	-0.0265	0.0031	-0.0476
FA-FA	CN	-14.3	-5.2	0.0281	0.0260	0.0070	0.0091
	CO[(b)]			0.0507	**0.0491**	-0.0345	-0.0329

Table S8 – cont.

	NH[a]			**-0.0765**	-0.0057	-0.0006	-0.0714
C1-C1	CN	-12.2	-2.8	0.0518	0.0559	-0.0086	-0.0127
	CO[b]			0.0265	**-0.0172**	-0.1011	-0.0574
	NH[a]			**-0.0829**	-0.0223	0.0014	-0.0592
C2-C2	CN	-15.7	-5.3	0.0747	0.0513	-0.0279	-0.0045
	CO[b]			0.0511	**0.0415**	-0.0893	-0.0797
	NH[a]			**-0.0694**	-0.0039	0.0010	-0.0645
C3-C3	CN	-11.1	-2.7	0.0021	0.0063	-0.0145	-0.0187
	CO[b]			0.0407	**0.0148**	-0.0187	0.0072
	NH(a)			**-0.0755**	-0.0206	-0.0022	-0.0571
C4-C4	CN	-16.3	-5.6	0.0697	0.0656	-0.0117	-0.0076
	CO[b]			0.0200	**0.0041**	-0.0537	-0.0378
	NH[a]			**-0.0601**	-0.0115	0.0006	-0.0480
C5-C5	CN	-16.0	-5.0	0.0141	0.0039	-0.0226	-0.0124
	CO[b]			0.0418	**0.0202**	-0.0926	-0.0710
	NH[a]			**-0.1067**	-0.0138	0.0006	-0.0923
C6-C6	NC	-21.0	-7.4	0.0368	0.0265	0.0243	0.0346
	CO[b]			0.0626	**0.0086**	-0.1297	-0.0757
	CO			0.1189	0.0621	-0.1152	-0.0584
	CN			0.0450	0.0362	-0.0303	-0.0215
C7-C7	NH[a]	-12.2	-3.1	-**0.0482**	-0.0109	0.0005	-0.0368
	NC			0.0524	0.0287	-0.0447	-0.0210
	CO[b]			0.0004	**-0.0716**	-0.1287	-0.0567
	CN			0.0098	-0.0014	-0.0048	0.0064
	CN			0.0528	0.0047	-0.0137	0.0344
C8-C8	NH[a]	-27.6	-8.7	**-0.0934**	-0.0185	-0.0188	-0.0937
	NC			0.0068	-0.0030	0.0100	0.0198
	CO[b]			0.0840	-**0.0677**	-0.1972	-0.0455
	NH[a]			**-0.0670**	-0.0131	-0.0015	-0.0554
	NC			0.0837	0.0174	-0.0366	0.0297
C9-C9	CN[b]	-11.9	-1.9	0.0184	**-0.0147**	-0.0702	-0.0371
	NC			0.0629	0.0341	-0.0208	0.0080
	NH[a]			**-0.0958**	-0.0120	-0.0007	-0.0845
	NC			0.1034	0.0419	-0.0441	0.0174
C10-C10	CN[b]	-20.3	-8.9	0.0159	**-0.0035**	-0.0783	-0.0589
	NC			0.0469	0.0045	-0.0304	0.0120
	CO			0.0390	0.0654	-0.0520	-0.0784

[a] Proton donor; [b] Proton acceptor

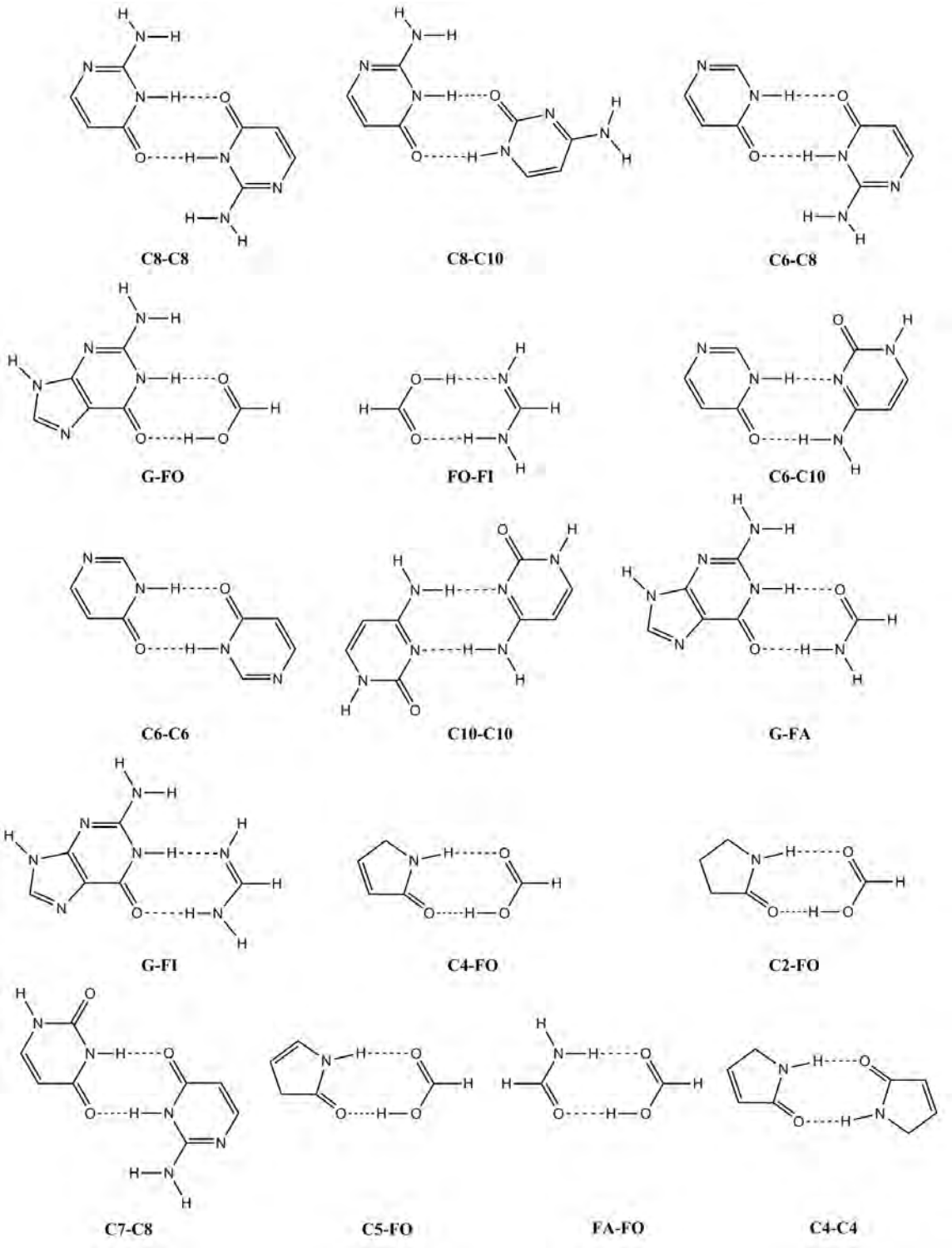

Figure S1: All complexes used in this work.

Figure S1 – cont.

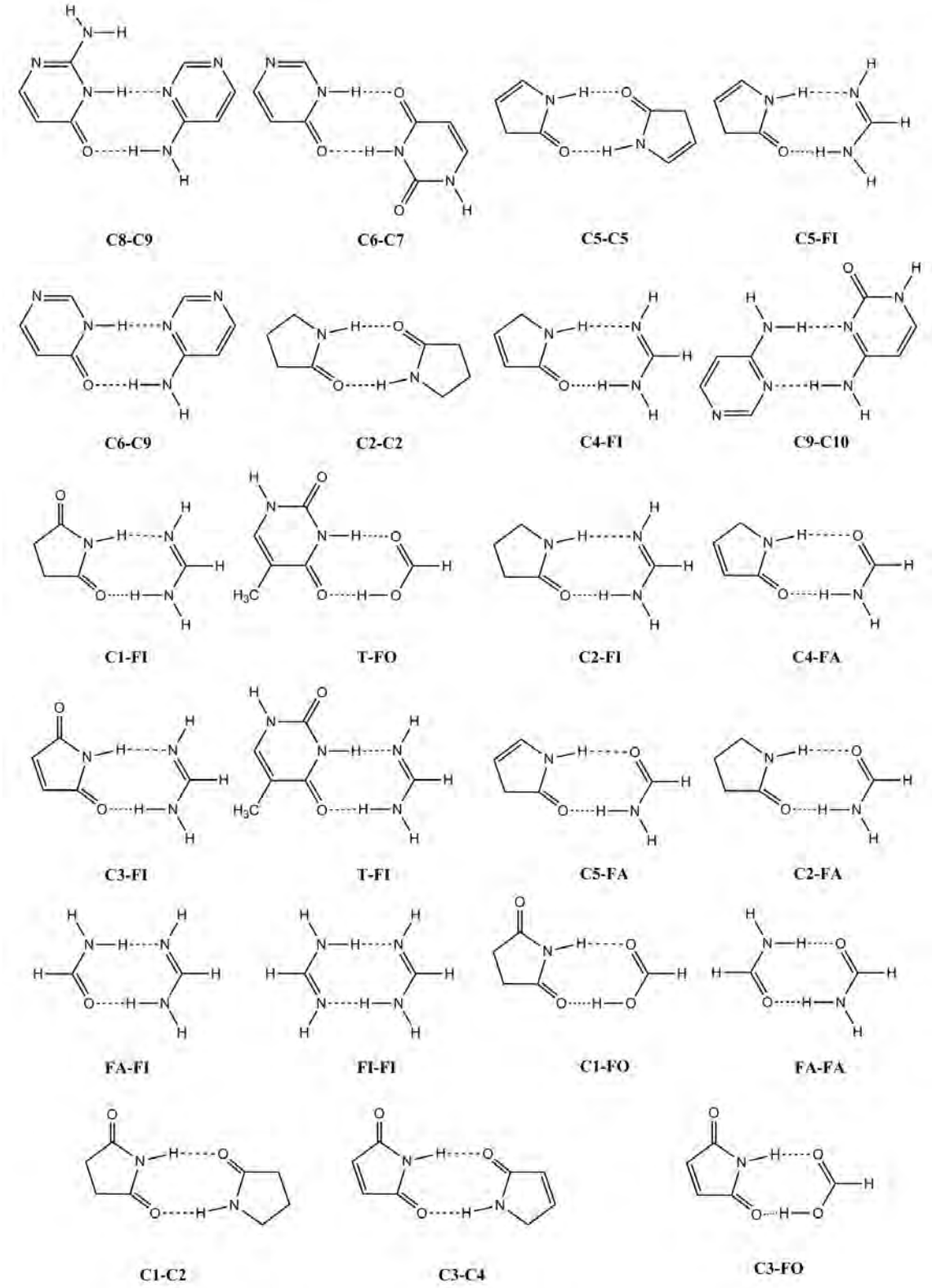

Figure S1 – cont.

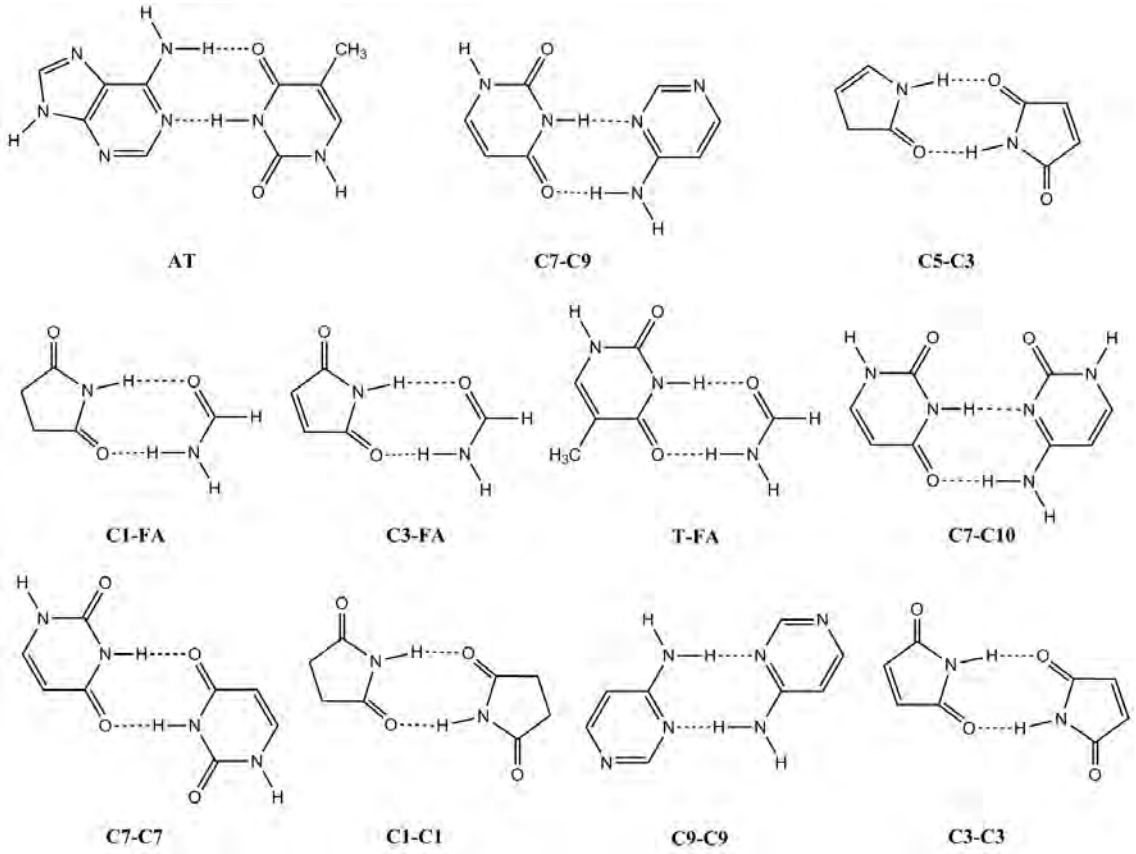

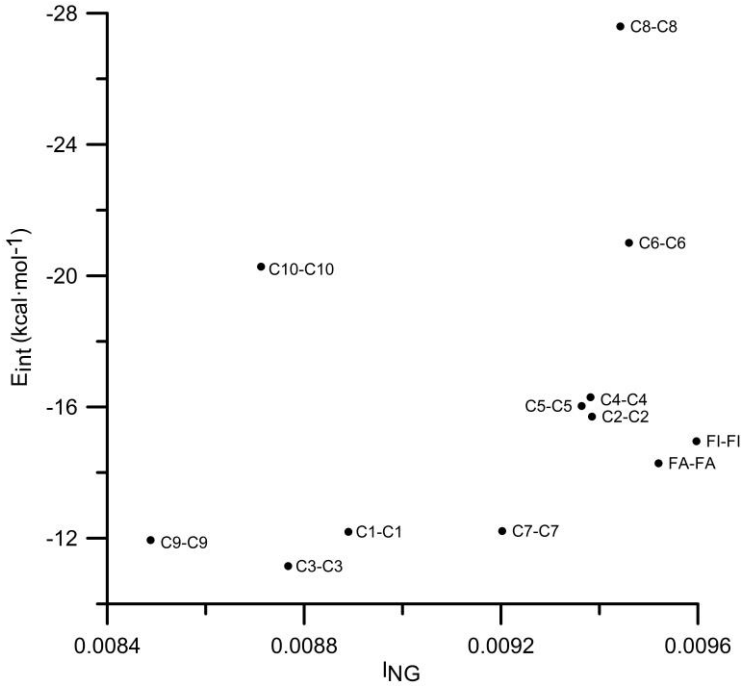

Figure S2: Interaction energy with respect to the n-center delocalization index, I_{NG}.

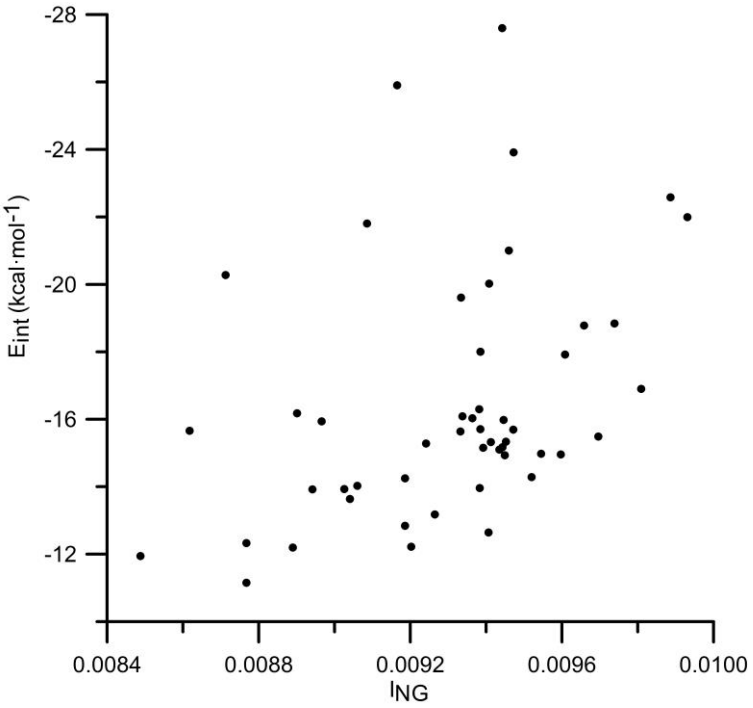

Figure S3: Interaction energy with respect to the n-center delocalization index, $I_{NG.}$

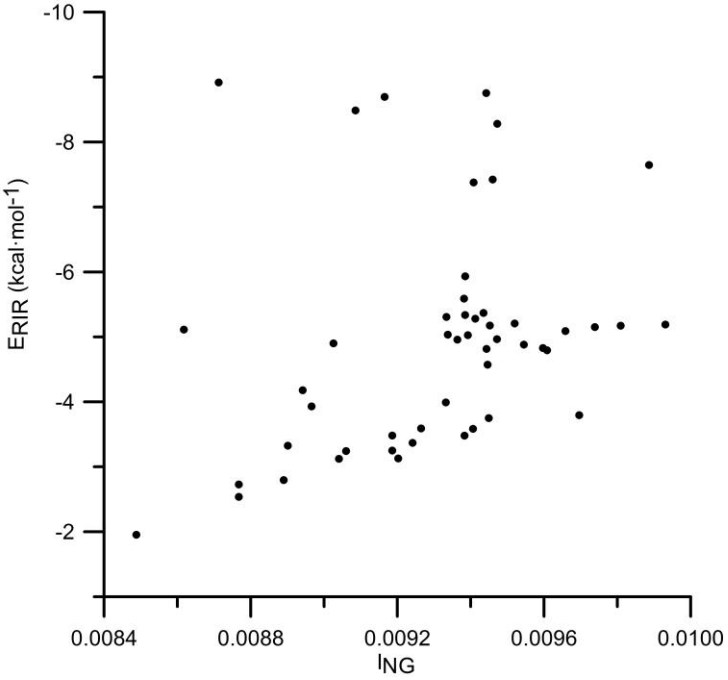

Figure S4: E_{RiR} with respect to the n-center delocalization index, $I_{NG.}$

Supporting information for CHAPTER 6

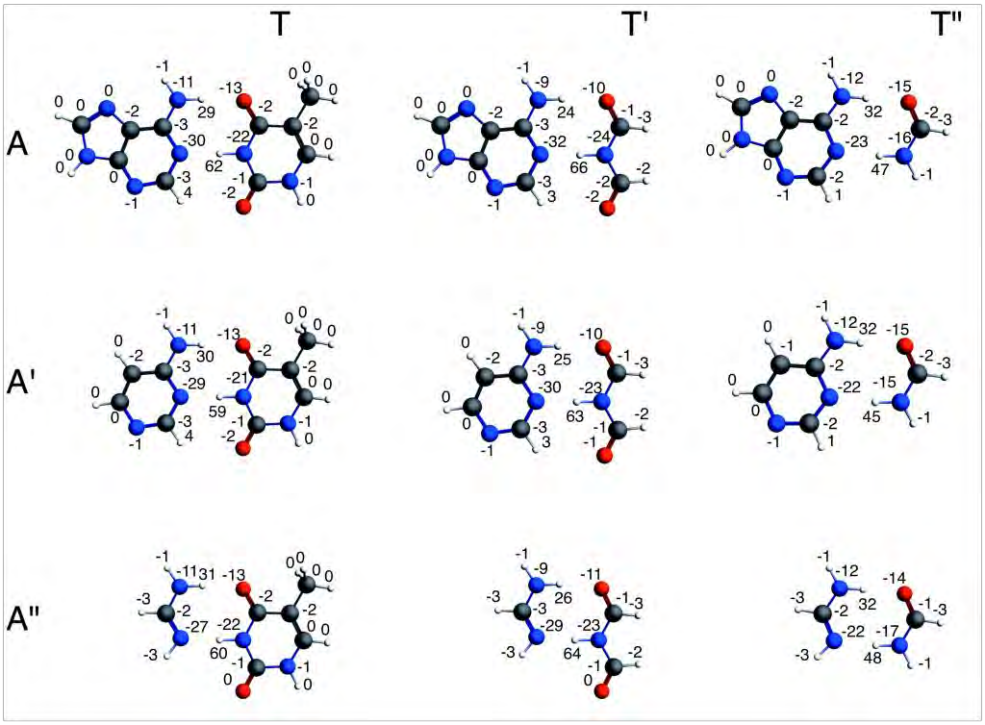

Figure S5: The σ component of Pauli VDD charges of AT and its smaller analogues (see eq. (6.11)).

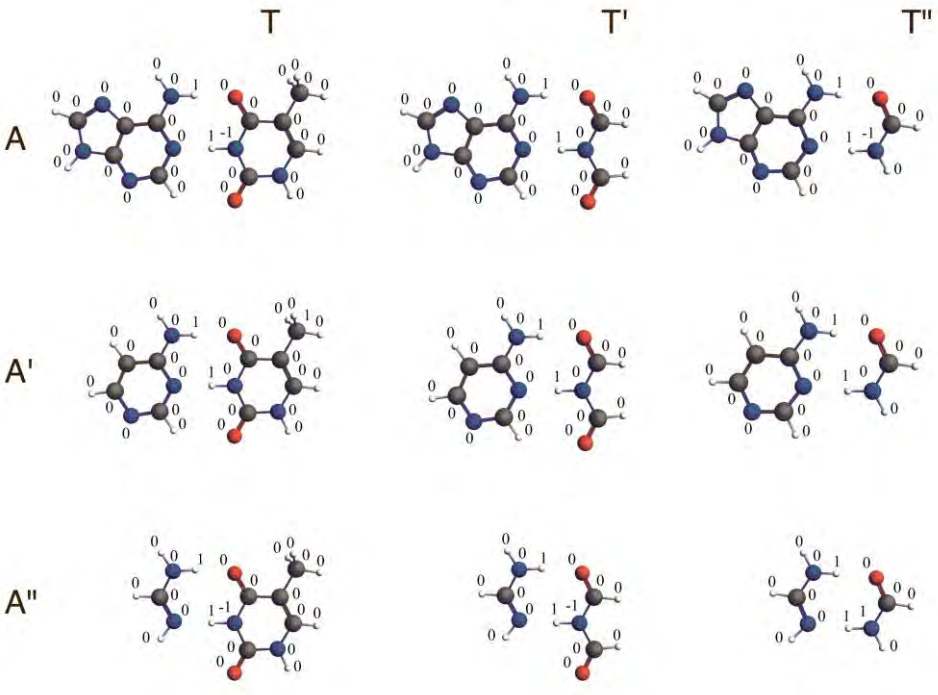

Figure S6: The π component of Pauli VDD charges of AT and its smaller analogues (see eq. (6.11)).

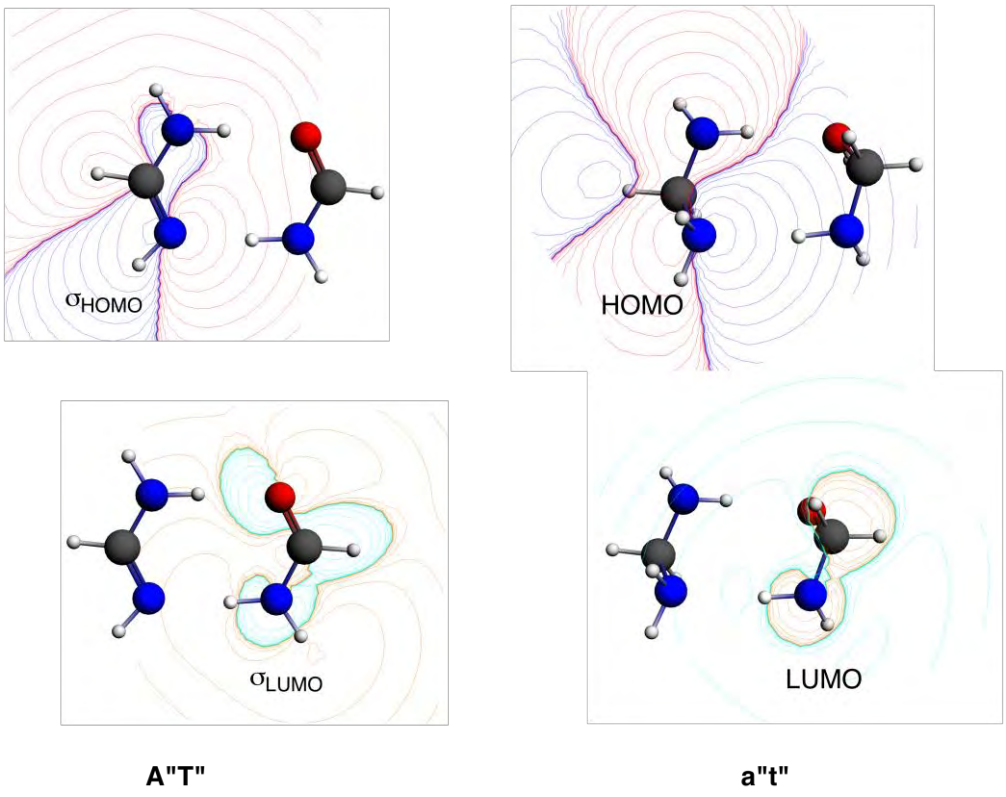

Figure S7: Frontier orbitals in the hydrogen bond N···(H)N of A”T” and a”t”.

Table S9: Hydrogen bond N–H···O in AT analogues.

	AT	AT	AT''	A'T	A'T'	A'T''	A''T	A''T'	A''T''
Energy gap $\lvert\varepsilon_A - \varepsilon_T\rvert$ (eV)									
$\lvert\varepsilon_{LUMO+1} - \varepsilon_{HOMO}\rvert$	5.94	6.40	5.76	6.41	6.88	6.22	6.34	6.80	6.14
$\lvert\varepsilon_{LUMO} - \varepsilon_{HOMO}\rvert$	5.70	6.16	5.53	5.48	5.95	5.30	5.66	6.11	5.46
$\lvert\varepsilon_{LUMO+1} - \varepsilon_{HOMO-1}\rvert$	6.75	7.18	9.72	7.23	7.66	10.18	7.17	7.60	10.09
$\lvert\varepsilon_{LUMO} - \varepsilon_{HOMO-1}\rvert$	6.51	6.95	9.48	6.30	6.74	9.25	6.48	6.90	9.41
Overlap **<A|T>**									
$\langle\sigma_{LUMO+1}\lvert\sigma_{HOMO}\rangle$	0.07	-0.06	0.09	-0.07	0.06	-0.10	0.08	0.07	0.11
$\langle\sigma_{LUMO}\lvert\sigma_{HOMO}\rangle$	-0.07	0.05	-0.10	0.08	-0.06	-0.11	0.07	-0.05	0.09
$\langle\sigma_{LUMO+1}\lvert\sigma_{HOMO-1}\rangle$	-0.05	-0.07	-	-0.04	-0.06	-	0.03	-0.06	-
$\langle\sigma_{LUMO}\lvert\sigma_{HOMO-1}\rangle$	0.05	0.07	-	0.05	0.08	-	0.04	0.06	-
Gross Population (electrons)									
σ_{LUMO+1} of A	0.01	0.01	0.01	0.01	0.01	0.02	0.02	0.02	0.02
σ_{LUMO} of A	0.01	0.01	0.02	0.02	0.01	0.02	0.01	0.01	0.01
σ_{HOMO} of T	1.97	1.98	1.95	1.97	1.98	1.95	1.97	1.98	1.95
σ_{HOMO-1} of T	1.99	1.97	2.00	1.99	1.97	2.00	1.99	1.98	2.00

Table S10: Hydrogen bond N···H–N in AT analogues.

	AT	AT'	AT''	A'T	A'T'	A'T''	A''T	A''T'	A''T''
Energy gap $\lvert\varepsilon_A - \varepsilon_T\rvert$ (eV)									
$\lvert\varepsilon_{HOMO} - \varepsilon_{LUMO+1}\rvert$	5.78	5.75	5.90	5.70	5.67	5.82	5.86	5.85	5.99
$\lvert\varepsilon_{HOMO} - \varepsilon_{LUMO}\rvert$	5.05	5.13	5.07	4.96	5.06	4.99	5.16	5.19	5.17
$\lvert\varepsilon_{HOMO-1} - \varepsilon_{LUMO+1}\rvert$	6.63	6.61	6.73	6.81	6.78	6.90	10.99	10.99	11.04
$\lvert\varepsilon_{HOMO-1} - \varepsilon_{LUMO}\rvert$	5.91	5.98	5.91	6.08	6.18	6.07	10.29	10.32	10.22
Overlap **<A|T>**									
$\langle\sigma_{HOMO}\lvert\sigma_{LUMO+1}\rangle$	0.18	-	-0.18	-0.16	-	-0.17	-0.30	-	0.27
$\langle\sigma_{HOMO}\lvert\sigma_{LUMO}\rangle$	-	-0.23	0.15	-	-0.22	-0.15	-	-0.34	0.23
$\langle\sigma_{HOMO-1}\lvert\sigma_{LUMO+1}\rangle$	0.15	-	-0.15	-0.15	-	0.16	-	-	-
$\langle\sigma_{HOMO-1}\lvert\sigma_{LUMO}\rangle$	-	0.19	0.12	-	-0.20	0.12	-	-	-
Gross Population (electrons)									
σ_{LUMO+1} of T	0.04	0.00	0.03	0.03	0.01	0.03	0.06	0.01	0.04
σ_{LUMO} of T	0.01	0.08	0.02	0.01	0.08	0.02	0.01	0.10	0.03
σ_{HOMO} of A	1.95	1.95	1.97	1.96	1.95	1.97	1.88	1.87	1.91
σ_{HOMO-1} of A	1.97	1.97	1.98	1.96	1.96	1.98	2.00	2.00	2.00

Table S11: Cartesian coordinates of AT and its smaller mimics optimized at the BLYP-D3(BJ)/TZ2P level of theory.

AT (E= -4494.40 kcal·mol^{-1}; nimag = 0)

N	2.800551000	0.016603000	0.000000000
C	3.428805000	-1.180122000	0.000000000
N	4.747802000	-1.416032000	0.000000000
C	5.451956000	-0.268506000	0.000000000
C	4.937625000	1.039101000	0.000000000
C	3.527395000	1.166001000	0.000000000
N	6.826787000	-0.101469000	0.000000000
C	7.068317000	1.266701000	0.000000000
N	5.961055000	1.983947000	0.000000000
N	2.888698000	2.352506000	0.000000000
H	2.767749000	-2.043922000	0.000000000
H	7.510691000	-0.848165000	0.000000000
H	8.074345000	1.664051000	0.000000000
H	3.440110000	3.199091000	0.000000000
H	1.861128000	2.393656000	0.000000000
N	0.001031000	0.010111000	0.000000000
C	-0.590462000	-1.240648000	0.000000000
N	-1.990595000	-1.190738000	0.000000000
C	-2.713088000	-0.014584000	0.000000000
C	-2.114205000	1.203780000	0.000000000
C	-0.648398000	1.245748000	0.000000000
O	0.005632000	2.304469000	0.000000000
O	0.028571000	-2.301068000	0.000000000
C	-2.869390000	2.506162000	0.000000000
H	1.062369000	0.016735000	0.000000000
H	-2.455104000	-2.091143000	0.000000000
H	-3.792785000	-0.132614000	0.000000000
H	-2.606213000	3.106455000	0.879309000
H	-3.951050000	2.334898000	0.000000000
H	-2.606213000	3.106455000	-0.879309000

AT' (E= -3452.12 kcal·mol^{-1}; nimag = 0)

N	2.815279000	0.018977000	0.000000000
C	3.445480000	-1.178306000	0.000000000
N	4.763109000	-1.411642000	0.000000000
C	5.466562000	-0.263743000	0.000000000
C	4.950218000	1.043181000	0.000000000
C	3.540897000	1.168658000	0.000000000
N	6.840339000	-0.094798000	0.000000000
C	7.079676000	1.273650000	0.000000000
N	5.971435000	1.989427000	0.000000000
N	2.906127000	2.358817000	0.000000000
H	2.786799000	-2.044136000	0.000000000
H	7.525545000	-0.840481000	0.000000000
H	8.085044000	1.672593000	0.000000000
H	3.460168000	3.203828000	0.000000000
H	1.883451000	2.410018000	0.000000000
N	0.035690000	-0.003637000	0.000000000
C	-0.630329000	-1.221321000	0.000000000
C	-0.613546000	1.204574000	0.000000000
O	-0.044866000	2.294913000	0.000000000
O	-0.066343000	-2.301967000	0.000000000
H	1.107208000	-0.005854000	0.000000000
H	-1.718108000	1.125193000	0.000000000
H	-1.735389000	-1.118594000	0.000000000

AT'' (E= -3107.58 kcal·mol^{-1}; nimag = 0)

N	-0.603891000	-0.816530000	0.000000000
C	0.208653000	-1.895251000	0.000000000
N	1.547779000	-1.935144000	0.000000000
C	2.071478000	-0.694105000	0.000000000
C	1.361753000	0.516819000	0.000000000
C	-0.053624000	0.430853000	0.000000000
N	3.404359000	-0.318667000	0.000000000
C	3.432004000	1.070535000	0.000000000
N	2.227134000	1.607846000	0.000000000
N	-0.847888000	1.516485000	0.000000000
H	-0.297531000	-2.859019000	0.000000000
H	4.195494000	-0.950569000	0.000000000
H	4.364654000	1.618366000	0.000000000
H	-0.409669000	2.427508000	0.000000000
H	-1.876265000	1.437735000	0.000000000
N	-3.503033000	-1.026989000	0.000000000
C	-4.198181000	0.129138000	0.000000000
O	-3.700113000	1.262821000	0.000000000
H	-2.459975000	-1.018370000	0.000000000
H	-4.004831000	-1.906089000	0.000000000
H	-5.297901000	-0.009327000	0.000000000

A'T (E= -3931.63 kcal·mol^{-1}; nimag = 0)

N	2.799056000	0.003769000	0.000000000
C	3.444114000	-1.174780000	0.000000000
N	4.766144000	-1.371488000	0.000000000
C	5.507753000	-0.235010000	0.000000000
C	4.962115000	1.035297000	0.000000000
C	3.547078000	1.137517000	0.000000000
N	2.887569000	2.320787000	0.000000000
H	2.802181000	-2.054761000	0.000000000
H	3.405903000	3.186451000	0.000000000
H	1.858826000	2.345702000	0.000000000
N	-0.014037000	0.003367000	0.000000000
C	-0.612438000	-1.245014000	0.000000000
N	-2.012452000	-1.186098000	0.000000000
C	-2.727604000	-0.005852000	0.000000000
C	-2.121796000	1.209330000	0.000000000
C	-0.656075000	1.242670000	0.000000000
O	0.005422000	2.297228000	0.000000000
O	0.000688000	-2.307995000	0.000000000
C	-2.870928000	2.515380000	0.000000000
H	1.044890000	0.004304000	0.000000000
H	-2.482535000	-2.083664000	0.000000000
H	-3.807997000	-0.117345000	0.000000000
H	-2.605637000	3.114526000	0.879456000
H	-3.953345000	2.348805000	0.000000000
H	-2.605637000	3.114526000	-0.879456000
H	5.589764000	1.923756000	0.000000000
H	6.588963000	-0.367365000	0.000000000

A'T' (E= -2889.15 kcal·mol^{-1}; nimag = 0)

N	2.813812000	0.010048000	0.000000000
C	3.459408000	-1.169456000	0.000000000
N	4.779901000	-1.365030000	0.000000000
C	5.522005000	-0.228940000	0.000000000
C	4.976022000	1.041199000	0.000000000
C	3.561806000	1.143261000	0.000000000
N	2.906270000	2.330162000	0.000000000
H	2.818934000	-2.050740000	0.000000000
H	3.426259000	3.194828000	0.000000000
H	1.882234000	2.363424000	0.000000000
N	0.018354000	-0.005933000	0.000000000
C	-0.657622000	-1.219616000	0.000000000
C	-0.619984000	1.207634000	0.000000000
O	-0.041019000	2.292896000	0.000000000
O	-0.101538000	-2.303482000	0.000000000
H	1.086445000	-0.016038000	0.000000000
H	5.603247000	1.929732000	0.000000000
H	6.602853000	-0.361654000	0.000000000
H	-1.725006000	1.138377000	0.000000000
H	-1.761716000	-1.107397000	0.000000000

A'T'' (E= -2545.00 kcal·mol^{-1}; nimag = 0)

N	0.391127000	-0.534936000	0.000000000
C	1.422188000	-1.395425000	0.000000000
N	2.727669000	-1.113854000	0.000000000
C	3.016799000	0.213051000	0.000000000
C	2.052082000	1.200950000	0.000000000
C	0.690800000	0.793176000	0.000000000
N	-0.334128000	1.675294000	0.000000000
H	1.153106000	-2.452017000	0.000000000
H	-0.138153000	2.665497000	0.000000000
H	-1.317590000	1.363362000	0.000000000
N	-2.408072000	-1.363286000	0.000000000
C	-3.326530000	-0.375549000	0.000000000
O	-3.071507000	0.836444000	0.000000000
H	-1.390902000	-1.137715000	0.000000000
H	-2.716009000	-2.327539000	0.000000000
H	-4.374130000	-0.736985000	0.000000000
H	2.319413000	2.255466000	0.000000000
H	4.073874000	0.474891000	0.000000000

A''T (E= -3074.34 kcal·mol^{-1}; nimag = 0)

N	-2.666651000	-1.236455000	0.000000000
C	-3.610193000	-0.350318000	0.000000000
N	-3.361475000	0.980729000	0.000000000
H	-4.126428000	1.637549000	0.000000000
H	-2.388106000	1.319902000	0.000000000
N	0.058831000	-0.527510000	0.000000000
C	0.984330000	-1.558737000	0.000000000
N	2.315623000	-1.112172000	0.000000000
C	2.677277000	0.218278000	0.000000000
C	1.756563000	1.215169000	0.000000000
C	0.337820000	0.840310000	0.000000000
O	-0.579757000	1.682175000	0.000000000
O	0.701365000	-2.751946000	0.000000000
C	2.111000000	2.678336000	0.000000000
H	-0.964045000	-0.825464000	0.000000000
H	3.013916000	-1.846066000	0.000000000
H	3.746224000	0.411473000	0.000000000
H	1.688707000	3.179912000	-0.879154000
H	3.196996000	2.820725000	0.000000000
H	1.688707000	3.179912000	0.879154000
H	-4.677729000	-0.607838000	0.000000000
H	-3.027795000	-2.189569000	0.000000000

A''T' (E= -2032.88 kcal·mol^{-1}; nimag = 0)

N	-1.110588000	-1.526761000	0.000000000
C	-2.345005000	-1.136921000	0.000000000
N	-2.703978000	0.168718000	0.000000000
H	-3.679281000	0.424946000	0.000000000
H	-1.986092000	0.903202000	0.000000000
N	1.023447000	0.277208000	0.000000000
C	2.348477000	-0.144816000	0.000000000
C	0.690458000	1.606812000	0.000000000
O	-0.459145000	2.046290000	0.000000000
O	2.697553000	-1.311213000	0.000000000
H	0.238824000	-0.457342000	0.000000000
H	-3.193033000	-1.833404000	0.000000000
H	-1.024101000	-2.542334000	0.000000000
H	3.071357000	0.698966000	0.000000000
H	1.565439000	2.286645000	0.000000000

A''T'' (E=-1688.82 kcal·mol^{-1}; nimag = 0)

N	1.460561000	1.198732000	0.000000000
C	2.074834000	0.056421000	0.000000000
N	1.432035000	-1.134432000	0.000000000
H	1.968167000	-1.988805000	0.000000000
H	0.400119000	-1.186897000	0.000000000
N	-1.434309000	1.138121000	0.000000000
C	-2.029066000	-0.071108000	0.000000000
O	-1.444617000	-1.164165000	0.000000000
H	-0.391468000	1.235326000	0.000000000
H	3.169959000	-0.032619000	0.000000000
H	-3.137408000	-0.022813000	0.000000000
H	2.125610000	1.972300000	0.000000000
H	-2.014779000	1.967661000	0.000000000

a''t'' (chair) (E=-2002.95 kcal·mol^{-1}; nimag = 0)

H	-0.162087000	1.572337000	0.294911000
H	-1.052303000	2.915502000	0.689211000
H	-3.069710000	1.954255000	0.315303000
H	-2.451525000	-0.094417000	1.519969000
H	-3.177129000	-0.502178000	0.091095000
H	-2.126066000	1.297733000	-1.042357000
N	-2.343879000	-0.077577000	0.503256000
N	-1.032720000	1.897779000	0.728438000
C	-2.199672000	1.328350000	0.059365000
H	2.364942000	-1.287349000	-0.010569000
H	1.351209000	-0.523423000	1.249450000
H	1.580539000	0.442263000	-1.407011000
N	0.320233000	-1.592836000	-0.192716000
H	-0.593454000	-1.153474000	-0.009920000
H	0.376945000	-1.923815000	-1.154588000
O	1.497257000	0.577301000	-0.446219000
C	1.421207000	-0.763577000	0.185706000

a''t'' (boat) (E=-1998.20 kcal·mol^{-1}; nimag = 0)

N	1.596007000	1.274078000	0.030909000
C	1.884819000	-0.097893000	0.513105000
N	1.477006000	-1.041115000	-0.524003000
H	1.895512000	-1.956161000	-0.364420000
H	0.458666000	-1.154777000	-0.549253000
N	-1.465130000	0.972679000	-0.475064000
C	-1.882114000	0.053063000	0.525107000
O	-1.675086000	-1.319241000	0.015331000
H	-0.504420000	1.313449000	-0.379963000
H	2.954769000	-0.269108000	0.713969000
H	-2.948572000	0.188639000	0.748304000
H	2.094007000	1.421695000	-0.849992000
H	-2.139020000	1.684708000	-0.722848000
H	1.348035000	-0.206679000	1.472891000
H	1.928785000	1.968226000	0.702988000
H	-1.786016000	-1.930206000	0.766921000
H	-1.303784000	0.140738000	1.459948000

A''T'' ***R(sp^3)***

N	1.390600000	1.179100000	0.000000000
C	2.063300000	0.070200000	0.000000000
N	1.483100000	-1.152400000	0.000000000
H	2.062800000	-1.977900000	0.000000000
H	0.455300000	-1.258300000	0.000000000
N	-1.749300000	1.152400000	0.000000000
C	-2.263400000	-0.093200000	0.000000000
O	-1.608600000	-1.145600000	0.000000000
H	-0.715100000	1.317800000	0.000000000
H	3.161600000	0.038000000	0.000000000
H	-3.372600000	-0.117700000	0.000000000
H	2.014600000	1.986100000	0.000000000
H	-2.382900000	1.942100000	0.000000000

a"t'' ***R(sp^2)***

H	-2.126100000	1.297700000	-1.042400000
N	-2.343900000	-0.077600000	0.503300000
N	-1.032700000	1.897800000	0.728400000
C	-2.199700000	1.328400000	0.059400000
H	-0.162100000	1.572300000	0.294900000
H	-1.052300000	2.915500000	0.689200000
H	-3.069700000	1.954300000	0.315300000
H	-2.451500000	-0.094400000	1.520000000
H	-3.177100000	-0.502200000	0.091100000
H	-0.793600000	-1.022600000	0.058100000
H	0.163900000	-1.808200000	-1.087100000
N	0.113800000	-1.474400000	-0.125800000
H	2.162700000	-1.195600000	0.051100000
H	1.162000000	-0.415600000	1.311700000
H	1.398100000	0.541200000	-1.347300000
O	1.318800000	0.679400000	-0.386600000
C	1.226500000	-0.659000000	0.248400000

Appendix D

Supporting information for CHAPTER *7*

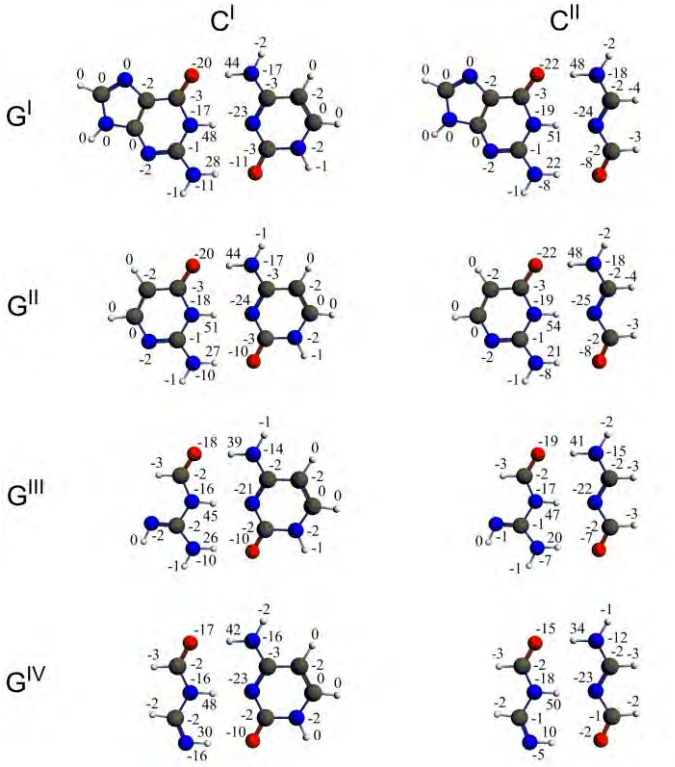

Figure S8: The σ component of Pauli VDD charges of $G^{I}C^{I}$ and its smaller analogues (see eq. (7.11)).

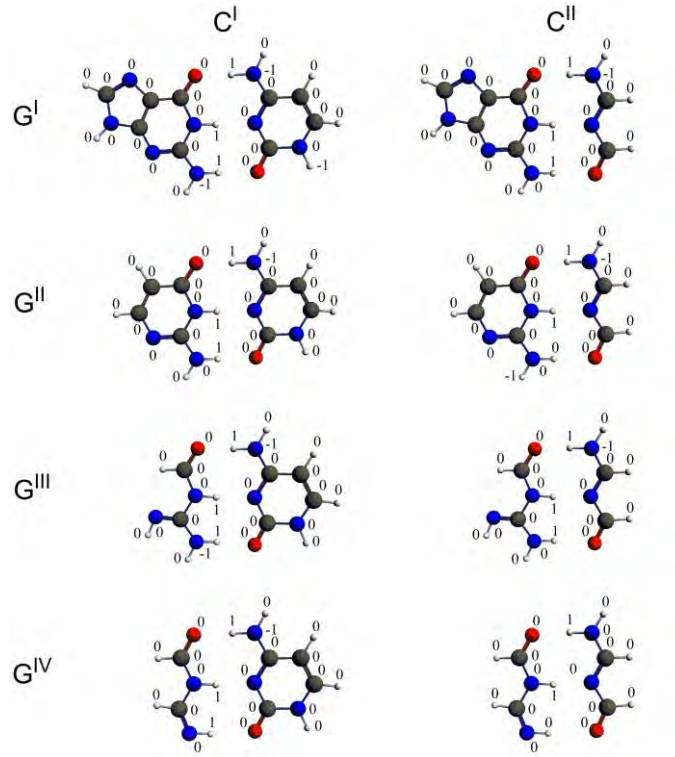

Figure S9: The π component of Pauli VDD charges of $G^{I}C^{I}$ and its smaller analogues (see eq. (7.11)).

Table S12: Hydrogen bond O···H-N in $G^{I}C^{I}$ mimics.

	$G^{I}C^{I}$	$G^{I}C^{II}$	$G^{II}C^{I}$	$G^{II}C^{II}$	$G^{III}C^{I}$	$G^{III}C^{II}$	$G^{IV}C^{I}$	$G^{IV}C^{II}$
Energy gap $\lvert\varepsilon_G - \varepsilon_C\rvert$ (eV)								
$\lvert\varepsilon_{HOMO} - \varepsilon_{LUMO+1}\rvert$	5.35	5.39	5.34	5.38	5.46	5.54	5.73	6.13
$\lvert\varepsilon_{HOMO} - \varepsilon_{LUMO}\rvert$	4.96	4.62	4.96	4.61	5.08	4.76	5.35	5.34
$\lvert\varepsilon_{HOMO-1} - \varepsilon_{LUMO+1}\rvert$	5.86	5.92	6.35	6.41	6.58	6.66	6.51	7.00
$\lvert\varepsilon_{HOMO-1} - \varepsilon_{LUMO}\rvert$	5.47	5.15	5.96	5.64	6.21	5.88	6.12	6.21
Overlap $\langle G \mid C \rangle$								
$\langle\sigma_{HOMO}\mid\sigma_{LUMO+2}\rangle$	-0.08	-0.07	0.09	0.07	-0.09	0.08	0.03	-0.07
$\langle\sigma_{HOMO}\mid\sigma_{LUMO+1}\rangle$	-0.05	-0.10	-0.05	-0.10	-0.05	0.10	0.03	-0.09
$\langle\sigma_{HOMO}\mid\sigma_{LUMO}\rangle$	0.08	-0.09	-0.08	-0.09	0.08	0.09	-0.03	0.08
$\langle\sigma_{HOMO-1}\mid\sigma_{LUMO+2}\rangle$	-	-	-	-	-	-	-0.09	-0.06
$\langle\sigma_{HOMO-1}\mid\sigma_{LUMO+1}\rangle$	-	-	-	-	-	-	-0.05	-0.08
$\langle\sigma_{HOMO-1}\mid\sigma_{LUMO}\rangle$	-	-	-	-	-	-	0.07	0.05
Gross Population								
σ_{LUMO+2} of C	0.02	0.01	0.02	0.01	0.02	0.01	0.02	0.01
σ_{LUMO+1} of C	0.01	0.04	0.01	0.04	0.01	0.03	0.01	0.03
σ_{LUMO} of C	0.02	0.03	0.02	0.03	0.02	0.02	0.02	0.02
σ_{HOMO} of G	1.94	1.93	1.93	1.93	1.94	1.94	1.98	1.96
σ_{HOMO-1} of G	2.00	2.00	2.00	2.00	1.99	1.99	1.95	1.98

Table S13 Hydrogen bonds N-H···N and N-H···O in $G^{I}C^{I}$ mimics.

	$G^{I}C^{I}$	$G^{I}C^{II}$	$G^{II}C^{I}$	$G^{II}C^{II}$	$G^{III}C^{I}$	$G^{III}C^{II}$	$G^{IV}C^{I}$	$G^{IV}C^{II}$
Energy gap $\lvert\varepsilon_G - \varepsilon_C\rvert$ (eV)								
$\lvert\varepsilon_{LUMO+2} - \varepsilon_{HOMO}\rvert$	5.52	5.55	5.93	5.96	5.99	6.04	6.27	6.34
$\lvert\varepsilon_{LUMO+2} - \varepsilon_{HOMO-1}\rvert$	6.13	6.57	6.52	6.96	6.59	7.05	6.89	7.32
$\lvert\varepsilon_{LUMO+1} - \varepsilon_{HOMO}\rvert$	5.23	5.27	5.52	5.55	5.30	5.35	5.54	5.70
$\lvert\varepsilon_{LUMO+1} - \varepsilon_{HOMO-1}\rvert$	5.85	6.29	6.12	6.55	5.90	6.36	6.15	6.68
$\lvert\varepsilon_{LUMO} - \varepsilon_{HOMO}\rvert$	4.32	4.36	4.32	4.36	4.29	4.34	4.86	4.82
$\lvert\varepsilon_{LUMO} - \varepsilon_{HOMO-1}\rvert$	4.93	5.38	4.92	5.36	4.90	5.35	5.47	5.81
Overlap $\langle G \mid C \rangle$								
$\langle\sigma_{LUMO+2}\mid\sigma_{HOMO}\rangle$	-0.04	0.10	-	-	-0.04	0.00	-0.07	0.01
$\langle\sigma_{LUMO+2}\mid\sigma_{HOMO-1}\rangle$	0.24	0.24	-	-	-0.18	0.19	-0.15	0.22
$\langle\sigma_{LUMO+1}\mid\sigma_{HOMO}\rangle$	-	-	-0.11	-0.10	0.08	-0.14	-	-
$\langle\sigma_{LUMO+1}\mid\sigma_{HOMO-1}\rangle$	-	-	0.25	0.24	-0.22	0.20	-	-
$\langle\sigma_{LUMO}\mid\sigma_{HOMO}\rangle$	0.14	-0.20	-0.14	-0.21	-0.13	-0.19	-0.12	0.22
$\langle\sigma_{LUMO}\mid\sigma_{HOMO-1}\rangle$	-0.22	-0.19	-0.22	0.20	0.20	0.18	0.32	-0.27
Gross Population								
σ_{LUMO+2} of G	0.03	0.03	0.01	0.01	0.02	0.02	0.02	0.03
σ_{LUMO+1} of G	0.00	0.00	0.03	0.03	0.02	0.02	0.00	0.00
σ_{LUMO} of G	0.05	0.05	0.05	0.05	0.04	0.04	0.07	0.06
σ_{HOMO} of C	1.96	1.96	1.96	1.97	1.96	1.97	1.97	1.98
σ_{HOMO-1} of C	1.95	1.94	1.95	1.94	1.95	1.95	1.94	1.94

Table S14: Cartesian coordinates of $G^{l}C^{l}$ and its smaller mimics optimized at the BLYP-D3(BJ)/TZ2P level of theory.

$G^{l}C^{l}$ (E= -4400.21 kcal·mol^{-1}; nimag = 0)

N	-3.186600000	-0.566000000	0.000000000
O	0.780800000	1.825700000	0.000000000
N	-1.247100000	0.723200000	0.000000000
C	-2.625000000	0.667000000	0.000000000
N	-3.398700000	1.751500000	0.000000000
C	-2.686100000	2.898800000	0.000000000
C	-1.289100000	3.074400000	0.000000000
C	-0.466200000	1.904300000	0.000000000
N	-3.200800000	4.178900000	0.000000000
C	-2.113900000	5.055600000	0.000000000
N	-0.959400000	4.428400000	0.000000000
H	-2.632600000	-1.431400000	0.000000000
H	-4.195200000	-0.607700000	0.000000000
H	-0.711600000	-0.169700000	0.000000000
H	-4.185900000	4.412000000	0.000000000
H	-2.253300000	6.128100000	0.000000000
O	-1.637200000	-2.995100000	0.000000000
N	2.235200000	-0.502900000	0.000000000
N	0.288300000	-1.726200000	0.000000000
C	2.412600000	-2.918900000	0.000000000
C	-0.398200000	-2.900900000	0.000000000
N	0.366500000	-4.097000000	0.000000000
C	1.731600000	-4.095600000	0.000000000
C	1.634100000	-1.701700000	0.000000000
H	3.496700000	-2.897300000	0.000000000
H	-0.164100000	-4.961400000	0.000000000
H	2.219700000	-5.064300000	0.000000000
H	1.672700000	0.381500000	0.000000000
H	3.244000000	-0.449700000	0.000000000

$G^{l}C^{II}$ (E= -3727.00 kcal·mol^{-1}; nimag = 0)

N	0.590136000	-2.485132000	0.000000000
O	-0.104936000	2.093105000	0.000000000
N	0.131646000	-0.203026000	0.000000000
C	-0.339945000	-1.497302000	0.000000000
N	-1.636436000	-1.799103000	0.000000000
C	-2.424021000	-0.701469000	0.000000000
C	-2.051999000	0.657935000	0.000000000
C	-0.657332000	0.968798000	0.000000000
N	-3.802988000	-0.686985000	0.000000000
C	-4.197392000	0.652422000	0.000000000
N	-3.176988000	1.479815000	0.000000000
H	1.597888000	-2.302170000	0.000000000
H	0.251265000	-3.436047000	0.000000000
H	1.162352000	-0.054640000	0.000000000
H	-4.395467000	-1.507949000	0.000000000
H	-5.241711000	0.933620000	0.000000000
O	3.528416000	-1.956949000	0.000000000
N	2.577932000	2.535133000	0.000000000
N	2.949284000	0.260314000	0.000000000
C	3.856789000	-0.770590000	0.000000000
C	3.402413000	1.497129000	0.000000000
H	1.528857000	2.383709000	0.000000000
H	2.955235000	3.473820000	0.000000000
H	4.479708000	1.718379000	0.000000000
H	4.935630000	-0.486686000	0.000000000

$G^{II}C^{I}$ (E= -3841.69 kcal·mol^{-1}; nimag = 0)

N	-1.447244000	-2.312188000	0.000000000
O	-1.381613000	2.311201000	0.000000000
N	-1.475996000	0.012692000	0.000000000
C	-2.170279000	-1.169076000	0.000000000
N	-3.503009000	-1.221880000	0.000000000
C	-4.138576000	-0.020318000	0.000000000
C	-3.522190000	1.213710000	0.000000000
C	-2.091706000	1.273591000	0.000000000
H	-0.420122000	-2.319190000	0.000000000
H	-1.966938000	-3.178136000	0.000000000
H	-0.432769000	-0.002376000	0.000000000
O	1.455817000	-2.281055000	0.000000000
N	1.371723000	2.322121000	0.000000000
N	1.393503000	0.023628000	0.000000000
C	3.522947000	1.203666000	0.000000000
C	2.029345000	-1.179312000	0.000000000
N	3.449272000	-1.157348000	0.000000000
C	4.165183000	0.005011000	0.000000000
C	2.078220000	1.181631000	0.000000000
H	4.075592000	2.136531000	0.000000000
H	3.906439000	-2.062798000	0.000000000
H	5.245909000	-0.089049000	0.000000000
H	0.322117000	2.307811000	0.000000000
H	1.856549000	3.208439000	0.000000000
H	-5.226502000	-0.079135000	0.000000000
H	-4.082959000	2.141518000	0.000000000

$G^{II}C^{II}$ (E= -3168.30 kcal·mol^{-1}; nimag = 0)

N	-0.692730000	-2.306668000	0.000000000
O	-0.525185000	2.312832000	0.000000000
N	-0.677721000	0.017194000	0.000000000
C	-1.395185000	-1.148907000	0.000000000
N	-2.727713000	-1.173142000	0.000000000
C	-3.335542000	0.042836000	0.000000000
C	-2.691629000	1.263882000	0.000000000
C	-1.261673000	1.289880000	0.000000000
H	0.331072000	-2.334743000	0.000000000
H	-1.224733000	-3.165177000	0.000000000
H	0.364870000	-0.026490000	0.000000000
O	2.317535000	-2.331055000	0.000000000
N	2.199040000	2.257780000	0.000000000
N	2.160413000	-0.045776000	0.000000000
C	2.861437000	-1.227055000	0.000000000
C	2.826998000	1.089652000	0.000000000
H	1.137849000	2.296664000	0.000000000
H	2.738459000	3.113717000	0.000000000
H	-4.424302000	0.008885000	0.000000000
H	-3.232343000	2.203426000	0.000000000
H	3.926556000	1.115979000	0.000000000
H	3.974270000	-1.148013000	0.000000000

$G^{III}C^{I}$ (E= -3439.65 kcal·mol^{-1}; nimag = 1)

N	-2.140963000	-1.997825000	0.000000000
O	-1.613958000	2.570074000	0.000000000
N	-1.964413000	0.305449000	0.000000000
C	-2.838037000	-0.816860000	0.000000000
N	-4.112787000	-0.625372000	0.000000000
C	-2.385709000	1.594300000	0.000000000
H	-1.115975000	-2.052305000	0.000000000
H	-2.662152000	-2.862284000	0.000000000
H	-0.938834000	0.144670000	0.000000000
O	0.761915000	-2.289480000	0.000000000
N	1.168858000	2.297599000	0.000000000
N	0.939692000	0.009122000	0.000000000
C	3.184620000	0.955794000	0.000000000
C	1.447029000	-1.255043000	0.000000000
N	2.862523000	-1.382685000	0.000000000
C	3.697623000	-0.303731000	0.000000000
C	1.745774000	1.083933000	0.000000000
H	3.831601000	1.825911000	0.000000000
H	3.220691000	-2.331684000	0.000000000
H	4.762470000	-0.511056000	0.000000000
H	0.131438000	2.395693000	0.000000000
H	1.745061000	3.127017000	0.000000000
H	-4.620490000	-1.513407000	0.000000000
H	-3.478656000	1.705440000	0.000000000

$G^{III}C^{II}$ (E= -2766.28 kcal·mol^{-1}; nimag = 1)

N	1.653115000	-1.814607000	0.000000000
O	0.368051000	2.596168000	0.000000000
N	1.110253000	0.429263000	0.000000000
C	2.154172000	-0.535821000	0.000000000
C	1.300723000	1.769337000	0.000000000
H	0.653011000	-2.032558000	0.000000000
H	2.302428000	-2.587486000	0.000000000
H	0.127958000	0.093564000	0.000000000
O	-1.263044000	-2.622751000	0.000000000
N	-2.303039000	1.851768000	0.000000000
N	-1.667122000	-0.366314000	0.000000000
C	-2.058639000	-1.686204000	0.000000000
C	-2.602158000	0.557422000	0.000000000
H	-1.298862000	2.163365000	0.000000000
H	-3.045108000	2.538908000	0.000000000
H	-3.671833000	0.300955000	0.000000000
H	-3.157854000	-1.879270000	0.000000000
H	2.355902000	2.074041000	0.000000000
N	3.379831000	-0.142143000	0.000000000
H	4.027126000	-0.934057000	0.000000000

$G^{IV}C^{I}$ (E= -3162.15 kcal·mol^{-1}; nimag = 0)

N	-3.399678000	-0.373171000	0.000000000
O	0.736697000	1.858063000	0.000000000
N	-1.237226000	0.671106000	0.000000000
C	-2.647941000	0.652132000	0.000000000
C	-0.501977000	1.812144000	0.000000000
H	-2.861529000	-1.255048000	0.000000000
H	-0.712852000	-0.237063000	0.000000000
O	-1.600598000	-2.979598000	0.000000000
N	2.300047000	-0.527886000	0.000000000
N	0.339983000	-1.731175000	0.000000000
C	2.450690000	-2.945088000	0.000000000
C	-0.369385000	-2.901366000	0.000000000
N	0.395128000	-4.106108000	0.000000000
C	1.757597000	-4.116472000	0.000000000
C	1.680170000	-1.724671000	0.000000000
H	3.534852000	-2.933150000	0.000000000
H	-0.142995000	-4.966130000	0.000000000
H	2.238932000	-5.088905000	0.000000000
H	1.749915000	0.348348000	0.000000000
H	3.308461000	-0.480991000	0.000000000
H	-1.107280000	2.738442000	0.000000000
H	-3.086266000	1.656364000	0.000000000

$G^{IV}C^{II}$ (E= -2488.57 kcal·mol^{-1}; nimag = 0)

N	-1.721503000	2.422728000	0.000000000
O	-1.389917000	-2.263302000	0.000000000
N	-1.461755000	0.038141000	0.000000000
C	-2.194872000	1.242199000	0.000000000
C	-2.023707000	-1.196348000	0.000000000
H	-0.689238000	2.437169000	0.000000000
H	-0.414966000	0.088028000	0.000000000
O	1.626506000	2.282496000	0.000000000
N	1.437126000	-2.314697000	0.000000000
N	1.402408000	-0.004549000	0.000000000
C	2.136756000	1.171550000	0.000000000
C	2.061285000	-1.137221000	0.000000000
H	0.396270000	-2.352815000	0.000000000
H	1.973190000	-3.171706000	0.000000000
H	3.160649000	-1.170850000	0.000000000
H	3.247976000	1.049549000	0.000000000
H	-3.278862000	1.085578000	0.000000000
H	-3.129497000	-1.192027000	0.000000000